UNIVERSITY OF BELGRADE

FACULTY OF TECHNOLOGY AND METALLURGY

Faisal Ali Alzarrug

SYNTHESIS AND CHARACTERIZATION OF DENTAL COMPOSITE MATERIALS REINFORCED WITH NANOFIBERS

Doctoral Dissertation

Belgrade, 2018

UNIVERZITET U BEOGRADU

TEHNOLOŠKO-METALURŠKI FAKULTET

Faisal Ali Alzarrug

SINTEZA I KARAKTERIZACIJA DENTALNIH KOMPOZITNIH MATERIJALA OJAČANIH NANOVLAKNIMA

Doktorska disertacija

Beograd, 2018

Supervisors

Dr Petar Uskoković, Full Professor, University of Belgrade, Faculty of Technology and Metallurgy,

Dr Dušica Stojanović, Associate Research Professor, University of Belgrade, Faculty of Technology and Metallurgy,

Members of Committee

Dr Vesna Radojević, Full Professor, University of Belgrade, Faculty of Technology and Metallurgy,

Dr Radmila Jančić-Hajneman, Full Professor, University of Belgrade, Faculty of Technology and Metallurgy,

Dr Ljiljana Brajović, Associate Professor, University of Belgrade, Faculty of Civil Engineering

Date:_____

ACKNOWLEDGEMENTS

I would like to express special appreciation and thanks to my supervisors, Dr Petar Uskoković and Dr Dušica Stojanović, who have been great mentors guiding me through the course of research and career with their constructive advice.

Also, I would like to thank Dr Vesna Radojević, Dr Radmila Jančić and Dr Ljiljana Brajović for serving as my committee members even at hardship. It is my appreciation for their detailed comments and suggestions - thus making my defense a memorable moment. Furthermore, I want to give a special thank you to Dr Vera Obradović, a research associate at the Innovation Center of the Faculty of Technology and Metallurgy, for her invaluable contribution to the work of this PhD thesis.

Last but not least, thanks go to my mum, wife and brothers for their tremendous support. They are the most important people in my world, and I dedicate this thesis to them.

SINTEZA I KARAKTERIZACIJA DENTALNIH KOMPOZITNIH MATERIJALA OJAČANIH NANOVLAKNIMA

Rezime

Cilj ovog istraživanja je ispitativanje mogućnosti upotrebe elektropredenih alumina punioca kao ojačanja za hibridne kompozitne materijale zasnovane na PMMA. Ispitivan je uticaj veličine i oblika elektropredenih alumina ojačanja na mehanička svojstva hibridnih kompozita i izvršeno je poređenje sa dva tipa kompozita dobijenih pomoću industrijskih alumina ojačanja: sferičnih čestica alumine i alumina viskersa. Sva ojačanja su dodata bez modifikacije površine, što čini proces veoma jednostavnim i snižava troškove procesiranja materijala.

Ova studija predstavlja ispitivanje uslova procesiranja na uniformnost, morfologiju i strukturu nanovlaknastih matova od poli (vinil butiral)/titanijum nanokompozitnih vlakana koja su dobijena brzim procesom elektropredenja sa više dizni. Kompozitna nanovlakna pokazuju poboljšanje termičkih, mehaničkih i antimikrobnih svojstava sa dodatkom nanoojačanja titanijuma.

Svrha ovog istraživanja bila je procena mehaničkih i optičkih svojstava kompozita na bazi PMMA, ojačanih poli (vinil butiral)/titanijum nanovlaknima. Štaviše, u ovom radu je izvršeno i ispitivanje različitog sadržaja poli (vinil butiral)/titanijum nanovlakana na mehanička i optička svojstva kompozita, kao i komparativna studija mehaničkih i optičkih svojstava kompozita.

Ključne reči: *elektropredenje, antimikrobna aktivnost, transparentni hibridni kompoziti, nanoindentacija, dinamičko mehanička analiza*

Naučna oblast: Tehnološko inženjerstvo, Nauka o materijalima i inženjerstvo materijala

SYNTHESIS AND CHARACTERIZATION OF DENTAL COMPOSITE MATERIALS REINFORCED WITH NANOFIBERS

Abstract

The goal of this research was to examine the feasibility of using electrospun alumina fillers as reinforcement for PMMA-based hybrid composite materials. The influence of the size and shape of electrospun alumina fillers on the mechanical properties of the hybrid composites was studied and compared with those of the two types of composites prepared using industrial alumina fillers: alumina spherical particles and alumina whiskers. All fillers were added without surface modification, which makes the process very simple and lowers the cost of the processing of the materials.

This study presents an investigation of processing conditions on the uniformity, morphology and structure of nanofibrous mats for poly (vinyl butyral)/titania nanocomposite fibers obtained by fast multi-needle electrospinning process. Composite nanofibers with the addition of titania nanofillers show improvement in thermal, mechanical and antimicrobial properties.

The purpose of this research was to evaluate the mechanical and optical properties of PMMA based composites reinforced with poly (vinyl butyral)/ titania nanofibers. Moreover, the effect of different contents of poly (vinyl butyral)/ titania nanofibers on the mechanical and optical properties of the composites as well as a comparative study of the mechanical and optical properties of the composites have also been conducted in this work.

Keywords: *electrospinning, antibacterial activity, transparent hybrid composites, nanoindentation, dynamic mechanical analysis*

Field of Academic Expertize: Technology engineering, Materials Science and Engineering

TABLE OF CONTENTS

CHAPTER 1

INTRODUCTION TO DENTAL MATERIALS

1. Introduction

A wide variety of materials have been applied as tooth crown and root replacements. These materials include animal or human teeth, bone, ivory, ceramics and metals. Restorative materials for the replacement of missing fragment in tooth structure have been improved over the past centuries [1].

There are different types of dental material used in dentistry, with characteristics that vary according to their application. The science of dental materials includes a study of their composition and properties and the way of the interaction with their environment. It has to be mentioned that the dentist and dental technician have a wide variety of materials at their disposal such as metals, alloys, rigid polymers, elastomers, ceramics, inorganic salts and composite materials (Figure 1). Numerous dental materials are put permanently into the patient's mouth or removed at times for cleaning. Such materials have to withstand the effects of a most hazardous environment like wide variations in acidity or alkalinity, temperature variations and high stresses which have impact on their durability [2].

A big challenge for a man is finding an appropriate material capable of fulfilling all the requirements needed for substitution of lost tooth structure. There have been many attempts with such restorative materials through the years, but the ideal replacement has not yet been discovered. Different reconstructions are used today and they include different metals, polymers and ceramics along with combinations of these materials.

Many of these materials work properly despite the fact that they are not ideal. Actually, it is complicated to make a perfect dental material because it is demanded that, at the same time, such a material has to be biocompatible, durable, refined, corrosion resistant and easy to process. Beside all above mentioned, along with its processing costs, the material should be relatively low in favour to make the use of

the material accessible to all socio-economical groups [3]. Most therapeutic materials are defined by physical, chemical, and mechanical parameters which are determined from test data. The material's accomplishment in the mouth and the performance of the material to be handled appropriately by the dental team present their precise and objective test [4].

The usage of suitable standards presents a great advantage in the knowledge of dental materials and their manipulation. The Dental Research Fellowship was established by the American Dental Association (ADA) in 1928. The work at the ADA includes a number of categories, such as measurements of clinically important physical and chemical features of dental materials with the development of new materials, instruments, and test procedures [5].

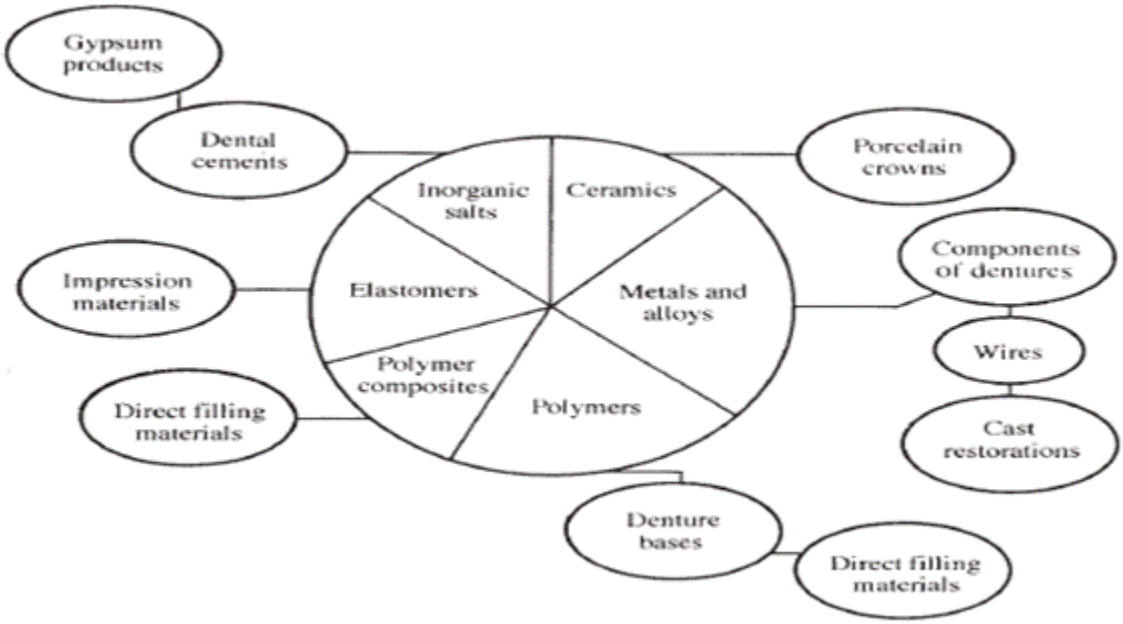

Figure 1. Plot of materials used in dentistry and some of their applications [2]

2. Classifications of dental materials

There are four groups of materials which are applied in dentistry: metals, polymers, ceramics and composites. The recent improved physical properties of these materials are not long-lasting and thus dentist and material scientists have been carrying over their research in the 21st century. It is assumed that a perfect restorative material would be biocompatible in the first place, bond permanently to tooth structure and copy the natural appearance of the structure. Further, the materal would display properties related to those of tooth dentin, and be capable of repairing missing or damaged tissues [3].

2.1 Metals

In dental practice, dental laboratory, dental restorations, implants and with instruments used to shape teeth, metals and alloys are heavily utilized. Metals and their alloys possess unique physical, chemical, optical, thermal, and electrical properties which are appropriate for plenty of dental applications. Tooth-coloured materials are commonly wanted for restorations but mainly metals bring stiffness and longevity for long-term dental applications. Metals display elastic and plastic behavior because they are ductile and malleable. Additionally, they are good electrical and thermal conductors with higher density than other materials, expose good toughness and can be polished. Metals may be drawn, cast or machined to generate dental restorations [6].

2.2 Polymers

Polymers consist of long chains of repeating covalently bonded units. These chains are composed of thousands of units which include carbon, hydrogen, and other

elements. The covalent bonds between the carbon atoms which form the backbone of the polymer molecule or chain define some properties of polymers.

A wide diversity of polymeric materials is caused by the variety of bonds between polymer chains. The fluctuating dipole is the weakest bond among them. Polymers do not have important permanent charges in the whole structure. The fluctuating dipole bonds are broken, and thus the chains easily slide by each other at room temperature where these polymer chains look like spaghetti. The polymer piece of spaghetti is twisted and curved by its way through the mass, which can quickly be bent. For instance, plastic bags are made of these materials. In case they are bent or stretched, the chains slide against each another. Chain slippage is increased by heating of such linear polymers and they are then molded or extruded [7].

2.3 Ceramics

The technological development of ceramics for dental applications has been impressive in the past forty years. This enhacement considerably increased the range of applications of ceramics in dentistry where they are needed due to their chemical inertness and versatile optical properties with excellent esthetics. Ceramics are still extensively used for covering metallic frameworks for dental restorations along with ceramic posts, abutments and implants. Dental ceramics in restorations fundamentally present oxide based glass-ceramic structures. They are characterised with three essential features: fabrication comfort of complex shapes, appropriate mechanical and corrosion resistance and suitable attraction form [8].

2.4 Dental composites

A composite presents any material which is composed of two parts: hard filler particles bordered by a hard matrix of a second material that wraps the filler particles together [9]. Three components make the dental material: resin matrix in form of

organic content, inorganic fillers and coupling agents. In most cases, the resin matrix consists of Bis-GMA (bisphenol-Aglycidyldimethacrylate). Due to high viscosity of Bis-GMA, it is mixed with short-chain monomers such as TEGDMA (triethylenglycol-dimethacrylate). The low the Bis-GMA content with the high content of TEGDMA produce higher polymerisation shrinkage [10].

Although by replacing Bis-GMA with TEGDMA the tensile is increased the flexural strength of the material is reduced. Long light polymerisation enhances the chain-linking of the individual monomers which influences less monomer release. The filler particles are made of quartz, ceramic or silica. With increasing filler content the polymerisation shrinkage, the water absorption and the linear expansion coefficient are diminished. On the contrary, with increasing filler content, the modulus of elasticity, wear resistance and the compressive and tensile strength usually increase [10,11].

Figure 2. A common microscopic structure of a composite material [9]

The microscopic structure of a typical composite material is shown in Figure 2. In the picture, the matrix is the lighter material that surrounds dark filler particles in form of irregular granules. Contrary to the composite in the picture on the left which has low density of filler particles, the composite material on the right side possesses high density of differently shaped filler particles closely packed together. It is evident that these composite materials could vary in physical properties to great

extent due to relative contents of both the matrix materials and the different filler particles [9].

3. Restorative dental materials

Dental restorative materials are remarkably composed materials designed for dental restorations (fillings). Missing tooth structure with its function and morphology usually caused by dental caries can be repaired by dental restorations. Dental professionals must choose the relevant material for dental recovery due to their knowledge of the materials properties [12].

3.1 Direct filling materials

3.1.1 Amalgam

Dental amalgam is a metal alloy which is usually composed of mercury, tin and silver, with small contents of zinc and copper. For more than 170 years dental amalgam has been an approved part of dental treatment and is advised to be the best direct restorative material for the last restorations in permanent teeth subject to high occlusion. The advantages of dental amalgam are: ease to make and to place it in the prepared tooth, economy in comparison with other materials, high longevity, durability, compressive strength and resistance to wear and minimal dimensional change with time [12,13].

3.1.2 Resin composite

Resin composite is a more favourable restorative material than many others due to its several properties. Several components make resin composite: a resin polymer matrix (organic), filler particles (inorganic), silane coupling agent, initiators and pigments. It is of great importance that resin composites possess highly aesthetic properties for almost invisible restorations of the teeth when they are judged precisely because of a wide range of shades similar to enamel which are dependent on the

pigments used. The resin composite's capability to resist wear and stress is determined by the type of inorganic filler particles and their content in the organic matrix. There are typically two types of filler particles: microfil and macrofil particles or a combination of the particles named "hybrids" [14].

Compared to macrofil particles favoured for their strength, larger fractions of microfil particles are ordinarily used for the anterior teeth as a resin composite containing more microfil particles which can be more easily polished for better aesthetic finish [15].

3.1.3 Glass Ionomer Cements (GIC)

Glass-ionomer cements were introduced to the world in 1972 by Wilson and Kent [15]. The chemical structure mainly consists of a fluoroaluminosilicate glass powder and polyacrylic acid liquid. There are many applications of this cement which include permanent cementation of crowns, bridges, orthodontic appliances, etc. Glass ionomer cements can chemically bond to base metals, stainless steel and tin-plated noble metals, and this is not the case with pure noble metals or glazed porcelain. Early preservation from moisture contamination and desiccation as well is required for clinical achievement with glass-ionomer cements. Postoperative sensitivity is determined by the initial low pH of glass ionomers. Anyway, this cement is considered acceptable due to its chemical bonding to tooth structure, fluoride release, bacteriostatic effect and appropriate compressive and tensile strength [16].

3.1.4 Resin modified Glass-Ionomer Cement

Resin modified glass-ionomer cement is a combination of glass-ionomer and composite resin. This filling is a mixture of glass, an organic acid and resin polymer which harden when light cured due to light activation of a catalyst in the cement that causes it to stiffen immediately. It stays better than glass ionomer, yet not as fine as

composite resin. It is not favored for biting surfaces of adult teeth. Usually, resin modified glass-ionomer cements can produce a better aesthetic result than traditional glass ionomers, but less good than pure composites due to their own setting reaction [17].

3.1.5 Compomers

Compomers or polyacid-modified composite resins are materials which consist of calcium aluminium fluorosilicate glass filler and polyacid components. They contain either or both fundamental components of a GIC. They are not water-based and thus no acid-base reaction can appear. Due to this property, they cannot absolutely be specified as glass ionomers. The acid-base reaction exists in the moist intra-oral environment and it favours fluoride release from the material. Before placement, an action of successful adhesion demands the use of dentine-bonding primers [18].

3.2 Indirect restorative materials

Indirect restorations are the ones where the teeth are firstly prepared. A dental impression is taken and sent to a dental technician who shapes the restoration as stated in the dentist's instructions.

3.2.1 Dental ceramics (Porcelain)

Dental ceramics are the materials which are modeled for producing dental prostheses for replacing missing or damaged dental structures [18]. As restorative materials, dental ceramics lack in their ability to withstand functional forces that are produced in the oral cavity. Thus, they have limited utilization in the premolar and molar areas, although their further enhancement has allowed their use as a posterior

long-stretch fixed partial prosthetic structure over dental implants [19]. Compared to dental metal materials, all dental ceramics display low fracture toughness.

3.2.2 Dental resin composites

The direct composite resins possess great optical and mechanical properties. Their use in larger posterior restorations is under consideration due to polymerization shrinkage in cavities with high C-factor. It is noticed that the adhesive interface is not able to withstand the stresses of polymerization in enamel-free cavity margins [20]. This leads to incorrect sealing resulting in microcracks and repeated caries. The realization of a proper nearby contact and the complete healing of composite resins in the deepest cavity regions still present a challenge. In spite of the development of some imperfections of direct-placement composites, no method has completely eliminated the problem of marginal microcracks correlated with direct composite [21].

3.2.3 Gold

Gold fillings possess outstanding durability and do not cause danger to the opposing teeth, although they conduct heat and cold. There exist two types of gold fillings - cast gold inlays and onlays made with 14 or 18 kt gold and gold foil formed from pure 24 kt gold that is polished layer by layer. They have been considered the standard of restorative dental materials for a long time. Some recent improvements in dental porcelains and consumer focus on aesthetic have raised the need for advanced composites and porcelain crowns. Gold fillings are very expensive but they endure for a long time - which means that gold restorations are less necessary. A gold crown can last for even 30 years [22].

4. Properties of dental materials

4.1 Mechanical properties

Restorations are exposed to heavy forces in the oral environment that affect teeth or material. Their act produces deformation, which can endanger material durability in the end. Certain materials in dentistry should have a minimum mechanical property requirement and be strong and tough enough to resist biting forces without fracture. Some of them should be solid enough to keep their shape under load. These properties of materials are defined by the stress-strain relationship gained by using a testing machine, Figure. 3 [23].

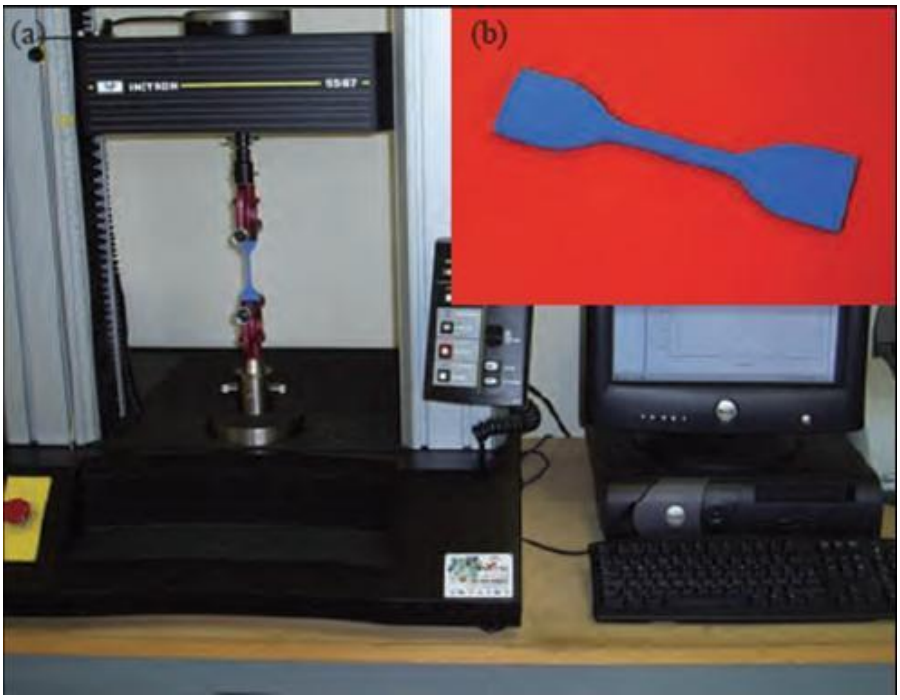

Figure 3. Testing equipment for mechanical properties [23]

Stress is the force per unit area produced in the body as a reaction to an externally applied force. Its units are kg/cm^2, N/m^2, PSI (pound per square inch) or Pascal, rather mega Pascal (MPa). It presents the internal reaction to the external force which is equal in power and opposite in direction to the applied external force.

Strain presents the change in length per unit length such as elongation or shortening when a stress is applied. It has no unit and is represented as a pure number (Figure 4) [24].

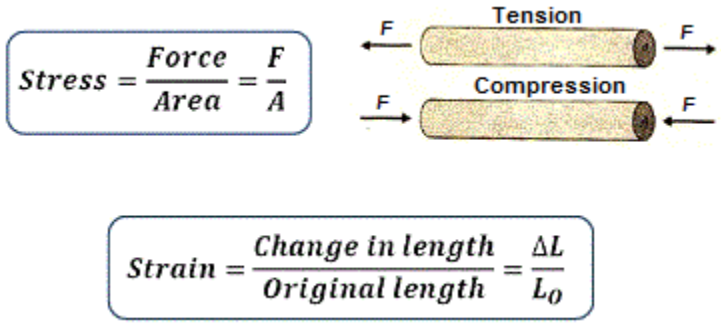

Figure 4. Material responses to external force [24]

4.1.1 Stress-strain relationship

Material's stress-strain curve displays the relationship between the stress and strain in concrete material. It is characteristic for each material and is found by reporting the amount of strain (deformation) at distinct intervals caused by stress (tensile or compressive loading). These curves inform of the material properties, such as the modulus of elasticity, E, etc. [25].

Stress-strain curves of various materials differ widely, and they depend on different tensile tests conducted, the temperature of the specimen and the speed of the loading. However, it is possible to recognize some typical characteristics among the stress-strain curves of various groups of materials and thus the materials are divided into two broad categories: the ductile materials and the brittle ones [26].

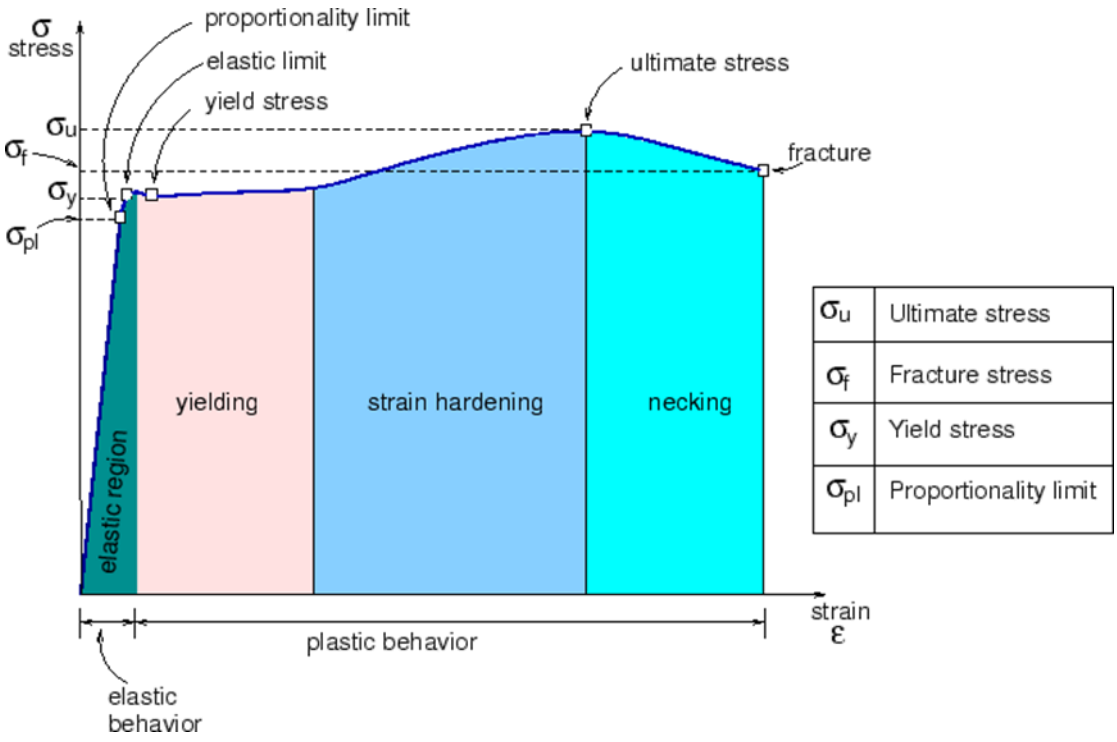

Figure 5. Typical regions and points on the stress-strain curve [26]

There are four typical regions which can be noticed in a stress-strain curve (Figure 5):

Elastic region - The region of the stress-strain graph with temporary deformation

Yielding - Where deformation is relatively large for small increases in the stress

Strain Hardening - Where the metal is becoming stronger with the strain increase

Necking and Failure - In the necking region the material starts breaking. A rupture occurs when the material completely breaks

4.1.2 Fatigue properties

Many restorative materials or dental prostheses are exposed to sporadic stresses which are too small to induce fracture over a long period of time. In these cases there is a possibility that the failure may appear by a fatigue process. This

includes the formation of a microleakage, probably caused by the stress concentration at a surface defect or the shape of the prosthesis reparation. This crack slowly increases until a fracture occurs. It is happens unexpectedly that final fracture often occurs at a low level of stress, and then patients claim that their denture plate fractured during biting of soft food [23].

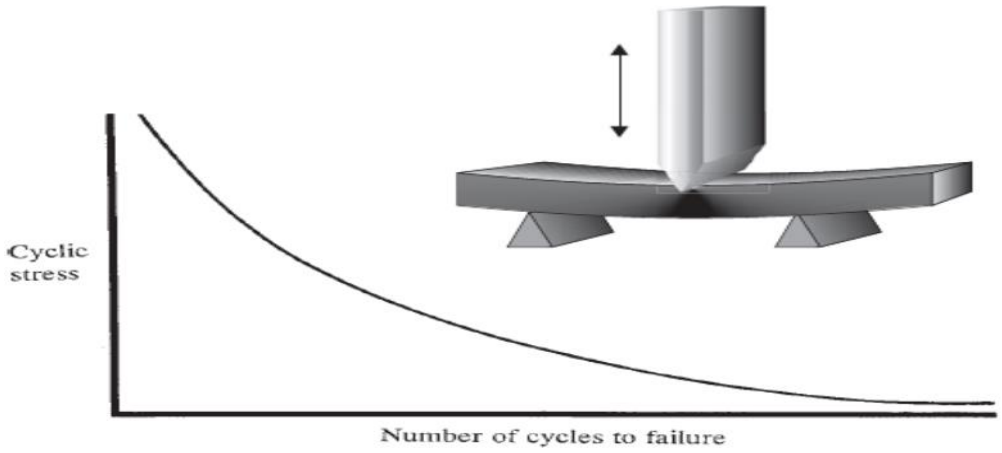

Figure 6. Fatigue testing results in a form of a graph cyclic stress versus a number of cycles to failure [23]

Fatigue properties are studied in two ways. The first approach is applying a cyclic stress at a given magnitude and frequency for observing the number of cycles demanded for failure. The result can be defined as the fatigue life of a material. Another method is choosing a number of stress cycles, like 10 000 and detecting the value of the cyclic stress required to induce the fracture in this number of cycles. This result is the fatigue limit. The most exact approach is to analyze numerous specimens at different cyclic stress levels for determination of the number of cycles to failure. These results are presented in the form of a graph displayed in Figure 6. It is observed that with the applied cyclic stress increase, there is a decrease in the number of cycles to failure [23].

4.1.3 Abrasion resistance

Wear presents the progressive loss of material due to relative motion of the contacting surfaces of a body [27]. Protection against wear and abrasion is a critical precondition for dental materials which are exposed to intense mechanical load during chewing [28,29].

Tooth wear is a complex phenomenon composed of biological, chemical, mechanical, and tribological elements. The whole tooth wear depends on muscular forces, patient diet routine and the nature of the restorative material used [30,31]. Much wear testing apparatus has been improved to estimate the clinical performance of numerous dental biomaterials, but they vary in the degree of difficulty and use different factors such as force, displacement, contact geometry, lubricant, opponent and cycles [32,33]. The two-body wear simulation devices are used for testing where the surfaces move opposed to each other in direct contact like during non-chewing movement inside the mouth [32]. Food particles in the mouth have a significant role in the wear of teeth and dental biomaterials during the process of mastication, and some simulation devices introduce abrasive slurries to imitate them as three-body wear [34].

4.1.4 Hardness

The hardness of a material provides a specification of the resistance to penetration when indented by a hard stiffness. The value of hardness in the form of the hardness number depends on the method used. Usually low values of hardness number imply a soft material and oppositely. Vickers, Knoop, Brinell and Rockwell are the typical methods used for hardness evaluation [23].

4.1.5 Elasticity

The yield stress is the value of stress after which the material becomes permanently deformed since the strain is not absolutely recovered after the applied load is removed. The yield stress is a significant property but it does not completely

characterise the elastic properties of a material since they are generally defined as the ability of a material to bear elastic recovery. A material is elastic when it undergoes full elastic recovery just after the removal of an applied load. In case the recovery occurs slowly, or if the slight permanent deformation remains, the material is viscoelastic [23].

4.2 Miscellaneous physical properties

4.2.1 Optical properties

4.2.1.1 Color and optical effects

Optical properties are required to allow a material to recover the function of damaged or missing natural tissues with appropriate color asthetics [35]. With the use of bleaching and whitening technologies esthetic application in restorative and prosthetic dentistry has received increasingly greater significance in recent decades [36].

4.2.1.2 Three dimensions of color

Color recognition is defined by three detached variables: **hue, value,** and **chroma**. The three parameters establish the three dimensions of “color space” which is displayed in Figure 7.

Hue is the dominant color of an object such as red, green, or blue. The continuum of these dominant wavelengths present in the spectral distribution creates the 3D color, Figure 7.

Value or the gray scale is located at Z-axis and it increases toward the high end (lighter) and decreases toward the low end (darker). Value is also defined by the “lightness” factor or varying levels of gray between the limits of white and black where teeth and other objects can be divided into lighter shades or darker shades [37-39].

Chroma is the degree of saturation of a specific hue, for instance, red range from scarlet-high saturation to light pink-low saturation. Chroma increases from the center radially outward with changes in a neighboring direction [38].

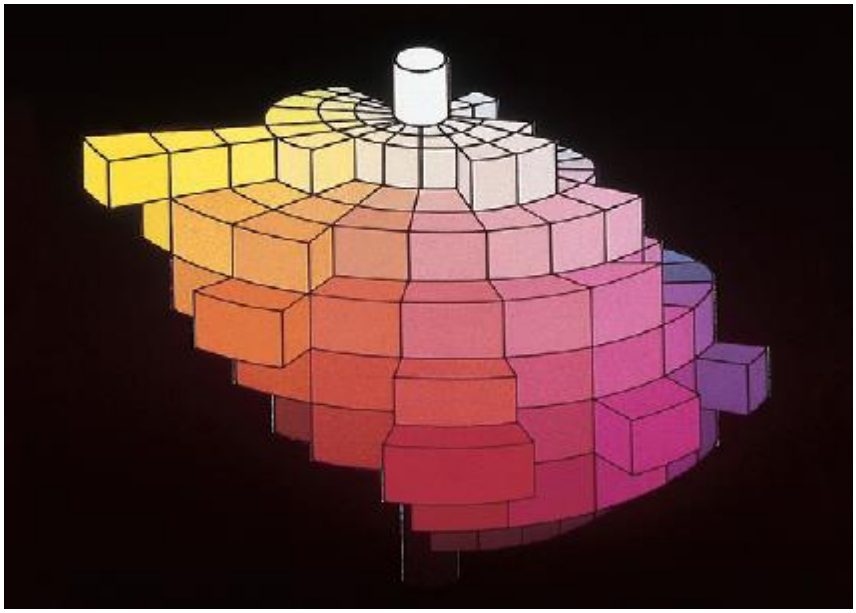

Figure 7. Three dimensions of color space [38]

4.2.1.3 Color matching

Color matching in dental practice is frequently carried out with the help of a shade guide (such as the one shown in Figure 8) to choose the color of ceramic veneers, crowns or inlays. The individual shade tabs in the Figure are grouped according to hue (A = red-brown, B = red-yellow, C = gray and D = red-gray), with the value 1 to 4, from lightest to darkest. This arrangement acts in accordance with the order introduced by Vita for porcelain with the system shade guides in decreasing order of value (from lightest to darkest: B1, A1, B2, D2, A2, C1, C2, D4, A3, D3, B3, A3.5, B4, C3, A4, C4) [39].

It is usually not easy to simply choose a shade for tooth or restoration from a shade guide and deliver the information to a technician or a lab. Supplementary information such as descriptions, photographs and drawings should also be sent for

successful esthetic results. Appropriate color match will be definitely better if the colour of certain teeth is available to the technician [39].

Figure 8. Tab arrangements of the Vitapan manufacturer classical shade guide. A - group division according to hue. B - "value scale", no group division. C - group division with alternative arrangement according to colour difference in relation to the lightest tab [39].

4.2.1.2 Pigmentation

Esthetic effects in a restoration are at times produced by including coloured pigments in resin composites, dental ceramics, denture acrylics and silicone maxillofacial materials. The colour makes a mix of pigments which results from the particular absorption by the pigments and the reflection of particular colours [39].

4.2.1.3 Opacity

Opacity is defined as a property of materials which blocks the passage of light (Figure 9). An object is white in case all of the spectrum colors from a white light source like sunlight are reflected from the object with the same intensity as received.

The object shows black when all the spectrum colors are absorbed identically. An opaque material can absorb some of the light and reflect the rest. For instance, the material appears green in reflected white light when red, yellow, orange, blue, and violet are absorbed [40].

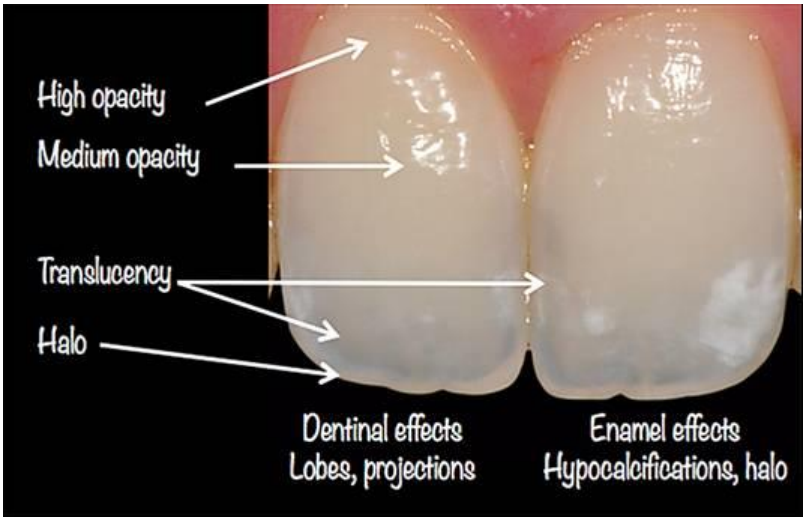

Figure 9. Illustration of halo, translucency and opacity [40]

4.2.1.4 Translucency

Objects cannot be seen through the material when translucency which presents a property of substances allow the passage of light, but dissipate the light. Resin composites, ceramics and denture plastics are translucent materials which are utilized in dentistry [40].

4.2.1.5 Transparency

Transparency is a property of material which enables the passage of light in a sense that little deformity occurs and objects can be clearly recognized through them (Figure 10), [41]. When transparent substances such as glass absorb certain wavelengths and transmit others they may be coloured. As an illustration, when a piece of glass absorbs all wavelengths excluding red, it would appear red because of

the transmitted light. In case that a light beam which contains no red wavelengths was shone on the glass, it would come out opaque, since the resting wavelengths would be absorbed [39].

Figure 10. Demonstration of transparency [41]

4.2.1.6 Index of Refraction

The ratio of the velocity of the light in a vacuum or air to the velocity in the medium is the index of refraction (n), a characteristic property of any substance (Table 1). The light slows from its air speed (300,000 km/sec) and may alter direction when it enters a medium. For instance, when a beam of air light hits the water surface at an angle, the light rays are bowed toward the normal.

A line drawn vertical to the water surface at the point where the light enters the water surface is called the normal [37]. If the light is traveling through water and contacts a water-air surface at an angle, the beam of light is bowed or refracted away from the normal. The index of refraction is used greatly for recognition of any substance. One of the most important applications of refraction is the regulation of the dispersed and matrix phase's refractive index in materials such as dental ceramics and resin composites, modeled to have the translucent image of tooth tissue. A perfect combination in the refractive indices appears in a transparent solid, because large characteristics result in opaque materials [38].

Table 1. Index of Refraction (n) of some materials [42]

Material	Index of Refraction
Feldspathic porcelain	1.504
Quartz	1.544
Synthetic hydroxyapatite	1.649
Tooth structure, enamel	1.655
Water	1.333

4.2.1.7 Optical Constants

Certain phenomena can be detected when light interacts with an object. Incident light can occur reflected, scattered (or maybe backscattered), absorbed or transmitted. These parameters are calculated to define the optical properties of the material more objectively (Figure 11). Turbid materials are dental materials like ceramics, resin composites, tooth structure or intensely light-scattering materials. The intensity of the incident light is weakened remarkably when the light passes through the specimen in a turbid material [41].

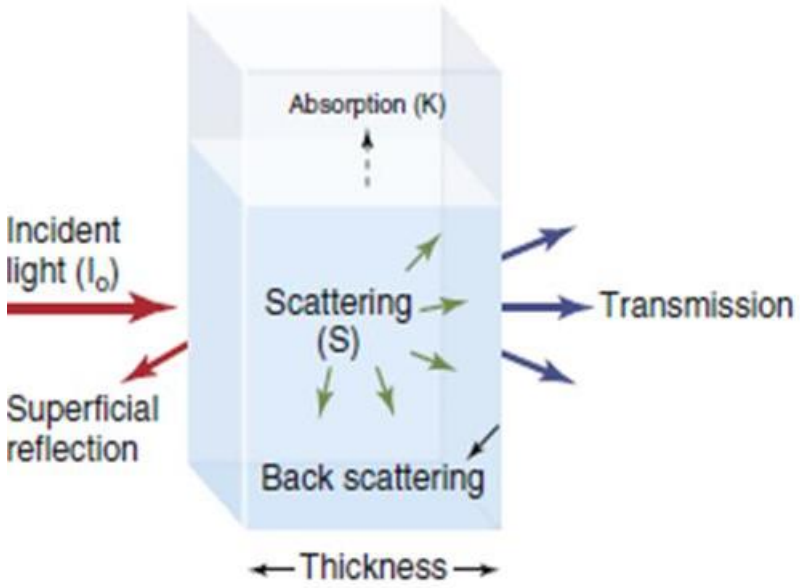

Figure 11. Illustrative of the possible light interactions with a solid [41]

These issues are important not only for shade matching but also in conditions where the restorative material is used to camouflage defects in the tooth being restored, such as blemishes. The optical properties of restorative materials described by the Kubelka-Munk equations can be solved algebraically by hyperbolic functions [41].

4.2.2 Dimensional changes

Dimensional preciseness is required for many dental materials. Dimensional changes which appear during impression recording, setting of direct restorative materials or casting of alloys dictate the success of various restorative procedures.

The handling of many materials includes the mixing of two or more components followed by chemical reaction which always come with dimensional changes. A contraction or an expansion occurs as a result of polymerization reactions. Dimensional changes can occur at each stage in multi-stage production of a restoration. In this case an expansion at one stage can be used to partly neutralize a contraction at another stage like constructing a cast metal restoration when the setting expansion of the investment material partly counterbalances the casting shrinkage of the alloy [23].

4.2.3 Density

Density is a basic property which induces design aspects of dental applications. For example, it would be necessary to consider density in case of choosing an alloy as construct components for upper denture since heavy alloy would produce large displacing forces making with holding difficult. In order to avoid these destabilizing forces a lower density alloy is used to keep its bulk to a minimum. These concerns become important when other design parameters are considered. For instance, when a square cross-section beam undergoes three-point bending, the force causing a given deflection at the beam centre is determined by the square of the thickness. Therefore, equal realization can be accomplished with a considerable

saving in weight with a rigid (high modulus of elasticity) but low density material [23].

4.3 Chemical properties

Chemical stability of a material placed in the mouth is one of the essential factors which define its durability. Materials should not dissolve, corrode, erode or either leach toxic ingredients into the oral fluids.

4.3.1 Solubility and erosion

The solubility of a material is simply a measurement of the dissolubility in a given fluid, like water or saliva. Furthermore, erosion is a process which links the chemical dissolution with a moderate mechanical action. Thus it is obtainable to consider a situation in which the surface layer of a material is weakened by dissolution and then dissociates by mild abrasion. In materials science the term erosion is usually used to indicate damage caused by the intrusion of particles on an object.

The degradation of natural hard tissues by acids (which occurrs naturally or exists in food/drinks) is described by erosion in dentistry and it includes the destruction of restorative materials with a combination of mild mechanical and chemical actions. For all restorative materials these properties are extremely important because weak resistance to erosion and a high solubility will shorten the effective existence of the restoration [23].

4.3.2 Leaching of constituents

Many materials in an aqueous medium absorb water by a diffusion process. By diffusion process of leaching ingredients of the material can be lost into the oral fluids. This may produce serious changes of material properties, when the leached material is maybe toxic or irritant. The presence of relatively large quantities of

plasticizer in the acrylic resin for their softness makes soft acrylic polymers adequate for cushioning the fitting surfaces of dentures.

The resin becomes hard and hence inefficient as a cushion by the slow leaching of plasticizer. Sometimes leaching helps to the benefit of the patient. For instance, slow leaching of some cements comprising calcium hydroxide produces an alkaline environment in the basis of deep cavities. The dual benefit is accomplished in this way -antibacterial resistance and secondary dentine formation [23].

4.3.3 Corrosion

The direct combining process of metallic and nonmetallic elements to produce a chemical compound through oxidation reactions is called chemical corrosion. Silver sulfide is formed by chemical corrosion with the discoloration of silver by sulfur. Dry corrosion is managed with dental gold alloys that contain silver, since it happens in the absence of water or another fluid electrolyte.

One more example is preparing particular dental amalgam products with the oxidation of silver-copper alloy particles which are mixed with mercury. It is very important to store the alloy in a cool and dry location to ensure a satisfactory shelf life since the alloy particles consist of a silver-copper eutectic phase and oxidation limits their reactivity with mercury, affecting the dental amalgam product setting reaction [43].

4.3 Biocompatibility of dental materials

Biocompatibility (tissue compatibility) is the capability of a material to operate with a relevant host response when it is applied. The suitability of the host response is crucial. Biocompatibility is sometimes defined as the ability of a material to bring out a proper biological feedback in a given utilization in the body. In this definition it is fundamental that a single material may not be biologically adequate in all appliances. One example is a material that is adequate for a full cast crown but it may be not acceptable for a dental implant. The prediction in a bone implant is that the material will allow the bone to combine with the implant with an appropriate

biological feedback for the implant called osseointegration [44,45]. Though the osseointegration is not an expectation in a full cast crown yet that the material will not cause inflammation of periodontal or pulpal tissues. Biocompatibility of a material depends on the physical function for which the material will be utilized and the biological response that will be demanded from it [46].

4.3.1 Biocompatibility tests

4.3.1.1 In vitro studies

In vitro analysis of the biocompatibility of materials happens outside of live organisms by applying cell cultures. These tests allow the inclusion of strategies to increase the closenesss to clinical practice, such the use of physical barriers like enamel or dentin discs. The development of these methods allows for estimation of cell function and existence, a kind of cell death, cell morphology, the expression of proteins and inflammatory channels, reactive oxygen species, etc [47, 48].

4.3.1.2 In vivo studies (with animals)

The animals used for testing in the laboratory are less expensive than clinical studies and they may be sufficiently controlled. However, the type, age and gender of the animal used in the studies may have an impact on the results attained in these tests [49] and cannot be regularly extrapolated to clinical conditions in humans [50]. Furthermore, the explanation of the responses observed is complicated, due to various events that occur together, such as the stress produced by the applications of the test materials in connection with the animals' tissues and probable local infections [51].

4.3.1.3 Clinical studies

The "gold standard" for the estimation of properties and performance of dental materials are realized with clinical studies by using the experimental results in

human volunteers [52]. Various experimental protocols are included in these types of studies which are related to cost and the difficulty of conducting them [53]. Biocompatibility would not be the main focus of clinical studies since their majority aims attention at mechanical properties of materials [54]. Clinical studies are usually more expensive and take more time. Their results are more difficult to control and interpret, especially when compared with the investigations produced in animals and in vitro tests. Strong ethical barriers are related to these studies using human bodies [55].

4.3.1.4 Correspondence between biocompatibility tests

It is usually not possible to obtain strong correspondence between the laboratory information and the set of clinical features in a short or long period [56]. This happens due to the fact that laboratory tests are static, but, on the contrary, the analysis of clinical properties includes dynamic examination like the change in the material after a while which, although appearing in vitro, does not certainly give back the same features as those detected in vivo [56].

CHAPTER 2

ELECTROSPINNING

2.1 Introduction

Electrospinning is the process of spinning fibers by electrostatic forces and this production has been present for more than one hundred years. This technique in its viable form started in the early 1930s. In 1934, Formhals patented his first invention relating to the electrospinning in 1934, and the apparatus produced artificial filaments applying electric charges. There has been an increased interest in electrospinning in the last 10 years, due to its large utilization in nanoscale properties and technologies. The diameters of polymer fibers which are produced by the electrospinning process differ from 3 nm to more than 5 μm [57,58]. The electrospinning setup has been attractive due to its simplicity and low-cost nature. The common electrospinning setup parts are: a high voltage source, a syringe pump and a collector (Figure 12).

In the electrospinning process, a polymer solution remains at a needle tip due to surface tension. The utilization of an electric field with the high-voltage source generates charges which are induced within the polymer and this results in charge repulsion in the solution. This electrostatic force fights with the surface tension. Finally, the charge repulsion prevails the surface tension, creating the initiation of a jet. The solvent evaporates from the jet when it goes down, and a suitable collector is used for the deposition of the polymer fiber [59]. Electrospinning offers a simple, special and many-sided technology for producing polymer and composite fibers within the micrometer or nanometer diameter dimensions [60].

With smaller pores and higher surface area than regular fibers, electrospun fibers possess smaller pores and higher surface compared to regular fibers and thus they have many applications in various fields like biomedical, pharmaceutical,

healthcare, tissue engineering scaffolds, biotechnology, protective clothing, filtration, nanocatalysis and environmental engineering [61].

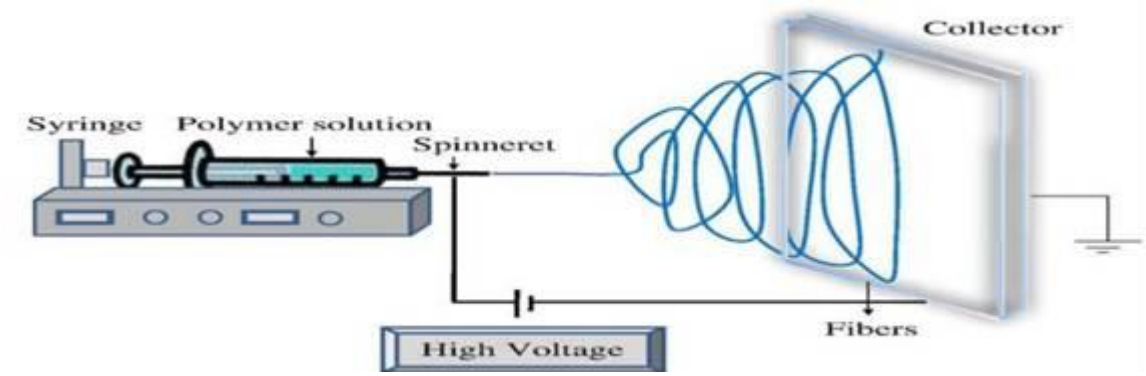

Figure 12. Basic electrospinning equipment [59]

In a typical electrospinning process, an electrical potential is employed between a droplet of a polymer solution or melt which is at the end of a syringe tube and a grounded collector. As stated before, when the applied electric field overpowers the surface tension of the droplet, a charged jet of polymer solution is thrown out at that moment. The shape and route of the charged jet is conducted by the electric field. The jet demonstrates bending fluctuations generated by repulsive forces among the charges carried with the jet. The jet stretches with spiralling loops and it is getting longer and thinner, the loops rise in diameter. In the end, the jet collects and solidifies on the target [62-64].

Electrospun fibers possess remarkable properties and serve as basic building blocks for the manufacturing of high strength structures. One example is carbon nanotubes (CNTs) and carbon black (CB) particles as fillers which are dispersed within the fibers to resemble the performance of silk fibers for toughness and high strength applications [63].

2.2 Process description

There are four main regions which characterize the electrospinning process: (1) the Taylor cone, (2) the steady jet, (3) the instability, and (4) the base. At the moment when a high voltage is applied to a liquid droplet, the liquid gets charged, and the droplet is extended because electrostatic repulsion works against the surface tension. Then, at a critical point, the liquid erupts from the surface making a stream. This stage of eruption is known as the Taylor cone. In case the molecular unity of the liquid is sufficiently high, stream breakup does not appear and a charged liquid jet is produced. When the breakup occurs droplets are electrosprayed [65,66].

On its way down, the jet dries, with the mode of the flow that changes from ohmic to convective as a result of the charge migrating to the surface of the fiber. The jet is then stretched by a whipping process which is created by electrostatic repulsion. This repulsion made small bends in the fiber that is finally deposited on the grounded collector (Figure 13). This elongation and, at the same time, thinning of the fiber, as a result of the bending instability, produce the uniform fibers with nanometer-scale diameters [66].

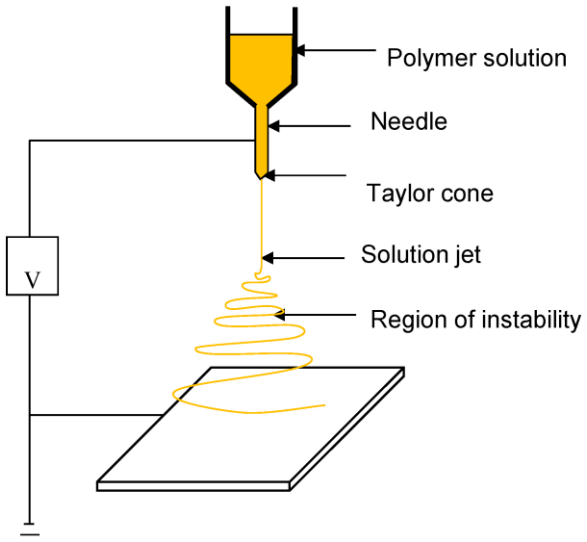

Figure 13. Electrospinning regions [66]

2.3 Working parameters

2.3.1 Process parameters

2.3.1.1 Applied voltage

The flow of the polymer jet towards the collector enables the charge transport owing to the applied voltage in electrospinning. The increase or decrease in the current is related to the mass flow of the polymer from the syringe tip. Deitzel et al have concluded that the change in the spinning current is connected with the change in the instability mode. They experimentally confirmed that an increase in applied voltage produces a change in the shape of the jet initiating point, and thus the morphology of fibers [67].

Several groups proposed that higher voltages increase the electrostatic repulsive force of the charged jet, favoring the narrowing of the jet and decreasing of fiber diameter. For instance, Yuan et al. [68] examined the effect of voltage on fiber morphologies and alignment with polysulfone (PSF)/DMAC/acetone (Figure 14).

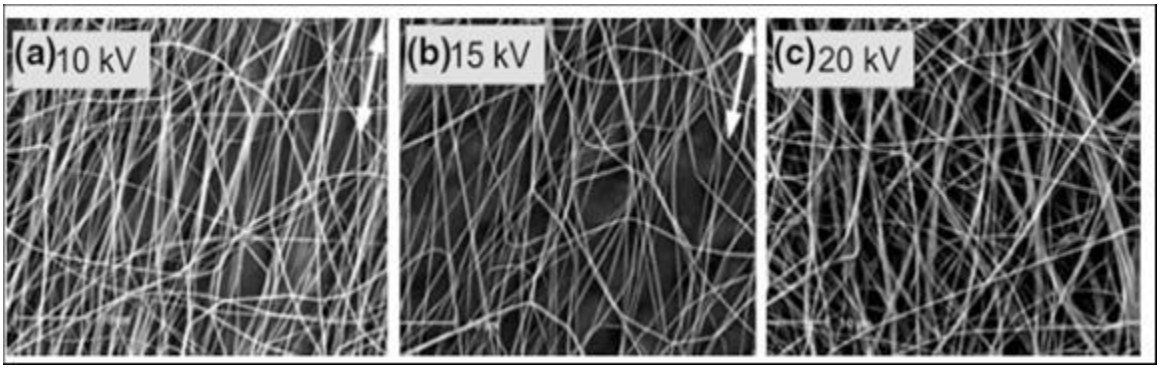

Figure 14. **SEM images of the ultrafine fibers electrospun from a 20 % PSF solution in DMAA/ acetone (9:1) under different voltage. The average diameters of fibers are: (a) 344 ± 51 nm, (b) 331 ±26 nm, and (c) 323 ±22 nm [69]**

3.1.2 Polymer flow rate

An important process parameter in electrospinning process is the polymer flow rate from the syringe which induces the jet velocity with the material transfer rate. Megelski et al. noticed that in the case of PS fibers the fiber diameter and the pore diameter increased with increasing the polymer flow rate [12]. When the flow rate increased, fibers were characterized with beaded morphologies, with the mean pore size increase from 90 to 150 nm [70].

3.1.3 Collectors

In the electrospinning process, collectors usually have a role as the conductive substrates to collect the charged fibers. Commonly, Al foil is used as a collector but it is problematic to move the collected nanofibers to other substrates for different applications. With the need of fibers sifting, various collectors have been developed such as wire mesh, rotating rods or wheel, liquid bath, grids, pin, parallel or gridded bar, etc. (Figure 15) [71].

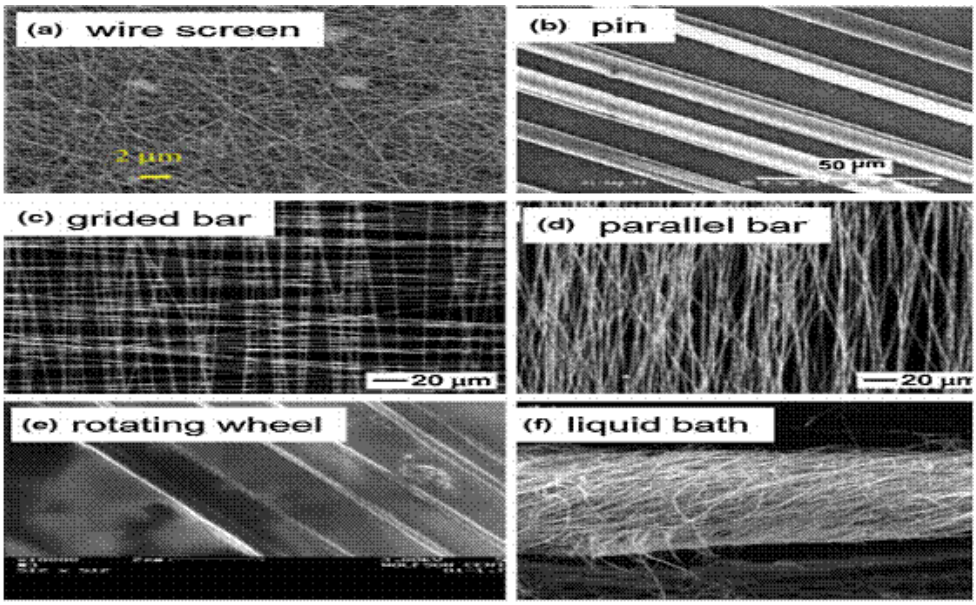

Figure 15. SEM images of electrospun fibers with different types of collectors [71]

3.3.1.4 Distance (H) between the collector and the tip of the syringe

It has been confirmed that the distance (H) between the collector and the tip of the needle also affects the fiber diameter and its morphology [71]. Generally, if this distance is too short, the solvent from the fiber will not have enough time to evaporate and the fiber will not solidify before reaching the collector. On the other hand, if the distance is too long, the bead structure of the fiber can be obtained. As it has been mentioned above, the important physical aspect of the electrospun fiber is their dryness from the solvent, which can be achieved by optimum distance. For instance, Yuan et al. [69] demonstrated that a long distance produces the thinner fiber diameter as shown in Figure 16.

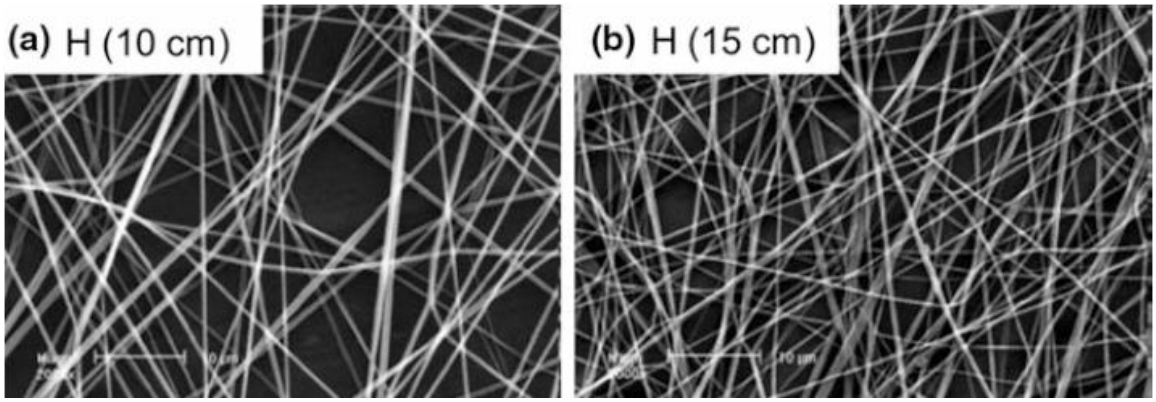

Figure 16. SEM images of the electrospun PSF fibers from 20 wt. % PSF/DMAC solution at 10 kV with two different distances. The diameters of (a) and (b) are 438 ±72 nm and 368 ±59 nm, respectively [71]

2.3.2 Solution Parameters

2.3.2.1 Concentration

A minimum solution concentration is required for fiber formation in the electrospinning process. It has been discovered that at low concentration of solution, a mixture of beads and fibers is collected. When the solution concentration increases,

the shape of the beads transforms from spherical to spindle-like and, in the end, consistent fibers with increased diameters are produced because of their higher viscosity resistance [72].

There are four critical concentrations going from low to high that should be observed:

1) When the concentration is very low, polymeric micro (nano)-particles will be produced. In fact, electrospray appears instead of electrospinning due to the low viscosity and high surface tensions of the solution.

2) By increasing the concentration, a mixture of beads and fibers will be obtained [73]

3) With the suitable concentration, smooth nanofibers can be produced [73]

4) When the concentration is very high, helix-shaped microribbons will be observed instead of nanoscaled fibers (Figure 17) [74].

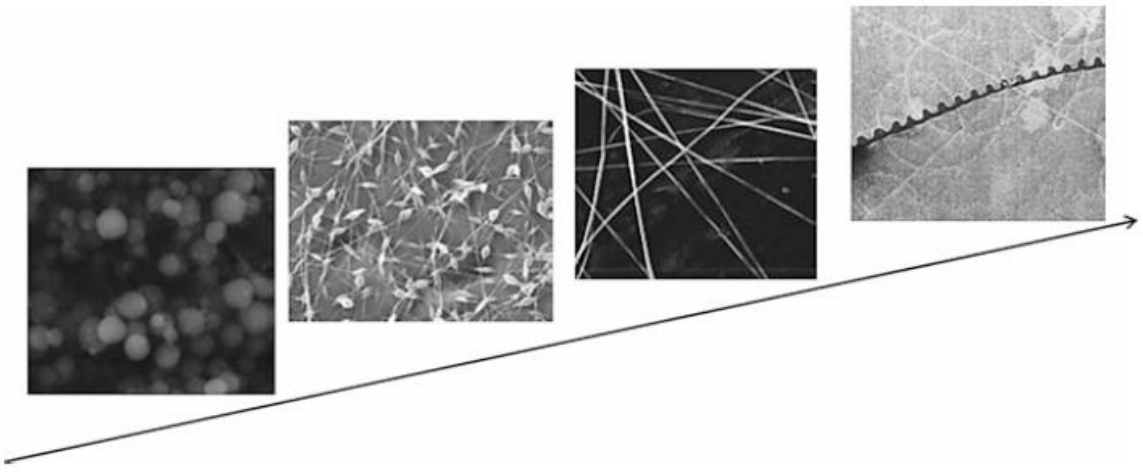

Figure 17. SEM images of the progression of the products with different concentrations during the electrospinning (from low to high) [75]

2.3.2.2 Molecular weight

Molecular weight of the polymer has a considerable effect on rheological and electrical properties like viscosity, conductivity, surface tension and dielectric strength [72]. This solution parameter is very important since it affects the morphology of electrospun fibers. Usually high molecular weight polymer solutions have been applied in electrospinning since they provide the relevant viscosity for the fiber formation. It has been observed that a solution with too low molecular weight tends to produce beads more than fibers while a high molecular weight solution provides fibers with larger mean diameters (Figure 18). The molecular weight of the polymer demonstrates a solution viscosity and the number of entanglements of polymer chains in a solution.

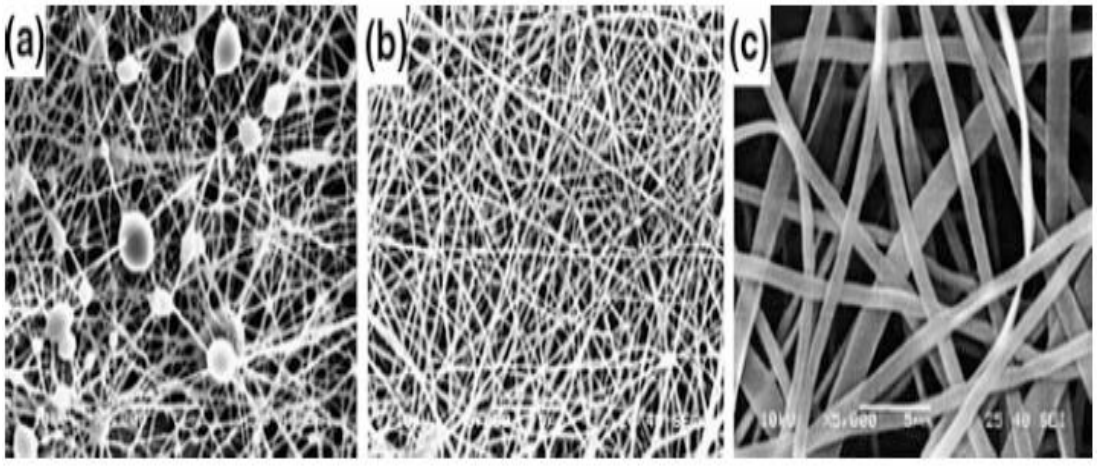

Figure 18. Images showing the expected structure in the electrospun polymer for various molecular weights: (a) 9000-10,000 g/mol; (b) 13,000-23,000 g/mol and (c) 31,000-50,000 g/mol (solution concentration: 25 wt. %) [71]

It is also important to refer to the fact that the molecular weight is not always crucial for electrospinning if adequate intermolecular interactions can be supplied by oligomers. For instance, Long and McKee successfully produced the oligomer-sized phospholipid fibers from lecithin solutions by electrospinning. They found that smooth fiber could be gained when the concentration of phospholipid is higher than 35 wt. % [76].

2.3.2.3 Viscosity

Viscosity has an important role in fiber size and their morphology during electrospinning process. The effect of viscosity appears in the same manner as concentration; low viscosity does not enable continuous fiber formation, while high viscosity generates drying of polymer solution at needle tip. Furthermore, different kind of polymer and polymer-solvent system displays different viscosity range [66,67].

2.3.2.4 Surface tension

During its fall through the air, the droplet of water comonnly adopts a spherical shape. Surface tension is the liquid surface property which is responsible for this phenomenon. In electrospinning process, the charges on the polymer solution need to be great enough to overcome the surface tension of this solution. As the solution current accelerates from the tip of the syringe to the collector, the solution is elongated while the surface tension of the solution may provoke this solution to break up into droplets. The process is called electrospinning when fibers are collected. On the contrary, when droplets are collected the process is known as electrospraying. The surface tension is also responsible for the formation of beads on the electrospun fibers. Due to these phenomena, it is significant to understand the behaviour of surface tension in a fluid [77].

There are uniform attractive forces among a liquid molecule in the solution and other liquid molecules which are surrounding it. After all, for a liquid molecule

placed at the surface of the solution, there is a greater attractive downward force by molecules below than by the gas molecules above as depicted in Figure 19.

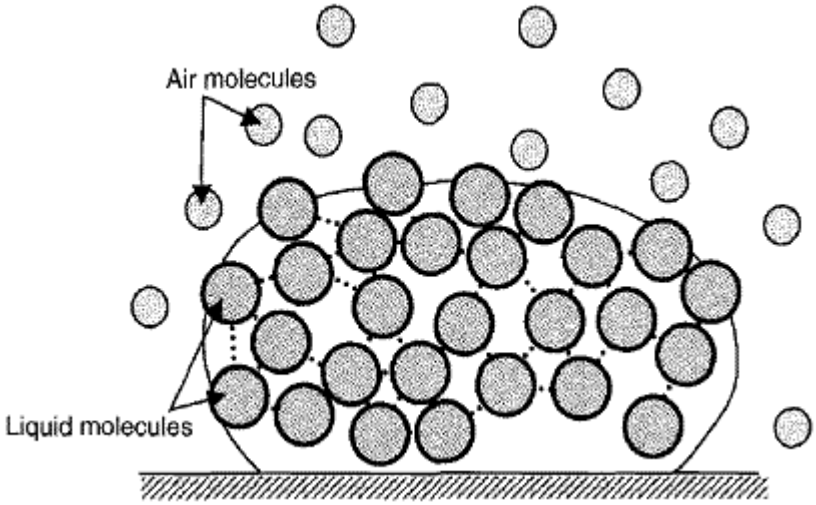

Figure 19. In the picture it is depicted that attractive forces among the liquid molecules are stronger than the ones of the air molecules [77].

The tension which causes a contraction at the surface of the solution is balanced by repulsive forces which increase from the collisions of molecules from the inside of the solution. With this net effect of the pulling of all the surface liquid molecules the liquid surface is contracted and the surface area is reduced. For this reason, a spherical shape is the lowest surface area to volume ratio for a droplet of water.

2.3.2.5 Conductivity/surface charge density

Polymers are generally conductive, with some exceptions of dialectric materials. The charged ions in the polymer solution are of great influence in jet formation. The conductivity of solution is usually directed by the polymer type, the solvent type and the ionisable salts. It has been discovered that with the increase of electrical conductivity of the solution, there is a considerable decrease in the

electrospun nanofibers diameter while with low conductivity of the solution, there is an insufficient elongation of a jet by electrical force to form a uniform fiber, and beads may also be noticed [72].

For instance, the electrical conductivity of the solution can be controlled by adding the ionic salts like KH_2PO_4, NaCl, etc [71]. Nanofibers with small diameter can be produced with the assistance of ionic salts. High solution conductivity can be also accomplished by applying organic acid as the solvent [71].

2.4 Polymers used in electrospinning

There are a plenty of polymers which are used in electrospinning. They are able to produce fine nanofibers within the submicron range that are used for various applications. Electrospun nanofibers have been made from various natural polymers, synthetic polymers or a blend of both along with proteins nucleic and even polysaccharides [78].

During many years, more than 200 polymers have been electrospun prosperously from natural polymers and they have been characterized considering their applications [79]. Some polymers which are used in electrospinning, with their characterization methods and applications have been listed in Table 2.

Table 2. Different polymers used in electrospinning, with their characterization methods and applications [79].

Polymers	Applications	Characterizations
Poly(glycolide) (PGA)	Nonwoven TE[a] scaffolds	SEM[b], TEM[c], *in vitro* rat cardiac fibroblast culture, *in vivo* rat model
Poly(lactide-co-glycolide)(PLGA)	Biomedical applications, wound healing	SEM, WAXD[d], SAXS[e], degradation analysis
Poly(ε-caprolactone) (PCL)	Bone tissue engineering	SEM, *in vitro* rat mesenchymal stem cell culture
Poly(l-lactide) (PLLA)	3D cell substrate	SEM, *in vitro* human chondrocyte culture
Polyurethane (PU)	Nonwoven tissue template wound healing	SEM, *in vivo* guinea pig model
Poly(ethylene-co-vinyl alcohol) (PEVA)	Nonwoven tissue engineering scaffold	SEM, *in vitro* human aortic smooth muscle cell and dermal fibroblast cultures
Polystyrene (PS)	Skin tissue engineering	SEM, *in vitro* human fibroblast, keratinocyte, and endothelial single or cocultures
Syndiotactic 1,2-polybutadiene	Tissue engineering applications	ESEM[f], XRD[g], FTIR[h]
Fibrinogen	Wound healing	SEM,TEM,mechanical Evaluation
Poly (vinyl alcohal)/cellulose acetate (PVA/CA)	Biomaterials	SEM, FTIR, WAXD, mechanical evaluation
Cellulose acetate	Adsorptive membranes/felts	SEM, FTIR
Poly(vinyl alcohol)	Wound dressings	SEM, EDX[i]
Silk fibroin, silk/PEO[j]	Nanofibrous TE scaffold	SEM, FTIR, XPS[k]
Silk	Biomedical Applications	SEM, TEM, WAXD
Silk fibroin	Nanofibrous scaffolds for wound healing	SEM, ATR-IR[l], ^{13}C CP/MAS NMR, WAXD, NMR[m], *in vitro* human keratinocyte culture
Silk/chitosan	Wound dressings	SEM, viscosity analysis, conductivity measurement
Chitosan/PEO	TE scaffold, drug delivery, wound healing	SEM, XPS, FTIR, DSC[n]
Gelatin	Scaffold for wound healing	SEM, mechanical evaluation
Hyaluronic acid, (HA)	Medical implant	SEM
Cellulose	Affinity membrane	SEM, DSC, ATR-FTIR[o]
Gelatin/polyaniline	Tissue engineering scaffolds	SEM, DSC, conductivity measurement, tensile testing
Collagen/chitosan	Biomaterials	SEM, FTIR

2.4.1 Natural and synthetic polymers

A variety of polymers has been electrospun till now and the electrospun nanofibers from these polymer solutions have been used in various applications in various biomedical applications - tissue engineering scaffolds, filtration membranes,

etc. Compared to synthetic polymers, naturally occurring polymers expose better biocompatibility and low immunogenicity, and thus are used in biomedical applications. Natural polymers are utilized in electrospinning due to their inherent capacity for binding cells and they carry specific protein sequences, such as RGD (arginine/glycine/aspartic acid).

In recent years, electrospinning of proteins, usually from gelatin, collagen, elastin and silk fibroin has been presented [80,81,82,83]. Usual natural polymers involve chitosan, gelatin, collagen, chitin, casein, cellulose acetate, fibrinogen, silk protein, etc. The scaffolds which are produced from natural polymers guarantee better clinical functionality. Still, incomplete denaturation of natural polymers has been reported in recent years and that requires concern. For the first time, it has been demonstrated that the properties of prominent natural biomaterial collagen are lost when it is electrospun into nanofibers out of fluoroalcohols such as 1,1,1,3,3,3-hexafluoro-2-propanol or 2,2,2-trifluoroethanol [84]. Collagen is a leading biopolymer and is used widely due to its extraordinary biological and physico-chemical properties for tissue engineering applications.

Presently, in most cases, the adopted method for electrospinning of pure collagen or collagen-poly (3-caprolactone) blends includes the use of highly volatile fluoroalcohols such as 1,1,1,3,3,3-hexafluoro-2-propanolor 2,2,2-trifluoroethanol as solvents [85,86]. Common synthetic polymers which are used in biomedical applications are hydrophobic biodegradable polyesters, like poly (έ-caprolactone), (PCL polyglycolide (PGA) and polylactide (PLA). All of them have been electrospun into nanofibrous scaffolds [87,88].

Electrospinning has been utilized for the fabrication of nanofibrous scaffolds from various biodegradable polymers, such as polyurethane (PU), poly (lactic acid) (PLA), poly (έ- caprolactone) (PCL), poly (glycolic acid) (PGA), copolymer poly (lactide-co-glycolide) (PLGA), and the copolymer poly (L-lactide-co-έ-caprolactone) [P(LLA-CL)] for wound dressings, bone tissue engineering, cardiac grafts and blood vessel substitutes [89-92].

2.4.1.1 Silk fibroin

The silkworm, Bombyx mori, makes natural silk which has been used as biomedical suture material for hundreds of years. In recent years, silk fibroin (SF) has fascinated scientists for its superior biocompatibility, biodegradability and mechanical properties [93]. Numerous forms of SF materials have been used in biomaterials such as fibers, films and sponges. Among these structures, electrospun regenerated silk fibroin (RSF) fibers have a lot of advantages, such as nanoscale diameter, circular cross-section and appropriate porosity [94]. This material can perfectly imitate the extracellular matrix (ECM) and it can be appropriate for cell attachment, multiplication and growth [69].

2.4.1.2 Hyaluronic acid

Hyaluronic acid (HA) presents one of the main components of the extracellular matrix and it is a natural linear polysaccharide built of repeating units of β-1-4-D-glucuronic acid and β-1-3-N-acetyl-Dglucosamine [95]. It has been widely recommended for many biomedical applications due to its biocompatibility, the angiogenic character of its degradation products, its positive impact in the healing process and its capacity as a drug release system [96]. At the beginning, it was problematic to produce uniform size fibers from hyaluronan using electrospinning because of the surface tension, high viscosity, and strong water retention ability of the hyaluronan solution. The water retention capacity might guide to the fuse of nanofibers electrospun on the collector due to the insufficient evaporation of solvents in electrospinning. It was successfully performed only after the improvement of blowing assisted electrospinning the forming of HA into nanofibrous nonwoven membranes from aqueous solution [97].

According to Um et al. (2004), there have been several approaches to make a hyaluronan solution that has sufficient molecular entanglement in a speedily evaporated solvent, while still controlling surface tension and low viscosity by applying the electroblowing technique. This successful fabrication of HA nanofibers

can be mostly associated with the two new parameters introduced: the temperature and the rate of air blow [98].

2.4.1.3 Chitosan

Chitosan is one of the most manifold and promising classes of the functional natural polymeric materials with special characteristics, such as biocompatibility and bioactivity, hydrophilicity, non-antigenicity, and non-toxicity (since its degradation products are natural metabolites) for application in separation and biomedical technologies [99].

A durable chitosan nanofiber filter (which possesses high surface area per unit mass along with strong mechanical strength) would have advantage over present technologies since chitosan is an environmentally friendly natural material with many polar and ionizable groups. Chitosan potential application can be found in the separating technology as nanofibrous membranes for neat filtration of toxic microbes and metals [100], and also as scaffolding materials in drug delivery system and tissue engineering, etc [101].

2.4.1.4 Collagen

Collagen, which presents the most numerous protein family in the body, has been extremely used for in vitro and in vivo tissue engineering. The collagen polymers of type I and type III are the most important structural elements of the extracellular matrix in various native tissues. Mainly, more than 80% of collagens in the body consist of type I, II and III and have similar features in all species. Collagen is highly preserved, almost non-immunogenic and it has been used in tissue engineering applications.

The main activity of collagen is to produce structural support to the tissue in which it is placed, but it is also known to separate many factors required for tissue care and regeneration. For this reason, it is also regarded as “ideal” scaffold material in the tissue engineering [102].

2.4.1.5 Gelatin

Electrospun gelatin nanofibers present a hopeful class of biomaterials which possess extraordinary structural and functional resemblance with native extracellular matrix (ECM) along with biocompatibility and non-cytotoxicity [103]. Gelatin is received from collagen, which is a main constituent of ECM proteins. Compared to its precursor collagen, gelatin is non-antigenic and economical material. The scientific community in the field of tissue engineering, drug delivery and wound dressing would be attracted by a green fabrication technique for electrospun gelatin nanofibers [104].

2.4.1.6. Fibrinogen

Another natural polymer for the fabrication of tissue engineering scaffolds as well as hemostatic and wound dressings is fibrinogen [105]. Fibrinogen presents a candidate material for use as an electrospun tissue-engineered scaffold because of its natural ability to activate cellular interaction, non immunogenic nature, undemanding degradability and build up increased cell migration [106].

Electrospun nanofibrous fibrinogen mats are highly appropriate for wound dressing and hemostatic products because of their high surface area to volume ratio available for clot formation. The electrospun mats of fibrinogen should exhibit structural integrity, which let them be efficiently removed from the collector [107].

2.4.2 Copolymers

Electrospinning with copolymers performs improvement of polymeric materials, which includes tailoring of mechanical strength, barrier properties and thermal stability and thus is often developed for engineering structural applications such as melt-blending, incorporation of inorganic fillers and copolymerization [108].

The utilization of copolymers is a useful method to fabricate new materials of desirable properties and when it is properly realized, the performance of the electrospun scaffolds based on copolymers can be considerably enhanced compared to homopolymers. Biodegradable hydrophobic polyesters usually have great mechanical properties but they are in deficit with cell affinity for tissue engineering. This deficit can be improved with the incorporation of a capable hydrophilic polymer segment which increases the cell affinity. Beside the cell affinity, other physical properties can be composed by the use of copolymers in electrospinning and they include: the mechanical properties, structure, pore size and distribution, morphology and biodegrability [109].

2.5 Characterization of electrospun nanofibers

It is very difficult to obtain single electrospun nanofibers, and thus the characterization of electrospun fibers presents one of the most challenging tasks. For understanding the electrospinning process, it is very important to determine accurately the entire process from polymer selection to mechanical testing. The polymers used in electrospinning are divided into three particular categories: physical and structural, mechanical and chemical [110]. Nowadays, these nanofibers have become popular among researchers due to their impressive micro and nano structural characteristics such as high surface area and small pore size. Their possibility of producing three dimensional structures that enable the development of advanced materials with delicate applications is very significant.

2.5.1 Geometrical characterizations

The physical characterization is related to structure and morphology of the nanofibers' internal structure which defines the physical and mechanical properties. Fiber diameter and their distribution with fiber orientation and fiber morphology (such as cross-section shape and surface roughness) present geometric properties of

nanofibers. Transmission electron microscopy (TEM), scanning electron microscopy (SEM), field emission scanning electron microscopy (FESEM) and atomic force microscopy (AFM) techniques are applied for the characterization of geometric properties [111, 112].

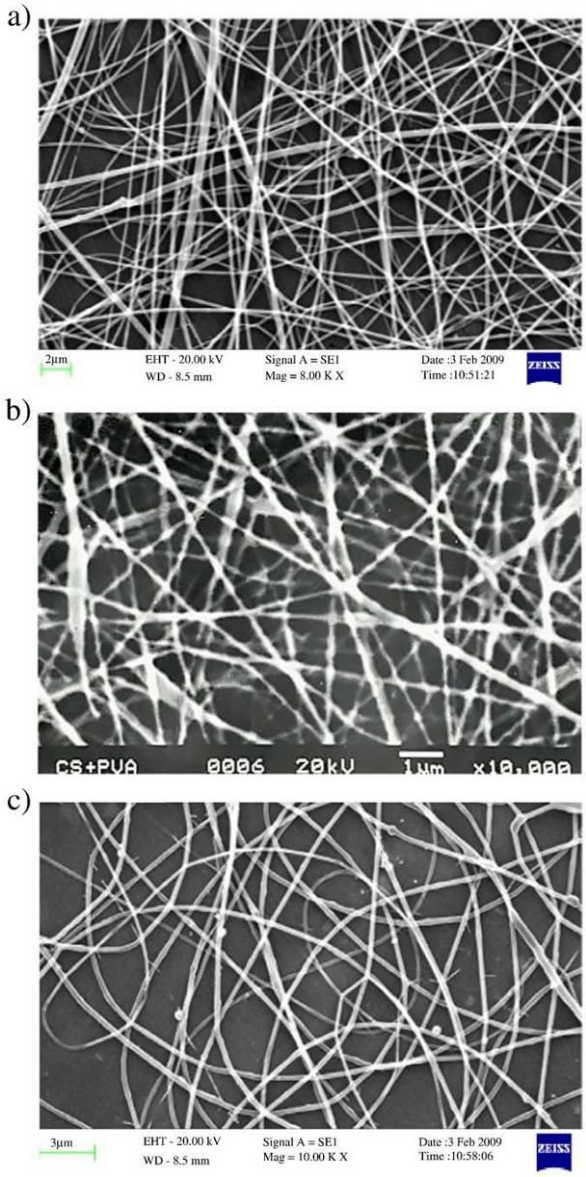

Figure 20. **SEM images of the electrospun polymer fibers: (a) 4% polyethylene oxide solution at 15 kV voltage (average fiber diameter (AFD) 250±50 nm). (b) Chitosan/poly vinyl alcohol (2% chitosan and 9% PVA in 50:50 ratios) at 17 kV voltage (AFD 200±32 nm).(c) Silk fibroin (6%) from non-mulberry tropical tasar silkworm, Antheraea mylitta at 15 kV (AFD 240±60 nm) [113].**

SEM is used for observing fiber diameters and morphologies, but the resolution is decreasing at extreme magnifications. The typical SEM images of polymer electrospun fibers are depicted in Figure 20. For SEM it is necessary for the samples to be electrically conductive, and thus the electrospun polymers must be coated with gold or platinum. This requirement may change the diameter readings at higher magnifications. However, SEM still presents a quick method for observing the fibers produced and it demands a very small sample size for its procedure [79].

Transmission electron microscopy (TEM) is another technique for observing fiber diameters for extremely small fibers (<300 nm) in which a beam of electrons is transmitted through a specimen to create an image. Atomic force microscopy (AFM) is another operation, used to analyse the fiber diameter. This accurate measurement becomes more complicated due to the tip convolution [113]. Porosity is a geometric parameter and with the pore size of nanofiber membranes it is important for the applications like template for tissue engineering, infiltration, protective clothing, etc [114,115].

The pore size measurement can be maintained by a capillary flow porometer and mercury porosimetry. With the usage of these methods researchers have presented highly porous structure of electrospun nanofibrous scaffolds with 91.63% porosity, a total pore volume of 9.69 mL/g, a total pore area of 23.54 m^2/g, and a pore diameter within range 2 to 465 μm [114].

2.5.2 Chemical characterization

Fourier transforms infrared spectroscopy (FTIR) and nuclear magnetic resonance (NMR) techniques are applied for the characterization of the molecular structure of a nanofiber [116]. If we mix two polymers together for the fabrication of nanofibers, the structure of the two materials can be analysed along with the intermolecular interaction by the use of these methods. For example, the presence of an aligned secondary structure 310-helix for silk fibroin dissolved in HFIP, has been

approved from the high resolution solution 13C-NMR and circular dichorism (CD) studies [117]. The NMR spectrum of electrospun nanofibers from a collagen and PEO blend, displayed a new phase structure generated from the hydrogen bonding between the ether oxygen of PEO and the protons of the hydroxyl and amino groups in collagen [54]. Super molecular structure describes the conFigureuration of the macromolecules in a nanofiber, identified by optical birefringence, small angle X-ray scattering (SAXS), wide angle X-ray diffraction (WAXD) and differential scanning calorimeter (DSC) [111].

2.5.3 Mechanical characterization

The correct evaluatuion of the mechanical properties of the nanofibrous matrix is very important for biomedical applications such as scaffolds. The scaffold must be capable of resisting the forces produced by growing tissue or during physiological activities such as pulsed blood flow [118]. The mechanical characterization is completed by using the tensile test loads to the samples made from the electrospun ultra fine non-woven fiber mats and adequate care must be taken in sample adjustment in order to avoid any possible sample damage [119].

There have been a variety of approaches of implementing mechanical characterization of nanofibers and nanowires by employing bending tests, resonance frequency measurements, nanoindentation and microscale tension tests. With single polymer fibers it is also possible to determine tensile strength, Young's modulus and the strain at break by carring out tensile tests. The determination of mechanical properties of single ultrafine Polycaprolactone (PCL) fibers is being performed by a commercial nano tensile testing system (Nano Bionix System, MTS, TN, USA) [120].

The tensile strength of some polymers has been presented in Table 3. The tensile testing for definement of the electrospun nanofibers mechanical strength is followed by the macroscale standards and includes the minimum number of the

assumptions which are necessary to get material properties. The aforementioned method is useful for fibers with diameters near 1 μm and provides the fiber testing until failure [121]. AFM is used for the determination of the elastic properties of electrospun membranes and it consists of a cantilever and tip arrangement that is applied for scanning of the surface by measuring the bending of the cantilever due to the opposition of the atomic shells of the tip and the sample atomic resolution which can be realized with a very slight contact. AFM Phase Imaging is a supplement of tapping mode which enables detection of alterations in composition and hardness [122].

The bending and shear moduli of the electrospun collagen fibers have been evaluated by AFM. These micromechanical bending tests were completed with native and glutaraldehyde cross-linked single electrospun fibers [123]. AFM nanoindentation method has been used to determine the elastic moduli of one-dimensional nanostructures like electrospun nanofibers and nanowires. Despite the fact that this method has been used satisfyingly for mechanical characterization, there are some difficulties, such as inaccuracies originating from the nanoindenter tip shape, the relative tip fiber configuration, and the effect of fiber surface roughness with the adhesion force between the sample and the indenter tip [124].

Table 3. **Mechanical strength of some common electrospun fibers [79].**

Polymers	Ultimate strength	Reference
Collagen II	3.3 ± 0.3 MPa	Shields et al. (2004)
poly(ε-caprolactone)	40 ± 10 MPa	Tan et al. (2005a)
Gelatin	4.79 MPa	Huang et al. (2004)
Cross-linked gelatin	12.62 ± 1.28 MPa	Zhang et al. (2006)
Silk fibroin	7.25 MPa	Ayutsede et al. (2005)
Poly(vinylchloride)/Polyurethane (25/75)	6.30 MPa	Lee et al. (2003c)
Polyethylene oxide	10 ± 0.2 MPa	Ojha et al. (2008)

2.6. Functional applications of electrospun nanofibers

2.6.1 Biomedical

Electrospun nanofibers are widely used in biomedical applications, such as tissue engineering scaffolds, drug delivery, wound healing, as affinity membrane, filtration, in immobilization of enzymes, healthcare, biotechnology, environmental engineering, defense and security, optical electronics, nanocatalysis, energy storage and in other numerous researches [125].

2.6.1.1 Tissue engineering scaffolds

Tissue engineering is a multidisciplinary study which includes biology, medicine and engineering. This field could transform the methods which can improve the health and quality of life for humanity worldwide [126]. An elemental principle of the tissue engineering is depicted in Figure 21. The function of tissue engineering is to replace or improve the function of a certain tissue or organ [127].

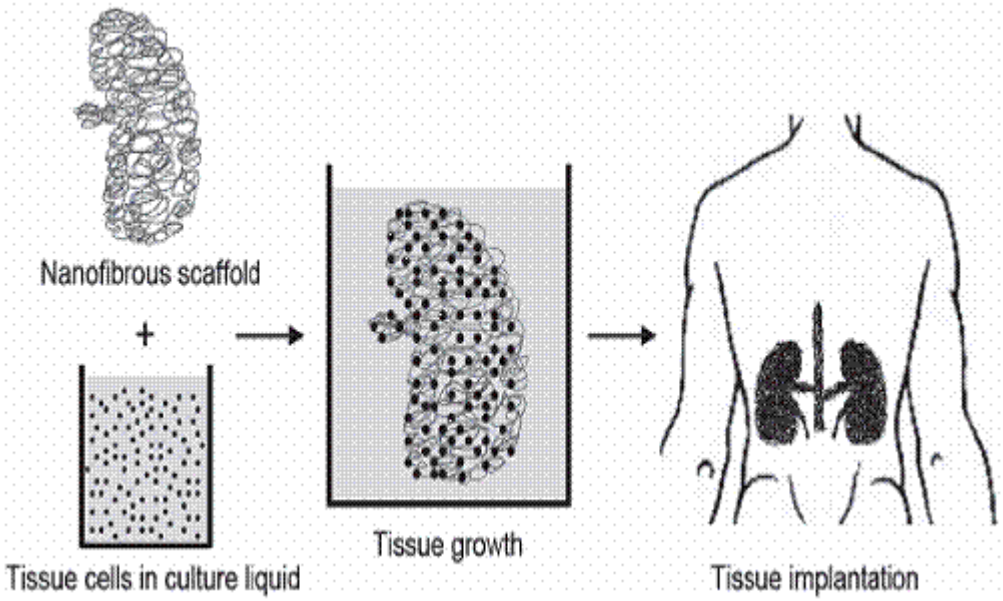

Figure 21. A primary principle of the tissue engineering [127]

The main technologies regarding this area can be organized into three categories: cell technology, technologies for in vivo integration and scaffold construct technology. The scaffold construct technology concentrates on creating, manufacturing and characterizing three dimensional (3D) scaffolds. The scaffolds are used for cell seeding and in vitro or in vivo culturing. In order to be functional, a scaffold must possess a high degree of porosity with an appropriate pore size distribution at the first place. Also, a large surface area is needed and biodegradability is often demanded, with the degradation rate which is in the coherence with the rate of neo-tissue formation. Beside aforementioned, the scaffold must have the required structural integrity with the appropriate mechanical properties to avoid its pores from disintegrating during neo-tissue formation. In the end, the scaffold should be biocompatible and non-toxic to cells, with positive interaction with the cells to develop cell adhesion, migration, proliferation and differentiated cell function [127].

2.6.1.1.1 Blood vessels

Based on their location and specific function, blood vessels differ in sizes, mechanical and biochemical properties, ultrastructural organization and cellar content. The vascular grafts should have particular characteristics. A fine blood vessel substitute (diameter less than 6 mm) has remained a big challenge.

The function of vascular endothelial cells (ECs) growth on the P(LLA-CL) cast film was improved compared on an electrospun poly(L-lactide-co-ε-caprolactone) (P(LLACL)) nanofibers. However, the electrospun nanofiber mats can provide good support at the time of the initial growth of vascular smooth muscle cells [128] and smooth film combined with electrospun nanofiber mat could model a valuable 3D scaffold for blood vessel tissue engineering.

The influence of the fiber diameter on endothelial cells culturing was investigated by using electrospun cellulose acetate (CA) fibers, with three fiber diameter ranges: 0.01-0.2, 0.2-1 and 2-5 μm [129]. It was observed that the endothelial cells displayed a growth inclination towards larger fibers. Poly(ε-

caprolactone) (PCL) nanofibers showed similar results with five different diameters [130] where a cell penetration increased with the increased fiber diameter and smooth cell delivery was observed only on the largest fibers (12.1 μm in diameter). Elastin/polymer blend nanofibers were used to be comparable to the mechanical characteristic of natural blood vessel, which has a low-strain mechanical reaction to blood flow and blocks pulsatile energy to be dissipated as heat [131].

2.6.1.1.2 Bones

For the bone tissue regeneration the natural polymers such as gelatin, silk, collagen and chitosan are recognazible as useful. Also, the PCL has long been examined as a bio-degradable nanofiber matrix for bone regeneration [132] and, within 4 weeks of culturing, Rat bone marrow has shown the secretion of type I collagen and calcium mineralization. The PLA nanofibers have also demonstrated good reaction toward MC3T3-E1 bone cells [133]. The PHB and poly(hydroxybutyrate-co-hydroxyvalerate) (PHBV) electrospun nanofibers have demostrated improved osteoblastic activity identical to flat membrane scaffolds [134].

Nanofibers from gelatin/PCL and PCL composite which included calcium carbonate nanoparticles and hydroxyapatite (HAp) nanoparticles for bone scaffolds have been studied beside the pure PCL nanofibers [135]. The cell attachment and growth on the scaffold was improved by the addition of 50% gelatin to PCL. In fact, this addition enhanced both the fiber mechanical strength and surface wettability [136]. Within one week of culture it has been notified that the cells moved up to 114 μm inside the scaffold. On the contrary, PCL nanofibers with these inorganic nanoparticles exposed higher osteoblast proliferation and differentiation.

2.6.1.1.3 Muscles

For culturing a smooth muscle cell, collagen nanofibers were first to be used. After 7 days of seeding, the cells were well integrated into the nanofiber network

while the cell growth on the collagen nanofibers was developed. Smooth muscle cells were also attached and generated well on other polymer nanofiber mats blended with collagen [137]. The inclusion of collagen into nanofibers was done in order to enhance fiber elasticity and tensile strength, and increase the cell adhesion as well.

The fiber surface wettability induces cell attachment. The fiber wettability was increased considerably when the PS nanofibers were treated with Argon plasma and cell attachment was increased by two folds [138]. Skeletal muscle cell morphologenesis and aligned myotube formation can be promoted by the alignment of nanofibers which cause cell orientation. An alignment factor of the cells cultured on the aligned nanofibers was 0.74, while the same factor was 0.19 on the randomly orientated scaffold [138].

2.6.1.1.4 Skin

Another ambition of the tissue engineering is the development of engineered skin. Skin coverage is required for large surface area wounds. The dominant mode of treatment is autologous skin grafting, but there are also other regenerative medicine technologies to be engaged [139].

Electrospinning has been used as one access for developing scaffolds for engineered skin and wound dressings, but less than other scaffold technologies [140]. However, several researchers have used electrospinning for skin tissue engineering. Most of the researches have been in vitro evaluations [141-143]. Also, electrospun polystyrene (PS) has been used as a model system for examining the influence of this system on engineered skin formation.

The effect of culturing cells in an air-liquid interface (this presents a common culture technique for skin culture) compared to submerged scaffolds was analyzed. The electrospun PS scaffolds had average fiber diameters of almost 10 μm. It was revealed that when fibroblasts, keratinocytes, and EC were cocultured, they could self arrange without other extra factors than the three-dimensional electrospun scaffold and the air-liquid interface [144].

2.6.1.1.5 Neural tissues

The injuries of the central and peripheral nervous system may profit from the use of the neural tissue engineering technologies that use scaffolds to promote the regrowth of nerves. In neurodegenerative diseases like Alzheimer's and Parkinson's diseases, the common pathological start is the agglomeration of insoluble filamentous aggregates which lead to early axonal dysfunction and pathology with possibly irreversible neuron degeneration [145].

Electrospun nanofibers are effective guidance substrates for nervous tissue recover. The NSC differentiation and neurite outgrowth with promoted NSC adhesion was maintained by PLLA nanofiber scaffold. This phenomenon was revealed by in vitro cell culture study of neural stem cells (NSCs) on a PLLA nanofiber scaffold. Further studies of aligned PLLA nanofiber or microfiber scaffolds confirmed that the orientations of NSC elongation and its neurite outgrowth were in the same direction to fiber alignment. Topographical guidance, neurite outgrowth and enhanced cell proliferation can be performed by the arranged fibers in the scaffold [146]. However, the impacts of the fiber diameter on cell culturing are still not defined. PLLA nanofibers possess higher neural stem cell distinction than microfibers, with similar cell orientation.

With the diameters of 283, 749 and 1452 nm, cell propagation and spreading increased with the decrease in fiber diameter concerning three types of PES nanofibers [147]. Another study demonstrated that the neurite length was the smallest on the finest fibers of three kinds of PLLA electrospun fibers [148].

2.6.2 Wound healing

Haemostatic ability, painless to patient, efficiency as bacterial barrier, adequate gaseous exchange ability, appropriate water vapour transmission rate absorption ability of excess exudates (wound fluid/pus), adherent to healthy tissue but non-adherent to wound tissue and ease of removal with low cost are ideal

characteristics of dressing for wound healing (Figure 22). The polymer nanofibrous membranes as medical dressing are still in the beginning with their research. However, the microfibrous and nanofibrous structures of electrospun materials provide the nonwoven textile with desirable properties for wound-healing polymer devices [149].

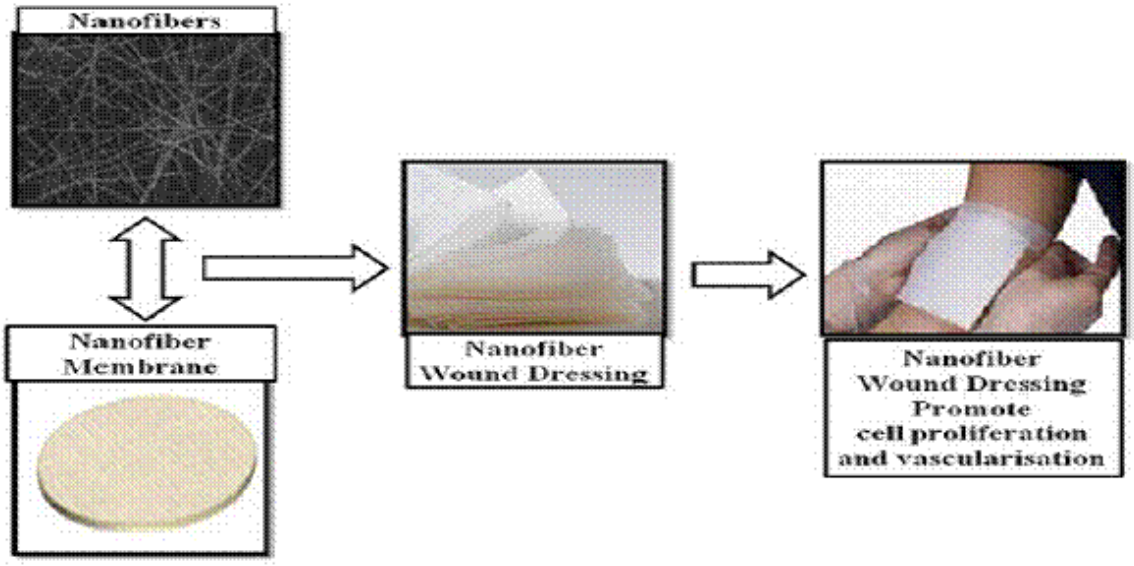

Figure 22. Nanofiber dressing [149]

2.6.3 Drug delivery

Nanofiber mats have been utilized as drug carriers in the drug delivery structure because of their overall qualitative characteristics. The drug delivery system depends on the assumption that dissolution rate of a particulate drug increases with increasing its surface area of both the drug and its corresponding carrier. The large surface area of the nanospun fibers contributes to speedy and efficient solvent evaporation. This phenomenon enables the incorporated drug limited time to recrystallize and this promotes the production of solid solutions or amorphous dispersions [150]. The delivery of pharmaceutical dosage can be made as rapid,

immediate, delayed or modified dissolution and it depends on the polymer carrier used. By incorporating the drugs in the polymer solution several researchers have successfully encapsulated drugs within the electrospun polymer fibers [151].

2.6.4 Filtration

The elimination of very small dust particles, bacteria and viruses from the ambient air and drinking water is linked with a majority of respiratory tract diseases in industrial zones. The filtration efficiency and the appropriate pressure drop (Δp) are required for the usage in filters. It is considered that nanofibers will be mainly used in the area of microfiltration and ultrafiltration (for the removal of particles in the range 100 nm - 15 μm and 5 -100 nm, respectively).

The nanofiber based filter which originates from the electrospinning process, has been observed by the Scanning Electron Microscope (Vega II, Tescan, The Czech Republic). Therefore, the realized SEM pictures have been used for the determination of the fiber diameter, fiber diameter/pore size distribution and nanofiber layer thickness for the 2D and 3D modelling of filtration efficiency [152].

For oil/water emulsion separation, nanofibers were also utilized as a supporting scaffold in ultrafiltration (UF). The announced UF mat had a three-layered composite structure - a conventional nonwoven microfibrous substrate, a crosslinked PVA electrospun nanofibrous mid-layer and a nonporous hydrophilic top layer [153-154]. The electrospun nanofibrous substrate maintained a well linked porous network with a large specific surface area. The UF filter possesses an excellent organic solute rejection capability with a high flux rate.

The chemical or physical crosslinking treatments are used to stabilize the porous structure of the nanofibrous mat for a long term filtration performance [155-156]. It was proved that filters which consist of the multiple thin nanofiber layers had a much better filtration performance compared to the single thick layer nanofiber mat because of the pressure drop during filtration [157].

2.6.5 Biosensors

Biosensors commonly contain bio-functional membrane and transducer. They have been extensively used for food, clinical and environmental objects. There are many parameters which influence the performance of a sensor. The parameters are dependent directly on the characteristics of the sensing membrane and they include selectivity, sensitivity, response time, aging and reproducibility. Sensitivity of the membranes plays a very significant role since there is a strong need for the analysis of gases and biological substances at low concentration. Nowadays present-day biomedical sensors with advanced micro fabrication and signal-processing facilities are becoming more accurate and low-cost [158].

The electrospun nanofibrous membranes are very attractive since they possess unique large surface area which is the most useful property for enhancing the sensitivity of conductometric sensors, whereas a larger surface area will absorb more of a gas analyte and transform the sensor's conductivity more considerably. The biosensors based on silk fibroin membranes have been widely used for investigating various substances such as hydrogen peroxide, glucose and uric acid. Besides this, the literature presents the engagement of other electrospun polymers as sensing interfaces like polypyrrole, polyaniline, nylon-6, poly(vinyl alcohol)(PVA), polyamic acid, nylon-6 and poly (acrylic acid)-poly (pyrene methanol) [159-160].

2.6.6 Protective clothing applications

Perfectly, protective clothing should have some fundamental properties like light weight, air and water vapour permeability, improved toxic chemical resistance and breathable fabric insolubility in all solvents. The electrospun nanofiber membranes are potential candidates for protective clothing utilization, thanks to their light weight, large surface area with high porosity, great filtration performance with resistant to the penetration of toxic chemical agents in aerosol form and their

capability to neutralize the chemical agents without blocking the air and water vapour permeability of the clothing [161].

2.6.7 Energy generation applications

The polymeric conductive membranes have the capability of applying like corrosion protection, electrostatic dissipation, photovoltaic device etc., because the surface area of the electrode is proportional to the rate of the electrochemical reactions. The conductive nanofibrous membranes are quite appropriate for use as porous electrodes as well as the polymer electrolyte membrane fuel cells (PEMFCs) and high performance batteries thanks to their high porosity and an important large overall surface area. The polymer batteries have been improved for cellular phones instead of the conventional, bulky lithium batteries [162].

2.6.8 Enzyme immobilization

The interpretation of immobilized enzymes is greatly dependent on the structure and characters of the carrier and carrier modification, such as providing biocompatibility, hydrophilicity, etc [163]. However, for the modified supports, the enzyme loading is generally significantly low, as well. As an alternative to the supports, porous materials such as membranes, porous particles and gel matrices have been used to obtain high enzyme loading [164]. The electrospun fibrous membranes are characterized by their fine porous structure which can effectively decrease the diffusion resistance of the substrates or products and, thanks to the large specific surface area, can extremely increase the catalyzing ability of the immobilized enzymes.

2.6.9 Affinity membrane

The affinity membranes present a broad class of membranes that particularly hold the specific target molecules by fixing a ligand or specific onto the membrane surface and demonstrate technological advances in membrane filtration and fixed-bed liquid chromatography. The membranes combine both the impresive selectivity of the chromatography resins and the decreased pressure drops connected with filtration membranes. Not many works have been written about the utilization of the electrospun nanofiber mesh as the affinity membrane and for this reason the surface must be functionalized with ligands before.

The ligand molecules should be covalently bonded on the membrane to block leaching of the ligands [165]. For IgG purification surface modified electrospun polyurethane nanofiber membrane with Protein A has been employed. Cellulose is a hydrophilic material extensively utilized in the membrane preparation. The affinity membrane for protein purification needs to be made up of hydrophilic materials which mostly have lower non-specific protein adsorption than hydrophobic synthetic polymers. Affinity membranes can be used as another approach for removing organic molecules from waste water.

For instance, a cyclic oligosaccharide with a hydrophobic interior and hydrophilic exterior named β-cyclodextrin has been added into a poly (methyl methacrylate) nanofiber membrane applying a physical mixing method for organic waste removal that can catch hydrophobic organic molecules from water by producing an inclusion complex which is used for affinity membrane application [166].

2.7. Nanotechnology and dentistry

Since the early 1990's nanotechnology has been part of the common scientific theory with possible medical and dental application. The nanostructures such as the nanoparticles, nanosphere, nanotubes, nanofibers, dendrimers and others have been investigated for numerous applications in biological tissues. Increasing interest in

nanotechnology for the future medical application has formed a new field called nanomedicine. Besides the conventional oral care methods and procedures, new nanoscale technologies have the capacity to transform dental practice by improving all aspects of dentistry (diagnostics, therapeutics and cosmetic) into an up- to- date-patient care [167].

There are two main approaches in nanotechnology. The first one is the 'bottom-up' approach, where the structure of materials and devices is done from the molecular parts that chemically gather on the principles of molecular distinction. Another one is the 'top down' approach, where the structure of materials and devices is completed from large parts without involmenent at the atomic level. There are some nanoparticles which are used and they involve nanopores, nanotubes, nanorods, nanobelts, nanospheres, dendrimers, quantum dots, etc. [168].

2.7.1 Application of nanotechnology in dentistry

2.7.1.1 Nanotechnology in dental material science

The introduction of the microfills established nanotechnology in dental material sciences. Nowadays, ordinarily used resin composites are nanofilled composites which contain filler particles in the range 20 – 600 nm and microhybrids. For example, better values have been achieved with assisted fluoride release in resin composites which contain calcium fluoride nanoparticles in a whisker-reinforced resin matrix than conventional and resin-modified glass ionomers [169].

There are also nanoparticles such as casein phosphopeptide-amorphous calcium phosphate (CPP-ACP) which act as mineral precursors for remineralization by connecting themselves to biofilms, bacteria, plaque, hydroxyapatite and the neighbouring soft tissues because of localizing bioavailability of phosphate and calcium [170]. Nanotechnology has become attractive to researchers, especially in case of dental implants due to biomaterials. It is of great importance to produce nanostructures with relevant chemical and structural properties and achieve an

increase in their surface osseoconductivity with improved durability and resistance to failure [171]. This will help with reducing the main restrictions of dental implants and coating.

The authors of one in vitro study reported that BIS-GMA/TEGDMA-based nano-composites can be remarkably reinforced by adding of nanofibrillar silicate crystals either alone or with nanofibers [172]. Correspondingly, by the incorporation of the nanosized $CaPO_4$ particles in the resin-based composites significant improvement in stress-bearing and ion releasing capacities has been observed [173]. These findings are very important for finding their prominent act in inhibition of dental caries.

2.7.1.2 Nanotechnology in prosthodontics

2.7.1.2.1 Impression materials

Special silicone impression materials are formed with incorporated nanofillers in vinyl polysiloxanes. This kind of material has some better flow and adhesiveness properties. It also has enhanced hydrophilicity, finer model pouring and improved detail precision with less voids at margin [174].

2.7.1.2.2 Implants

The incomplete bone formation around the biomaterial directly after the implantation is the most common cause of failure of implants. The integration and adhesion to the surrounding tissues can be improved by coating of nanoparticles over the dental implants. The ‘macro’, ‘micro’ or ‘nano’ structured surface of the implant plays a crucial role in verifying biocompatibility because it is in direct touch with the tissues. The nanostructured materials can possess some improved mechanical, magnetic, electrical, and optical properties compared to the ordinary micron or macro-scale complements [175].

2.7.1.3 Periodontics

Several important developments have been produced at the intersection of oral biology and nanomaterials. The creating of nanofibers which provide the materials for the three dimensional cell structure and tissue engineering are included in these developments. Nanoparticles are improved as a host in biotechnological and biomedical applications such as enzyme immobilization, drug delivery and DNA transfection.

Triclosan-loaded nanoparticles are fabricated and analysed by the emulsification-diffusion process for developing the treatment of periodontal diseases with this new delivery system. Drugs are put into the nanospheres made of a biodegradable polymer which favor the gradually release of the drug when the nanospheres degrade. Another possible option with this is the site-specific drug delivery. For example, the drug tetracycline in arestin is locally applied to a periodontal pocket by its incorporation in microspheres [177].

2.8 Nanostructures used in dentistry

Modern nanostructures use precisely fabricated nanocarriers like nanoparticles, nanofibers, nanotubes, nanospheres, nanorods, nanoshells, nanoscale cantilevers, nanopores, dendrimers, quantum dots (QDs) and liposomes to point at specific tissues and organs. These nanostructures may help in the diagnosis, treatment for dental disease and may provide anticancer agents in dentistry [178].

2.8.1 Nanoparticles

A nanoparticle (Figure 23A) is a particle with one dimension which is 100 nm or smaller in size. Nanoparticles influence the properties of many materials which they form and they are utilized in the resin-based composite (RBC) restorations with 2-year publicated clinical results [178]. The focus is on the nanoparticles function for dental composites and interfacial silanes changes. For a couple of years they have

been used for coating and bonding of inorganic fillers into RBC matrices with adjusting newer forms of silane bonding agents for the application of nanoparticles in RBCs.

Nanohybrid RBCs are currently the most promising form of nanotechnology with nanoparticles and relevant alterations of actual RBC systems that have provided important clinical helpfulness. Surface modification of TiO_2 nanoparticles by the organosilane inside a resin matrix enhanced the microhardness and bend strength of dental RBCs, which was reported by Xia et al. [179].

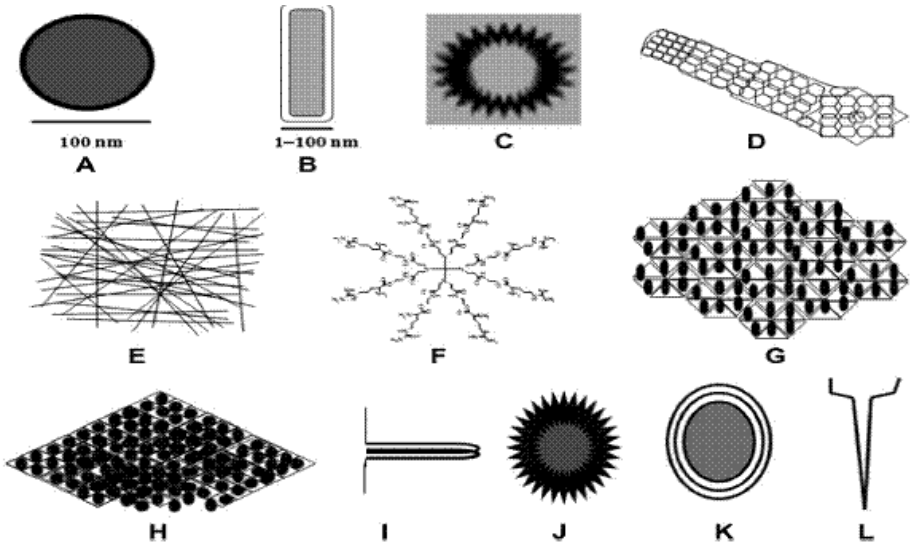

Figure 23. Nanostructures in dentistry: (A) nanoparticle; (B) nanorod; (C) nanosphere; (D) nanotube; (E) nanofibers; (F) dendrimers; (G) quantum dots; (H) nanopores; (I) nanocantilever; (J) nanoshell; (K) liposome; (L) nanoneedle [178]

It was discovered by Mayworm et al that the dental composites containing nanopartcles have increased wear resistance after their deposition in artificial saliva [180]. The material's wear resistance is increased with the storage of artificial saliva, manifesting that post-healing of material bulking takes place and saliva consumption appears just on the composite surfaces. This effect was approved by FTIR

spectroscopy and Vickers hardness analyses before and after artificial saliva operation. The bulk microhardness of the materials increases with the decreasing of composite surface microhardness after deposition in artificial saliva. It has also been reported that radiopaque Ta_2O_5/SiO_2 filler nanoparticles spread in a methacrylic matrix outcomes in adhesives with great adhesive strength which have radiopacity better than enamel and dentin.

2.8.2 Nanorods

The most widely accepted methods in nanotechnology present self-assembly of nanoscale structures, the utilization of surfactants as reverse micelles or microemulsions for the synthesis. The immitation of the natural biomineralization process to form the dental enamel, the hardest tissue in the human body, was carried out by Chen et al. For this purpose, they used nanorod-like calcium hydroxyapatite crystals in enamel prisms which were highly aligned micro units arranged almost parallel to each other. Important physicochemical properties of the enamel are determined by this organized structure [181].

2.8.3 Nanotubes

Nanotubes present nanometer-scale tube-like formations which have been investigated whether they are suitable for certain dental applications. Titanium oxide nanotubes have been exposed in vitro to increase speed of HA formation, mostly in the context of bone growth applications for dental implants. Modified single-walled carbon nanotubes (SWCNTs) with silicon dioxide attach to them by specialized organosilane bonding agents have been displayed enhance the flexural strength of RBCs [182].

Furthermore, recent nanostructured titania poly (methyl methacrylate), PMMA, is a broadly used polymer when the transparency is of extreme importance.

PMMA has an appropriate biocompatibility and has been utilized as a healing material in medicine and dentistry. For almost 50 years reinforced polymer composites have been used in restorative components which are applied in medicine and dentistry [183].

A real challenge presents the biocompatibility of bone cements reinforced by carbon nanotubes. The silica-doped TiO_2 nanotube layers with high aspect-ratio and different concentrations of silica particles were produced through anodization in NaCl electrolyte which had various concentrations of water glass (24 g/L or 48 g/L Na_2SiO_3) by electrochemical anodic oxidation of Ti in electrolytes with chloride [184].

The biomimetic apatite storage act under simulated body fluid (SBF) exposed great silica doping of the outcome nanotube layers with the plentiful OH groups on their surfaces. The results show that the HA growth on nanotubes probably due to silica doping greatly improves the fast nucleation of HA, particularly for the tubes in their amorphous like state, which usually need a lot of time for apatite induction.

2.8.4 Nanofibers

Nanofibers present fibers with diameter dimension less than 1000 nm. They are used for biomedical applications such as ceramics containing HA and fluor-HA [185]. Nanofibers in the appropriate proportion with distribution of the fibers/crystals and nanofibrillar silicate crystals were found to enhance the physical properties of the dental composites. This particularly refers to a mixture of the 2'-bis-[4-(methacryloxy propyl)-phenyl]-propane (Bis-GMA) with a thinning agent triethyleneglycoldimethacrylate (TEGDMA) [186].

Great potential for dental tissue engineering application could be the nanofibrous (NF)-poly(L-lacticacid) (PLLA) which strengthen dentin-like tissue formation and odontogenic differentiation of human dental pulp stem cells (DPSCs).

Nanofibers have improved physical and mechanical properties due to their high surface area to volume ratio and high aspect ratio [184].

2.8.5 Nanospheres

Nanospheres have also been studied for their possible evolution to therapeutic systems to imitate nanoscale processes for essential progress in the natural tooth. During the secretory phase of enamel, the amelogenin-rich organic matrix gathers to make nanosphere structures that are combined along the growing enamel crystallites [184].

2.9 Transparent PMMA/PVB-fiber composites

Poly (methyl methacrylate) (PMMA) is a famous transparent thermoplastic polymer. Earlier, it has been used as a model polymer for preparing nanofiller-reinforced transparent nanocomposites, such as PA-6 nanofibers. PMMA is a tough, strong, but lightweight material at the same time with a density of 1.17-1.20 g/cm^3 (less than half that of glass). PMMA burns at 460 °C (860 °F) forming as products water, carbon monoxide and dioxide, and formaldehyde among all other compounds. It possesses good impact strength that is higher than both polystyrene and glass [187].

With 3 mm of thickness, PMMA has up to 92% of visible light transmittance, with a 4% reflection from all of its surfaces due to its refractive index (1.4905 at 589.3 nm). Like typical window glass, PMMA filters ultraviolet (UV) light at wavelengths lower than 300 nm, allows infrared light of up to 2,800 nm to pass and blocks IR of wavelengths up to 25,000 nm. PMMA has a maximal water absorption ratio where tensile strength decreases (0.3-0.4% by weight) and its coefficient of thermal expansion is considerably high at $(5\text{-}10)\times10^{-5}$ $°C^{-1}$ [187].

Poly (vinyl butyral) (PVB) is a thermoplastic polymer which has various applications due to its extraordinary properties. PVB dissolves in alcohols but does not swell in water due to its hydrophilic/hydrophobic bivalent character. This material

has a great potential for doping of fibers with various useful components coupled with slow releasing properties for antibacterial compounds and anticancer drugs [59].

The impacts of nanofiber alignments on the mechanical and optical properties of PMMA-based nanocomposites were studied. The methods for making optically-clear fiber-modified polymer composites are coming from the match of refractive index of matrix polymers and selected fibers. PMMA as the matrix polymer has been used in numerous transparent materials applications. Due to its chemical, mechanical, and optical properties PVB has been utilized in many commercial applications like coatings (onto a laminate), adhesives for glass laminates, mixing into a resin and matrix polymer in fiber-reinforced thermoset composites. PVB has the same refractive index as PMMA, and, for this reason, it is chosen for the fabrication of electrospun fibers [188].

Figure 24 depicts the effect of a translucent material when it is held a little above the image. The difference in refractive index between matrix and fiber and the diameter of fibers affect the scattering of light in the polymer fiber composites. For instance, PMMA and polyacrylonitrile (PAN) have a little difference between their refractive indexes (1.49 and 1.52, respectively) but it produces significant difference in haze [188].

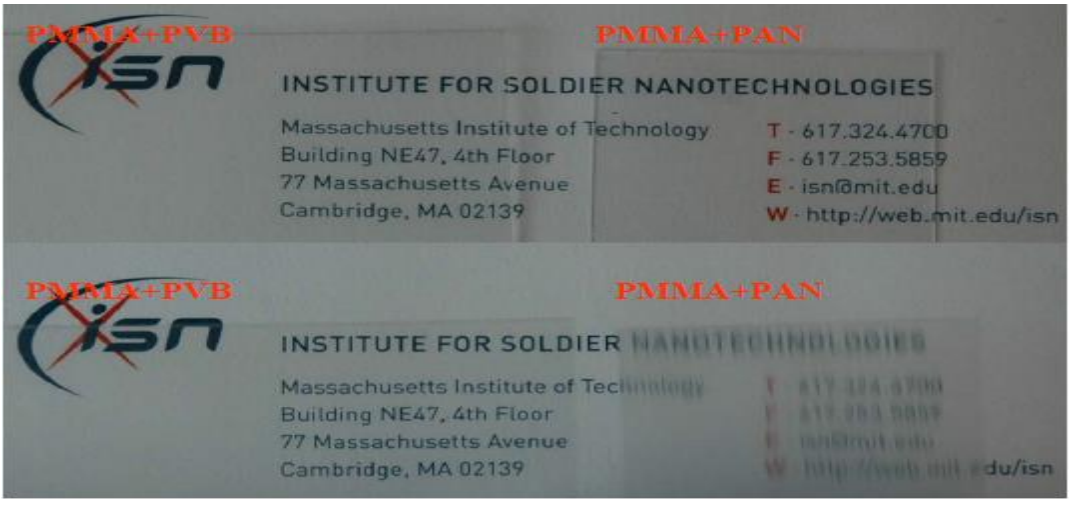

Figure 24. Two composites with comparable transmittance - the PMMA+PVB composite on the left has 3.5% haze (left), while the PMMA+PAN composite has 20% haze (right)

Electrospinning is a simple and powerful method of the submicron PVB fibers production. Furthermore, electrospinning has the following benefits: (1) producing of very fine fibers (diameter range 100 nm - 500 nm) that can decrease the scattering of light when there is a small disproportion in the refractive indices; (2) producing of a fibrous mat with a large surface area to mass ratio which enables improved bonding to the matrix material; (3) enabling the dye to disperse in the spin solution and it does not endanger the chemical stability of the dye in the processes of spinning and composite fabrication. The electrospun fibers have a wide variety of applications such as biodegradable electrospun fabrics for the drug delivery and tissue engineering, high surface area fabrics for protective clothing and highly effective filtration membrane materials [188].

2.9.1. Optical Properties of PMMA/PVB-fiber composites

The optical transparency of a usual PMMA/PVB-fiber composite containing 20 wt.% of electrospun PVB fibers is depicted in Figure 25. The refractive indices of PMMA and PVB correlated perfectly. Similar to the PMMA control, these PMMA/PVB-fiber composites are absolutely transparent in the visible light spectrum.

Figure 25. Translucent PMMA electrospun PVB-fiber composite [188]

2.9.2 Transparent PMMA/PVB-fiber composites with chromatic functionality

PMMA/PVB-fiber composites with chromatic functionality have been attempted to develop. The first approach was to prepare dye-impregnated PVB fibers for application in the consecutive composite fabrication. A UV dye, Fluorescent 28, was chosen for the use in this workability study. First, the dye was dissolved in the PVB solution (concentration of 1 mg/cc). The PVB-dye solution was then electrospun into a mat which was selected in advance. The in-situ casting process holds the electrospun fiber patterns in place. For this reason it is a usable approach for fabrication of PMMA composites with desired fiber pattern models. The final PMMA PVB-fiber composites fluoresce at locations with PVB fibers when they are exposed to a UV excitation. Successful fiber patterning in combination with chromatic functionality is displayed in Figure 26. It is obvious that the UV dyes were within the electrospun fibers during the composite fabrication which indicates the stability of the impregnated dye probably due to interaction of hydrogen bonding between PVB and the selected dye [188].

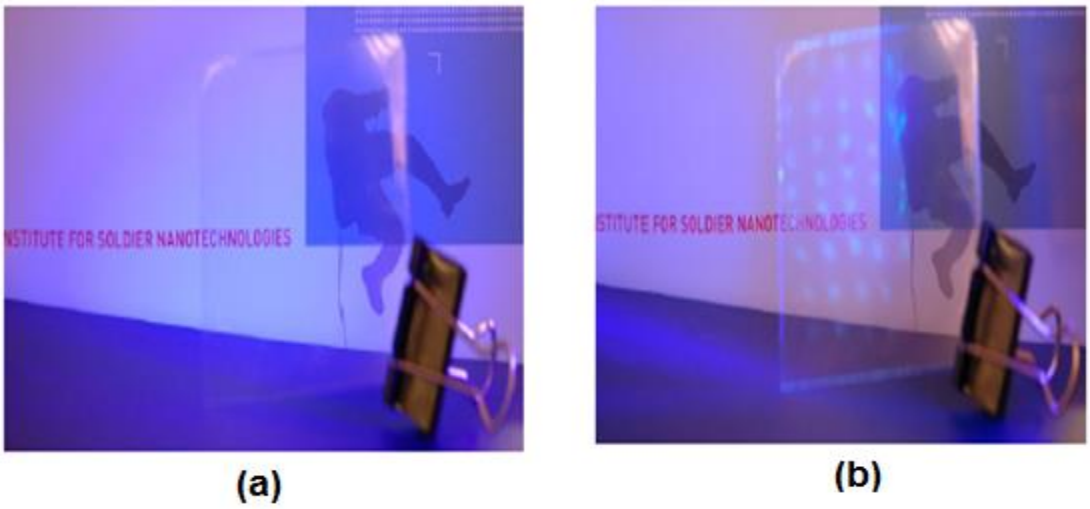

Figure 26. A transparent PMMA composite with arranged and dye-embedded PVB-fibers: (a) before UV excitation; (b) after UV excitation [188]

CHAPTER 3

THE USE OF DIFFERENT ALUMINA FILLERS FOR IMPROVEMENT OF THE MECHANICAL PROPERTIES OF HYBRID PMMA COMPOSITES

3.1 Introduction

Poly (methyl methacrylate) (PMMA) is a widely used polymer in cases when the transparency is of utmost importance. PMMA has a favorable biocompatibility and has been used as a restorative material in dentistry and medicine [189]. Reinforced polymer composites have been used for nearly 50 years in restorative components utilized in medicine and dentistry [190,191]. The use of this material has recently increased as a result of consumer demands for esthetic restorations, coupled with the public concern of mercury-containing dental amalgam [192]. Composites are now used in over 95 % of all anterior direct restorations teeth and in 50 % of all posterior direct restorations teeth [193]. In medicine, fiber-reinforced composites have been used in orthopedics as implants, and load bearing surfaces [194]. In addition, hydroxyapatite composite implant materials have become a promising alternative to acrylic cement in stabilizing fractures and cancellous screw fixation in elderly and osteoporotic patients [195,196]. The first use of poly (methyl methacrylate) as a dental device was for the fabrication of complete denture bases [197,198]. Although numerous new alloplastic materials show promise, the versatility and reliability of PMMA cause it to remain a popular and frequently used material [199,200].

The use of PMMA-based composites is based on the need to achieve favorable mechanical properties with appropriate polymer-reinforcement bonding, and benefit from the biocompatibility of PMMA. The even distribution of composite reinforcement particle plays a pivotal role in the durability of a material during long-time service. This is the situation where the properties of the composite are important

and when the even distribution of the reinforcement plays a vital role for enabling the material to be used safely and for a long time.

The deagglomeration and distribution of particulate reinforcements in the matrix can be achieved using several techniques of which ultrasonication of the reinforcing particles in the monomer is one of the most efficient techniques for the fabrication of composites with the desired mechanical properties [201]. Electrospinning is a process that enables the production of fine fibrous ceramic structures enabling particles having to obtain shapes with a good capacity for reinforcement to be obtained [202]. Alumina fibers are among the fibers that are easily produced using electrospinning and there are several reported chemical fabrication routes [203,204]. The fibers can be easily produced from precursor chemicals and then transformed into oxides by heat treatment in air [205]. The obtained fibers have promising potentials for use as reinforcements in composite materials. The process can be controlled using different process parameters, such as mass flow of the precursor, the voltage of electric field, chemical composition of the precursor and the distance between the syringe and the collector. By varying the mentioned parameters, the shape and dimensions of the fibers could be adjusted. The products mostly have a fibrous structure, but sometimes it is possible to obtain different shapes of the precursor. Appearance of the fiber shapes could be analyzed using image analysis techniques with precise measurement scales [206]. Usually, this technique is coupled with scanning electron microscopy in order to capture the real morphology of the fabricated materials.

Elastic modulus and hardness at ambient temperature and under heating cycles are essential for composite characterization. Nanoindentation is a technique that enables the determination of elastic modulus and hardness of a material on submicron scales. In the case of a composite material having nanoparticles as reinforcement, it is essential to elucidate the uniformity of mechanical properties that could be compromised due to uneven particle distribution or weak particle–matrix bonding.

Dynamic mechanical analysis (DMA) is a sensitive technique that measures the thermo-mechanical response of materials with respect to temperature and the

frequency of the applied sinusoidal stress. This analysis enables the determination of the storage modulus (E'), loss modulus (E''), damping factor (tan δ) and the ratio between loss modulus (E'') and storage modulus (E') (Cole–Cole plot). DMA also enables the determination of the glass transition temperature (T_g) of the composite and an evaluation of the contact between the reinforcement and the matrix. A comparison of the results of these methods gives the possibility to study the mechanical behavior of the composite and to evaluate the influence of the shape and quantity of the reinforcement.

The goal of this research was to examine the feasibility of using electrospun alumina fillers as reinforcement for PMMA-based hybrid composite materials. The influence of the size and shape of electrospun alumina fillers on the mechanical properties of the hybrid composites was studied and compared with those of the two types of composites prepared using industrial alumina fillers: alumina spherical particles and alumina whiskers. All fillers were added without surface modification, which makes the process very simple and lowers the cost of the processing of the materials.

3.2 Experimental

3.2.1 Materials

Aluminum chloride hydroxide (Locron L) was purchased from the Clariant company in the crystallized state of $Al_2Cl(OH)_5$ 2.5·H_2O. The PVA used had 130,000 molecular weight, and was purchased under the label Mowiol 18-88 (Aldrich). Mecaprex KM, PRESI (Grenoble, France) autopolymerizing acrylic resins consisted of KM powder (PMMA powder containing dibenzoyl peroxide (DBPO) initiator) and of KM liquid monomer (methyl methacrylate monomer - MMA with N, N-dimethyl-p-toluidine used as an activator). The spherical aluminum oxide nanoparticles and alumina whiskers were commercially available from Aldrich.

3.2.2 Methods

3.2.2.1 Fast preparation of electrospun alumina fibers

For the preparation of alumina ceramic fibers, a fast electrospinning procedure was used. The precursor was based on alumina chloride hydroxide and poly (vinyl alcohol), which served to enable the good spinnability of the solution and to ease the handling of the precursor fibers. The procedure for precursor preparation was selected so as to enable the preparation of mixtures having a desired ratio of aluminum oxide to the polymer in the solution. A 5 wt. % aqueous solution of polymer was used and the aluminum chloride hydroxide was added into the solution. The desired mass ratio of aluminum chloride hydroxide to polymer in the mixture was 5 to 1. The solution was then stirred using a laboratory mixer for 1 h at 30 °C to obtain a homogeneous solution. The resulting solution contained air bubbles that disappeared after 24 h.

An Electrospinner CH-01 electrospinning apparatus (Linari Engineering, Italy) was used for the fiber preparation. A high-voltage supply (SPELMANN PCM50P120, USA) capable of producing 30 kV was used in the experiments. The polymer solutions were supplied to the nozzles using R100E type syringe pumps (Razel Scientific Instruments, USA). The solution was placed into the 20 ml plastic syringe having a needle of 0.8 mm orifice. The voltage used to have a stable process was of 28 kV and the mass flow rate was 20 ml/h. The process was conducted in air at an ambient temperature of 21 °C. The distance between the needle and the collector was fixed at 15 cm. Aluminum foil was placed at the bottom of the installation. After completion of the electrospinning, the electrospun fibers were calcined at 1100 °C for 1 h in order to obtain electrospun alumina fillers [206]. The XRD pattern of the sample calcined at 1100 °C indicated that the α-alumina phase was formed (Figure 3.2b). Two industrially available fillers were selected in order to compare the prepared electrospun alumina fillers. These were spherical aluminium oxide nanoparticles, declared to have diameters of less than 50 nm, and alumina whiskers characterized with diameters of 2 – 4 nm and lengths of 200 – 400 nm. Thus very

different alumina fillers were examined, spherical alumina nanoparticles, with the length to diameter ratio of 1, and alumina whiskers having a length to diameter ratio of approximately 100.

3.2.2.2 Preparation of hybrid PMMA composites

Alumina spherical nanoparticles, alumina whiskers or electrospun alumina fillers were added to KM liquid. The mixture was sonicated for 60 min and KM powder was dispersed in the mixture. The mixing was performed by hand for 2 min and the mixture was poured out in a cast form having dimensions suitable for DMA and nanoindentation testing. The form was covered using a glass cover to ensure that the surface of the specimen remained smooth. A PMMA/MMA mass ratio of 0.75 was used as this ratio enables minimization of shrinkage as suggested by the manufacturer (PRESI) and as previously reported in the literature [207].

The polymerization of the monomer was realized at a temperature of 25 °C. The manufacturer's suggestion states that the polymerization is considered to be completed in 20 min at a temperature between 20 and 23 °C. The obtained composites were then exposed to a temperature of 37 °C for 30 days before they were mechanically tested in order to obtain the stabile composition of the polymer matrix of the composite [208]. The compositions of the composites PMMA/alumina whiskers and PMMA/alumina spherical nanoparticles prepared for analysis in this study are summarized in Table 4. The samples prepared using the alumina spherical nanoparticles as the filler were denoted P1, P3 and P5 for the addition of 1 wt. %, 3 wt. % and 5 wt. % of the filler, respectively. The samples using alumina whiskers as fillers were denoted W1, W3 and W5 for the addition of 1 wt. %, 3 wt. % and 5 wt. % alumina whiskers, respectively. The samples using the electrospun bimodal alumina product having the same contents of fillers as those having industrially produced alumina fillers are annotated as F1, F3 and F5 for the respective contents of 1 wt. %, 3 wt. % and 5 wt. % alumina electrospun fillers, respectively.

Table 4. The compositions of composite specimens prepared using the PMMA as the matrix and different fillers.

Sample	Quantity of fillers (g)	Mass MA+initiator (g)	Mass MMA (g)
PMMA	-	2.290	1.710
P1	0.045	2.540	1.910
P3	0.135	2.540	1.870
P5	0.225	2.440	1.830
W1	0.045	2.540	1.910
W3	0.135	2.540	1.870
W5	0.225	2.440	1.830
F1	0.045	2.540	1.910
F2	0.135	2.540	1.870
F5	0.225	2.440	1.830

3.2.3 Characterization

3.2.3.1 DMA analysis

Dynamic mechanical analysis was used to examine the performance of the PMMA matrix composite reinforced with alumina spherical nanoparticles, alumina whiskers and electrospun alumina fillers in order to analyze the influence of the size and shape of the alumina filler on the behavior of the fabricated composites. The storage modulus revealed the ability of the composites to store elastic energy associated with recoverable elastic deformation. Together with tangent delta, the storage modulus describes the behavior of the composite under stress in a defined temperature range. The effect of the structural changes of neat polymer matrix was

also confirmed by a Cole–Cole plot where the loss modulus data are plotted as a function of the storage modulus. Dynamic mechanical analysis was performed (DMA Q800, TA Instruments) under a nitrogen atmosphere and the single cantilever mode. Storage modulus (E'), loss factor (tan δ) and the Cole–Cole plot were calculated for rectangular specimens of size 35 mm × 13 mm × 3 mm at frequency ω = 1 Hz. Temperature range was changed from room temperature to 150 °C at a heating rate of 3 °C/min.

3.2.3.2 Nanoindentation

The nanoindentation test was performed using a Hysitron TI 950 TriboIndenter equipped with *in situ* SPM imaging (Hysitron, MN). The Berkovich indenter had an average radius of curvature of about 100 nm. The tests were performed in force-controlled feedback mode. The indentation maximum load was set at 4 mN for each tested sample. The loading and unloading times as well as the hold time at the peak force were all set to 25 s. For each loading/hold/unloading cycle, the applied load value was plotted with respect to the corresponding position of the indenter. The resulting load/displacement curve provides data specific to the mechanical nature of the material under examination.

All the results were obtained using the Oliver & Pharr method [209], employing a supposed sample for the reduced elastic modulus calculation. Established models were used to calculate the values of the quantitative hardness (H) and reduced elastic modulus (E) for such data. The specimens were polished using alumina paste having abrasive grains up to 0.02 μm until the average roughness (RA) of samples containing alumina particles was 38.89 nm, with alumina whiskers was 28.09 nm and with electrospun alumina fillers was 25.24 nm. (Figure 27). The specimens were about having dimensions 3 × 3 × 2 mm and were placed on the specimen holder in the nanoindenter. On each tested sample, nine indentations were

made at random positions ensuring that the distance between indents was at least 7.5 μm.

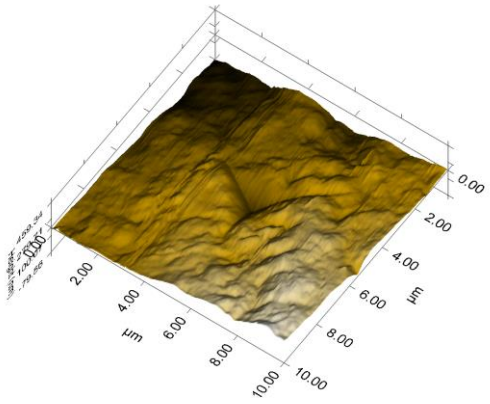

(a)

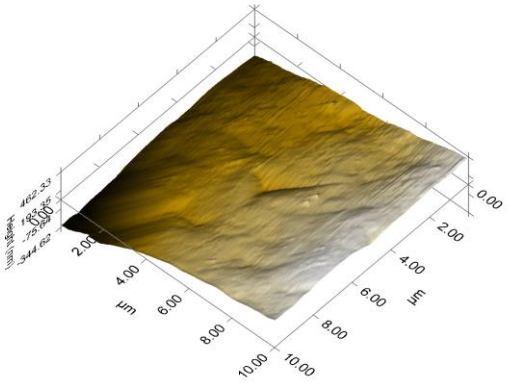

(b)

Figure 27. 3D photograph nanoindentation measurement a) PMMA/alumina particles and b) PMMA/alumina nanofillers

3.2.3.3 XRD analysis

Crystallographic phases formed in the heat treated fibers were determined by X-ray diffraction analysis. The XRD patterns were recorded on an Ital Structure APD2000 X-ray diffractometer in the Bragg–Brentano geometry using CuKα radiation (λ = 1.5418 Å) and the step-scan mode (range: 20−75° 2θ, step-time: 0.50 s,

step-width: 0.02°). The corund structure of the alumina fillers was confirmed by comparison of the XRD data to the standard card 93096-ICSD.

3.2.3.4 Analysis of morphology of the specimen

The morphology of the electrospun alumina fillers and the morphology of the samples were examined using a field emission scanning electron microscope (FESEM), MIRA3 TESCAN, operated at 20 kV. The electrospun alumina products were analyzed after heat treatment and prior to use as reinforcements. The bimodal size and shape distribution of the electrospun alumina fillers were measured using Image-Pro Plus 4.2 analysis software (Media Cybernetics) by manual measurements of the particle and fiber diameters.

3.3 Results

3.3.1 Characterization of the morphology of the electrospun alumina fibers

The product of electrospinning was characterized after heat treatment so the product that was used as reinforcement could be well known from the morphological point of view. The field emission scanning electron microscope was used for morphological characterization of the product as it enables better visibility of fine fibers produced using this method (Figure 28). These images were used to evaluate the content of spherical micron sized particles and nanofibers in the composition. This was realized using the image analysis technique as in the images these features could be separated. The volume fraction of the particles and fibers was evaluated according to the surface occupied in the image. The content of fibers in the product was 45 vol. % and the content of spherical micron sized particles were 55 vol.%. The particles and fibers were also characterized using the image analysis technique and the mean diameter of the particles in the electrospun product was 3.5 μm and that of

electrospun nanofibers was about 310 nm. The corresponding histograms of the distribution of the diameters of the particles and nanofiber are given in Figure 29.

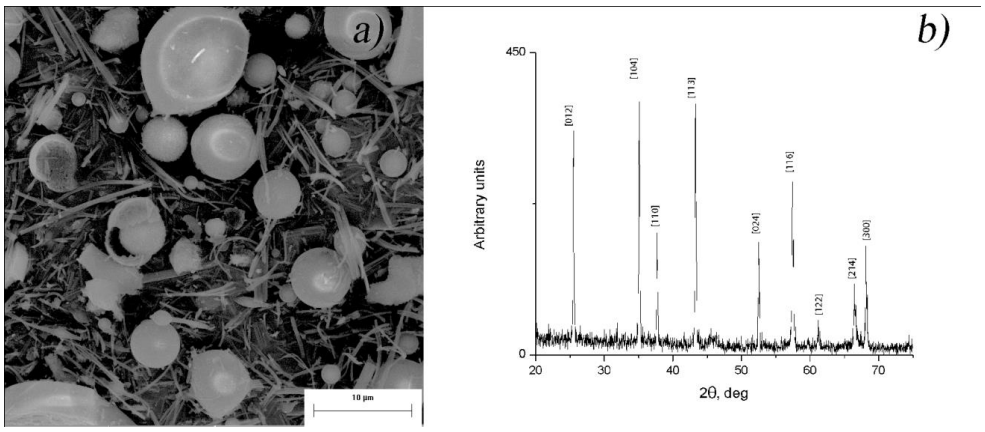

Figure 28. FESEM micrograph of the electrospun fillers showing the bimodal size and shape distribution, spherical particles and nanofibers in the composition, b) XRD pattern of the bimodal alumina product calcinated at 1100 °C.

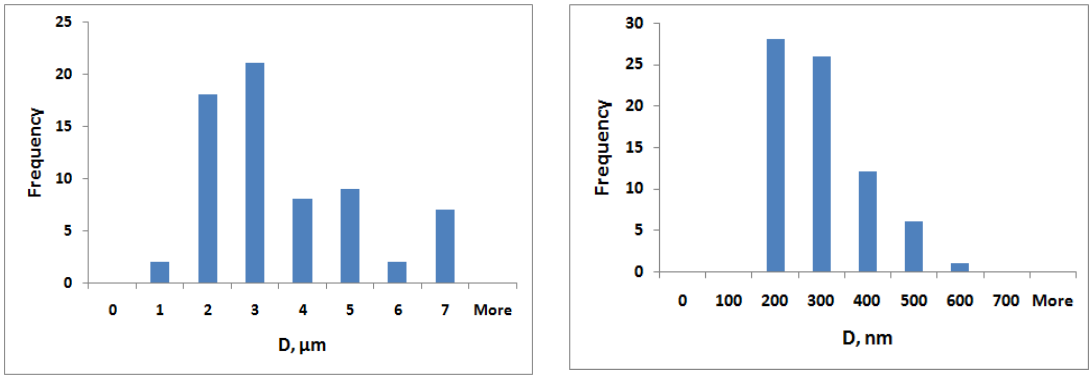

a) **b)**

Figure 29. Histograms of particles (a) and nanofibers (b) obtained by electrospinning of an aqueous PVA solution of aluminum chloride hydroxide after heat treatment at 1100 °C.

Ahmed Ben Hasan et al. [207] characterized the industrially available alumina spherical nanoparticles and alumina whiskers prior to utilization and the average mean diameter of agglomerates were found to be 87 µm and 1.1 µm for alumina spherical nanoparticles and alumina whiskers, respectively. The micrographs of

composites having PMMA and different contents of bimodal alumina fillers are presented in Figure 30.

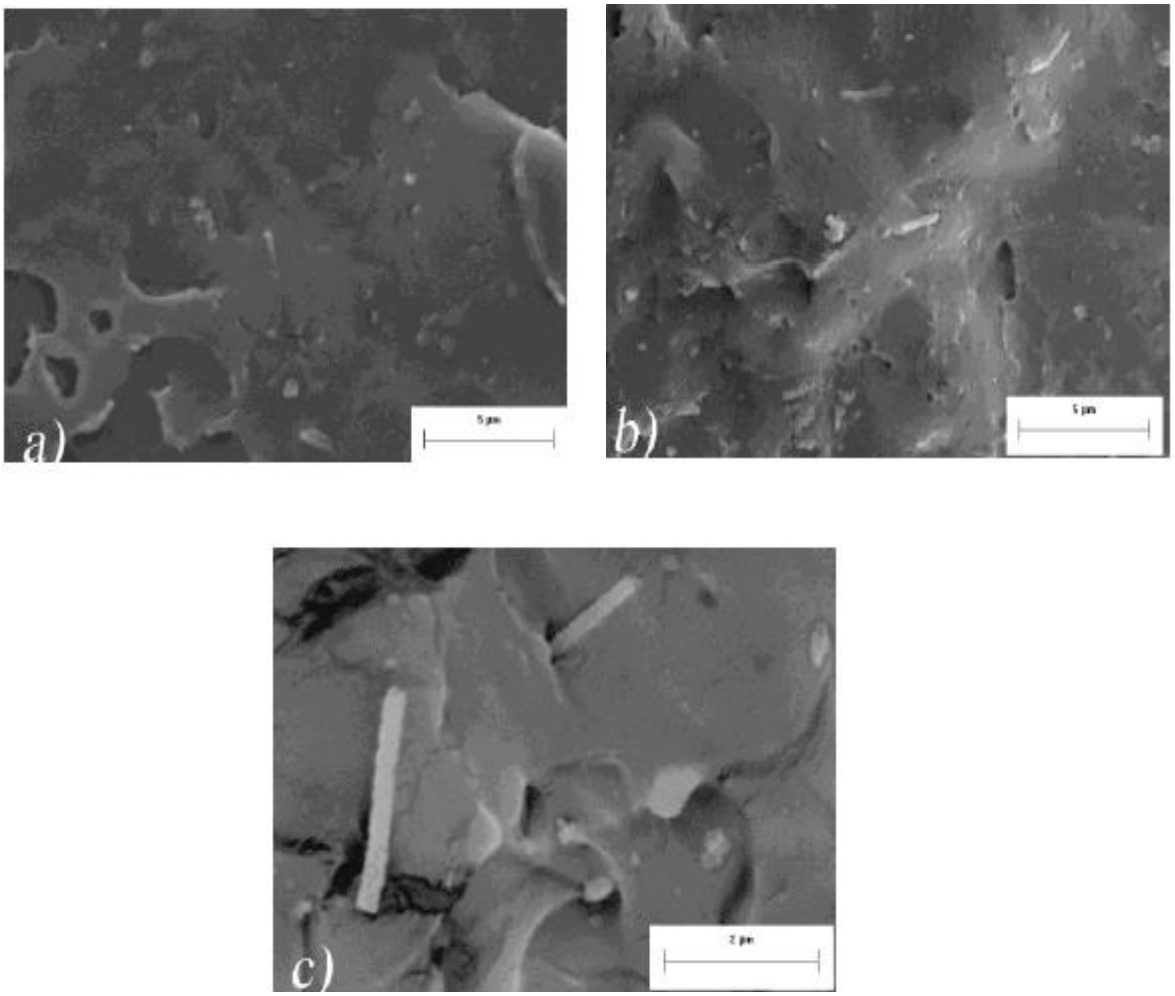

Figure 30. The SEM micrographs of hybrid composite of PMMA and a) 1 wt. % of bimodal alumina filler, b) 3 wt. % of bimodal alumina filler and c) 5 wt. % of bimodal alumina filler.

Hybrid composite containing 1 wt. % and 3 wt. % electrospun fillers had a good distribution of fibers in the volume of the matrix, whereas the specimen containing 5 wt. % showed some tendencies of agglomeration of the fibrous and particulate filler and this resulted in a less homogeneous distribution.

In the image of the cross section of the composite having 5 wt. % of the electrospun filler, the product established looser contact to the matrix and this could

explain the deterioration of the mechanical properties compared to the composites having 3 wt. % of electrospun alumina fillers.

3.3.2 Characterization using DMA

The main goal of the addition of the ceramic fillers into the polymer matrix was improvement of the mechanical properties. The obtained mechanical properties of composites having electrospun alumina fillers were compared to the composites reinforced using the commercial spherical nanoparticles and commercial alumina whiskers. Comparison of the influence of the filler size and shape on the mechanical properties of the composites showed that the elongated form of the filler, *i.e.*, the whiskers, was favorable to the improvement of the mechanical properties. Comparison of the mechanical properties of the composites showed that the improvement was the most obvious when the electrospun alumina fillers were used as the reinforcement.

Table 5. Properties of composites obtained from DMA testing

Sample	PMMA	F1	F3	F5	P3	W3
E′, (30 °C), MPa	1186	1379	2371	1937	1288	1932
T_g (°C)	95.6	95.6	100.4	101.9	93.9	98.5
Tan δ	1.45	1.22	1.16	1.17	1.00	1.17

The composites having 1 wt. %, 3 wt. % and 5 wt. % of bimodal alumina fillers as reinforcement were compared to the polymer without reinforcement using dynamic mechanical testing. The comparison of storage modulus at a temperature of 30 °C showed that any addition of bimodal alumina fillers increased the modulus; thus, the addition of 1 wt. % of electrospun fillers increased the storage modulus by about 16 % and the addition of 5 wt. % of electrospun bimodal fillers increased the storage modulus by 63 %. The composite having 3 wt. % of alumina fillers increased the value of the storage modulus by about 100 % and the obtained value was almost the double that of the polymer without any reinforcement. Thus the samples having 3

wt. % of bimodal alumina fillers and better values of modulus measured by DMA than the samples containing 5 wt. % of electrospun fillers. The properties of the composites obtained from DMA testing are presented in Table 5, Figures (31-33) and in a previous work [207].

The T_g values were determined from the DMA measurement and the values were compared to the PMMA without the addition of reinforcement. The T_g of PMMA was 95.6 °C and the T_g for the composite with spherical alumina particles was 93.9 °C. The composite obtained by the addition of 3 wt. % of whiskers had a T_g at 98.5 °C. The highest value of the T_g was observed for the composite obtained using electrospun alumina fillers. A comparison of the T_g value of the pure polymer to that of the composite containing 1 wt. % electrospun alumina fillers showed that the values were approximately the same. Addition of 3 wt. % of electrospun alumina fillers increases the T_g value by about 4.8 °C and the addition of 5 wt. % fillers increased the value by more than 6 °C. The values of the T_g increased with the addition of electrospun alumina fillers, indicating that the thermal stability of the composites increased with the addition of the reinforcement.

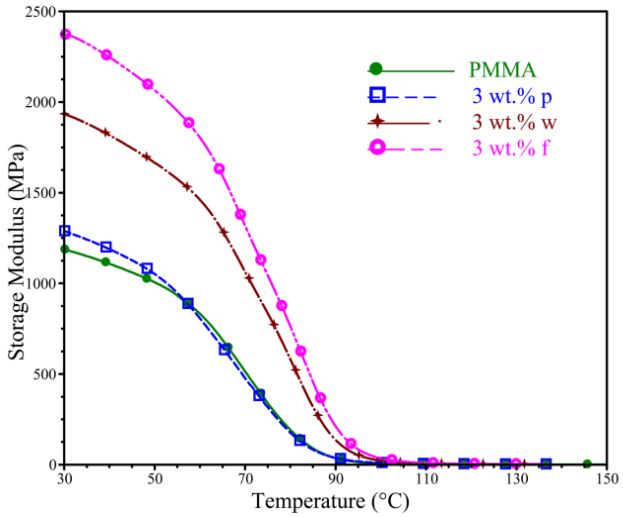

Figure 31. Comparison of storage modulus obtained from DMA analysis of composites of a PMMA matrix with alumina fillers of different shapes

In this study, all reinforcements had the same chemical composition, but the shapes of the fillers were different. A comparison of the composites having fillers of the same chemical composition and quantity of reinforcement but having different shapes is presented in Figure 31. It could be seen that the behavior of the composite having electrospun alumina fillers has the highest value of all composites at all examined temperatures.

The improvement in values of storage modulus for the addition of spherical alumina particles as a filler is not very important and at temperatures above 110 °C, the values of storage modulus are slightly lower than those for the polymer without any added filler. The improvements observed with the addition of whiskers were present over the whole studied temperature range. The improvements in storage modulus values were most visible for the composites containing electrospun alumina fillers for the temperature range from 30 °C up to 150 °C. The increase in the values of the storage modulus compared to that of the pure polymer matrix was 9 % for the spherical alumina particles, 63 % for the alumina whiskers and 100 % for the electrospun alumina fillers.

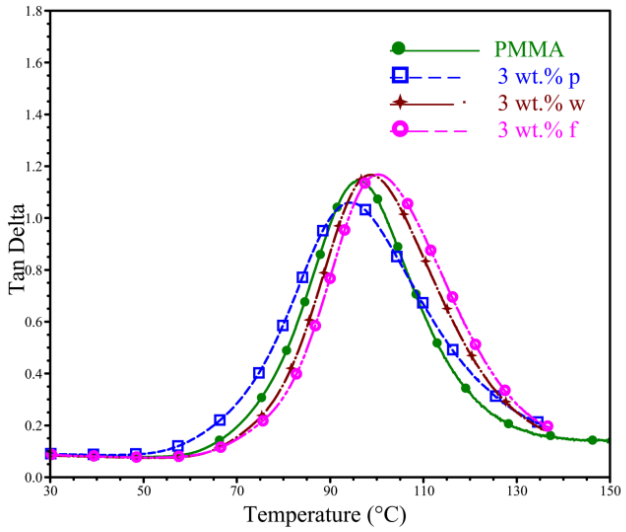

Figure 32. Values of tan δ measured at temperatures from 30 °C to 150 °C for the PMMA matrix and the matrix containing alumina fillers having different shapes.

Comparison of results obtained from the DMA testing of the specimens having the same quantity of spherical particles and electrospun fillers added showed that the maximum value of tan δ was higher for the specimen with the electrospun alumina filler than the one containing spherical nanoparticles (Figure 32). The decreasing height of the tan δ peak is due to the reduced fraction of the polymer matrix, and the better behavior is attributed to the fact that more polymer chains are restricted in the polymer/nanoparticles interphase.

The bonding established between the spherical nanoparticles and the matrix was better compared to that obtained using the electrospun product in the same matrix. This finding could be explained by the fact that the electrospun product was heat treated at 1100 °C and this heat treatment destroyed the hydroxyl groups at the surface of the filler. On the other hand, the crystals in the structure of the electrospun alumina fillers (Figure 32) were very well defined and the product obtained has a pure corundum structure, and addition of such fillers resulted in a product having higher values of the T_g.

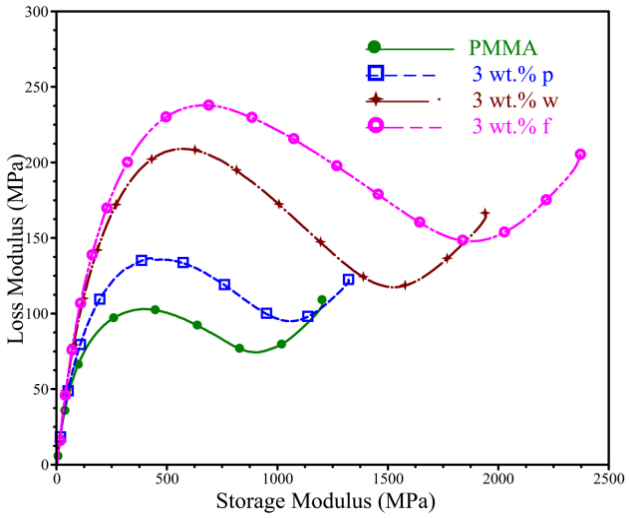

Figure 33. *Cole – Cole* plots for hybrid composites.

In comparison with the pure PMMA matrix, the composites obtained in this study all had hybrid structures, probably due to the presence of dispersed and agglomerated spherical alumina particles and alumina whiskers that were not

modified. This can be seen in Figure 33 showing the *Cole–Cole* plot [210] of the polymer and hybrid composites with the same amount of different fillers. The highest level of hybrid behavior had the one prepared using electrospun bimodal alumina fillers as it has two sorts of filler having different sizes and shapes.

3.3.3 Characterization using the nanoindentation

Nanoindentation measurements were performed on nine positions for every sample in order to obtain an overview of the possible inhomogeneity of the sample. The mean values of the nine measurements were used for further analysis, Figure 34. and 35. The data about the reduced modulus of elasticity and hardness of the samples were analyzed, Figure 35. The relative increases of the values of hardness and modulus obtained using nanoindentation are given in Table 6.

Table 6. Values of reduced modulus and hardness with standard deviation and increase relative to the polymer without fillers

	E_r (GPa)	**St dev**	**H (GPa)**	**St dev**
PMMA	4.39	0.378	0.287	0.090
F1	4.95	1.096	0.292	0.117
F3	10.28	3.073	0.741	0.456
F5	8.94	2.575	0.633	0.347
P1	4.70	0.665	0.242	0.0514
P3	4.85	1.212	0.31	0.0780
P5	4.73	0.627	0.29	0.0425
W1	4.27	0.493	0.26	0.0529
W3	8.60	1.900	0.47	0.1458
W5	4.62	0.515	0.29	0.0784

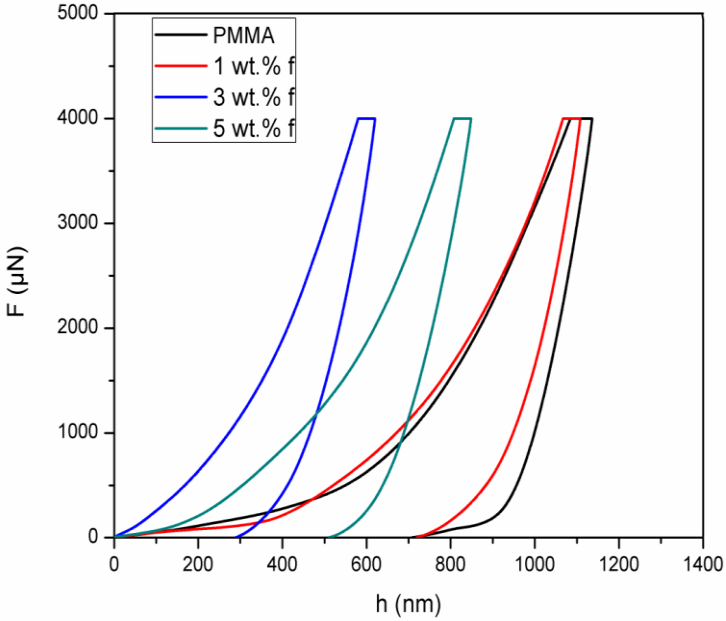

Figure 34. Nanoindentation curves for the best performing specimens obtained using 1 wt. %, 3 wt. % and 5 wt. % of electrospun alumina fillers

For the addition of 1 wt. % of alumina fillers, the increases of the reduced modulus of elasticity obtained from the nanoindentation experiments were modest. The addition of 3 wt. % of the alumina fillers did increase the values of modulus significantly for alumina whiskers and alumina electrospun fillers. The increase in the modulus was most significant for alumina electrospun fillers. The addition of 5 wt. % of electrospun alumina fillers and alumina whiskers did not additionally improve the values of modulus of elasticity. The improvement was less important in the cases of the addition of alumina spherical particles. This suggests that the morphology of the filler is very important for an improvement in the mechanical properties.

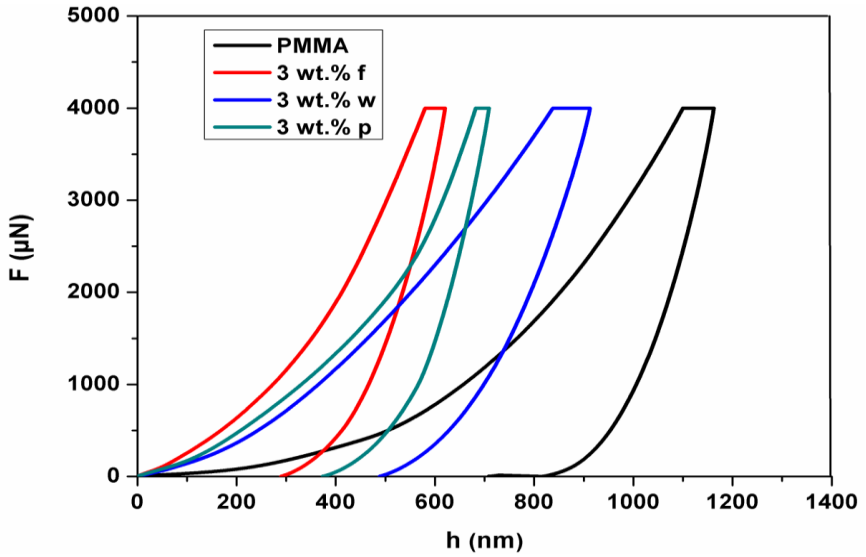

Figure 35. Nanoindentation curves for the best performing specimens obtained using 3 wt. % of fillers having a different morphology showing that the best modulus was observed in specimens having electrospun nanofibers as the filler. The two other fillers having spherical nanoparticles and whiskers had lower values of the reduced modulus of elasticity

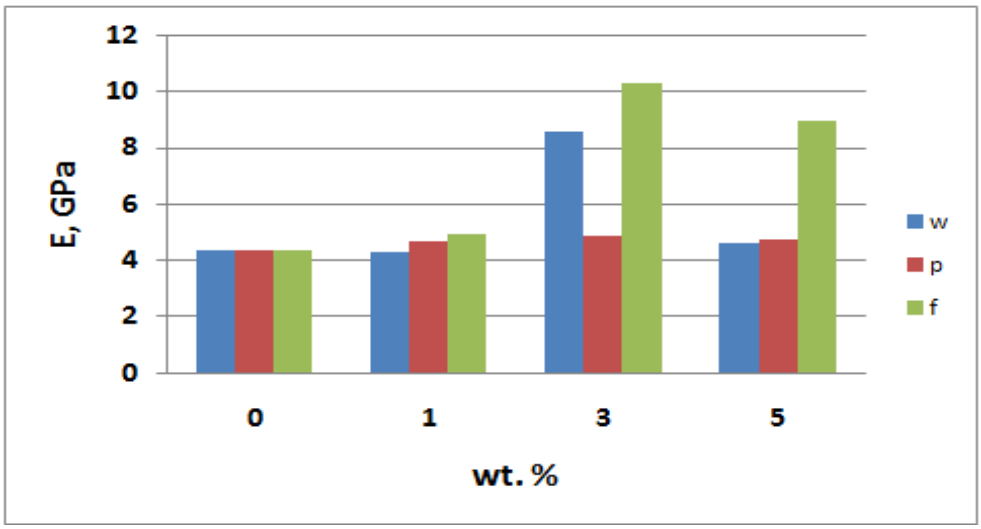

a)

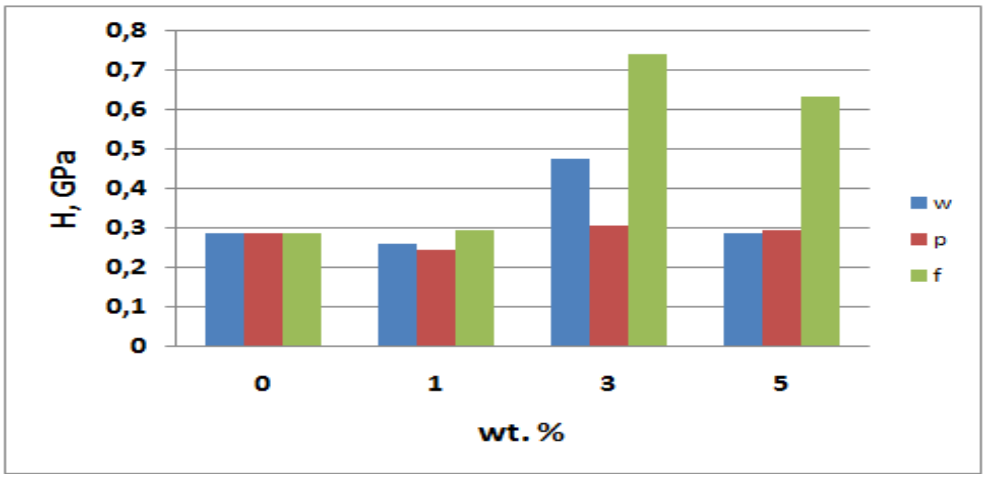

b)

Figure 36. Mean values of reduced elastic modulus (a) and hardness (b) measured using the nanoindentation technique for specimens containing different fillers

Mean values for reduced elastic modulus and hardness measured using nanoindentation are presented in Figure 36. The addition of 1 wt. % of any of the used fillers did not improve the hardness values. The addition of 3 wt. % of the whiskers and electrospun alumina product resulted in improvements in the reduced elastic modulus and hardness, whereas the addition of the spherical nanoparticles did not improve significantly the hardness of the obtained composite. The improvement of elastic modulus for addition of electrospun product was 134 % compared to the polymer without any additions. The addition of 5 wt. % electrospun product did not improve the values of the reduced modulus. Furthermore, the hardness values was significantly improved to 157.8 % on addition of 3 wt. % electrospun product, while the improvement of the hardness was 120.2 % for the sample containing 5 wt. % of electrospun product.

3.3.4 Comparison of nanoindentation and DMA data for mechanical properties

Obtained composites were tested using two different methods, giving data that could lead to an interpretation of the observed mechanical properties of the specimens. Comparison of the modulus values obtained by means of nanoindentation with those obtained by means of DMA revealed that the former technique yielded significantly higher values than the latter. This result is mainly attributable to the difference in the applied forces, but the obtained data are in accordance for the modulus values obtained using the two different methods. The best performance observed by both methods exhibited the material having 3 wt. % of electrospun alumina fillers.

3.4 Conclusion

Fast electrospinning was used to produce alumina fillers suitable for the preparation of composite materials. The conditions of the filler fabrication resulted in a product having a size and shape distribution that could be characterized as bimodal. Fine fibers having nano dimensions were produced as well as a product characterized by the presence of micron-sized particles. These two fractions were calcinated at 1100 °C and the obtained bimodal alumina product represented filler that improved the mechanical properties of the material. The quantity of the added filler was changed and the best mechanical performance was observed for 3 wt. % of added filler. The obtained results were compared to the mechanical properties of composites obtained using commercially available fillers in the form of spherical nano particles and in the form of whiskers. The addition of the whiskers resulted in a product with better mechanical properties than was obtained by the addition of the spherical nanoparticles. The addition of the electrospun alumina product having micron-sized particles and nano-sized fibers gave a composite with the best performance from those studied when 3 wt. % of this product was added to fabricate the composite.

CHAPTER 4

MULTISCALE CHARACTERIZATION OF ANTIMICROBIAL POLY(VINYL BUTYRAL)/TITANIA NANOFIBERS COMPOSITES

4.1 Introduction

Electrospinning presents a simple, unique, and versatile technology for fabricating polymer and composite fibers within the micrometer or nanometer scale range [211, 212]. Electrospun fibers are being used in membrane-based filtration, drug delivery, tissue engineering, in protective clothing, and reinforced composites.[213, 214]. The fiber production rate of the electrospinning setup with a single-needle is low. There have been attempts for creating the optimal needle arrangement with the best needle number for the multi-needle electrospinning process [215-218].

Poly (vinyl butyral) (PVB) is a thermoplastic polymer which has wide application due to its excellent properties [219]. The basic feature of PVB electrospun fibers is its hydrophilic/hydrophobic bivalent character, which enables to dissolve this material in alcohols but does not allow it to swell in water. This fiber material also has a great perspective for doping of fibers with various functional components with slow releasing properties, such as anticancer drugs [220], antibacterial compounds [221], and any type of nanoparticles [222]. The presence of titania nanofillers in polymers can alter the thermomechanical [223–224], optical [225], photocatalytic, and electrical properties of the polymers [226, 227]. Titanium dioxide nanotube is one of the promising nanostructured oxides with tubular structure. Fabricating methods of titania-based nanotubes comprise the assisted-template method, the sol-gel process, electrochemical anodic oxidation, and hydrothermal treatment [228]. Composites

with titania nanotubes (TTNTs) were shown to possess the highest fracture toughness and elastic moduli compared with other studied composites [229].

This work reports fabrication of electrospun materials based on PVB mats reinforced with titania nanofillers. The morphology of the resulting fibers was analyzed by optical microscopy, field emission scanning electron microscopy (FESEM) and transmission electron microscopy (TEM). In this study, the antibacterial activity of nanofiber composite mats with an immobilized antibacterial agent was tested. Finally, the enhancements of the thermo-mechanical properties of electrospun PVB non-woven mats were demonstrated by dynamic mechanical analysis (DMA) and nanoindentation testing (TriboIndenter Hysitron). This novel type of nanofibrous composite material combines the significant mechanical and antibacterial properties.

4.2 Materials and Methods

A powder PVB (Mowital B60H, Kuraray Specialities Europe) and absolute ethanol (Zorka Pharma, Šabac) were used for preparing the PVB solution (10 and 8 wt.% in acetic acid and ethanol in 1:2 wt./wt. ratio). TTNTs can be obtained by standard alkaline hydrothermal treatment, according to the previously published procedure [228]. An open-ended multiwall morphology of the scrolled nanotubes was observed (the average sizes of outer and inner diameters were about 10 and 7 nm, and the length distribution was up to few hundreds of nanometers). The TTNTs were characterized by quasianatase, axially symmetric, and distorted octahedral coordination with a large fraction of five-coordinated sites on the surface [230, 231]. Commercial nanoparticle (Aeroxide P25) TTNPs with a mean diameter of 21nm were obtained from Evonik-Degussa, Germany, and have a composition of 70% anatase and 30% rutile phase [232]. The Gram-negative bacterium *Escherichia coli* (ATCC 25922) was used for the antibacterial test.

The TTNTs and TTNPs were put into the PVB acetic acid/ethanol solution with a concentration of 1 and 3 wt.% with regard to the PVB, respectively. The suspension was mechanically stirred at a frequency of 8000 min^{-1} (Ultra Turrax Ika T25 disperser) during 2 h. This study reports fabrication of pure PVB fiber mats with 10 wt.% content of polymer both, single, and multiple needles. Initially, we have started experiments with 10 wt.% PVB, but the multi-needle spinning with this solution gave material in the fibers which were sealed to each other (Figure 38).

Therefore, the content of PVB was decreased to 8 wt.%, and this working solution was also used for synthesis of nanofibrous composite mats. The single and multi-needle systems (14 needles) used in this work are depicted in Figure 37.

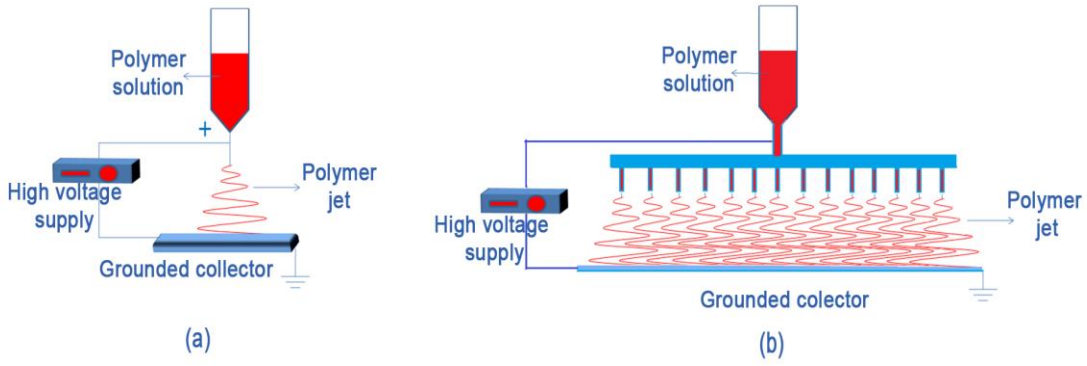

Figure 37. Schematic presentation of the single and multi-needle electrospinning setup

The electrospinning setup used for the experiments in this work is Electrospinner CH-01 (Linari Engineering). A set of experiments was conducted with the single needle where the applied voltage was V = 28 kV, while the flow rate was Q= 0.5 ml/h. Another experimental set was performed with the multineedle system (14 needles) where the applied voltage was V = 28 kV and the flow rate was Q= 7 ml/h. The distance between the needle tip and the collector was h = 10 cm in both cases. All the experiments were conducted at room temperature (25–27°C) and a

relative humidity of 30–40% within a closed chamber. The as-spun nanofibers were collected on an alkaline-resistant fiberglass mesh in the form of patterned nanofibrous mats and kept to dry in air for 15 h.

4.3 Characterization

The morphologies of the electrospun fibers were investigated by optical microscope (OLYMPUS CX41), field emission scanning electron microscope (FESEM, TESCAN, MIRA3 XMU) at 20 kV and transmission electron microscope (TEM) (JEOL 100CX II instrument) at 100 kV (Figs. 38-40).

The antibacterial activity was evaluated by using the gram-negative *Escherichia coli* (*E. coli*) bacteria ATCC 25922 and agar disk diffusion method. The electrospun fiber mats were compressed using N 840 D Hix Digital Press (Hix, Corp., USA) under pressure of 3.5 bar. In brief, nanofiber samples (12 mm in diameter and 80 mg in weight) were sterilized by UV irradiation for 30 min and placed on tryptone soy agar plate (TSA-Torlak, Serbia) inoculated with approximately 10^7 CFU/plate of *E. coli*. The agar plates were incubated for 24 h at 37 °C and antimicrobial activity was evaluated by presence of zone of inhibited growth.

Dynamic mechanical analysis (DMA, Q800 TA Instruments) of the PVB fiber mats (200 mg) was conducted in the dual cantilever mode (using the stainless steel sample holder) at a frequency of 1 Hz and in the temperature range from 30 ºC to 100 ºC by using a heating rate of 3 ºC/min. All experiments were performed in triplicate.

The nanoindentation testing of the PVB fiber mats was used for determination of the nanomechanical properties, which included indentation hardness (*H*), reduced elastic modulus (E_r) and H/E_r ratio. The testing was carried out using Hysitron TI 950 TriboIndenter equipped with in-situ scanning probe microscopy (SPM) with a Berkovich diamond tip for depth sensing indentation [232]. The indentation maximum load was set at 2 mN with the load-hold-unload of 10-20-10 s for each segment. Nine indentation measurements were performed for each sample. All tests

were performed at room temperature. Finally, H, E_r and H/E_r ratio were calculated from unloading segments of the partial unload function according to the standard Oliver-Pharr method [233].

4.3.1. Morphological characterization

Figure 38 shows a random orientation of electrospun PVB fibers generated from the single-needle with the flow rate of 0.5 ml/h. Contrary to that, the PVB fibers produced at a flow rate of 7 ml/h from the multi-needle system show mainly aligned orientation.

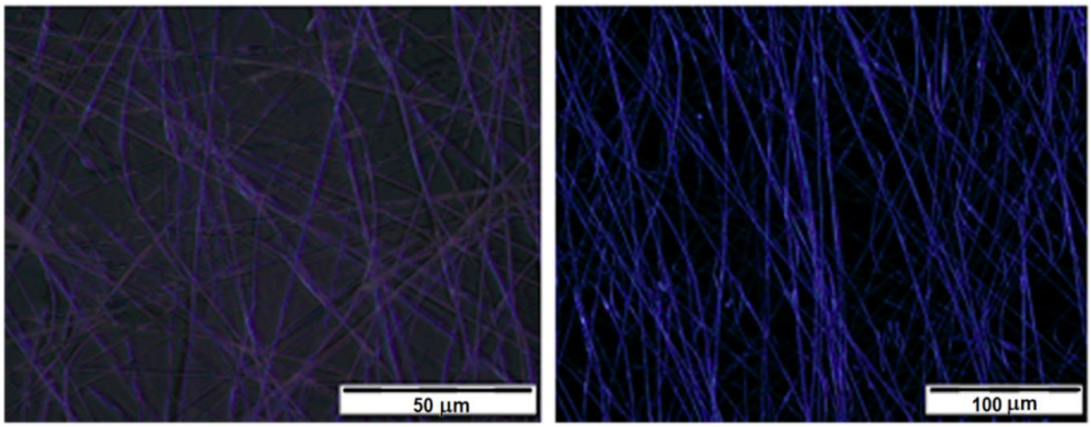

Figure 38. The optical, electron microscopic image of randomly (left) and aligned oriented (right) PVB nanofibers

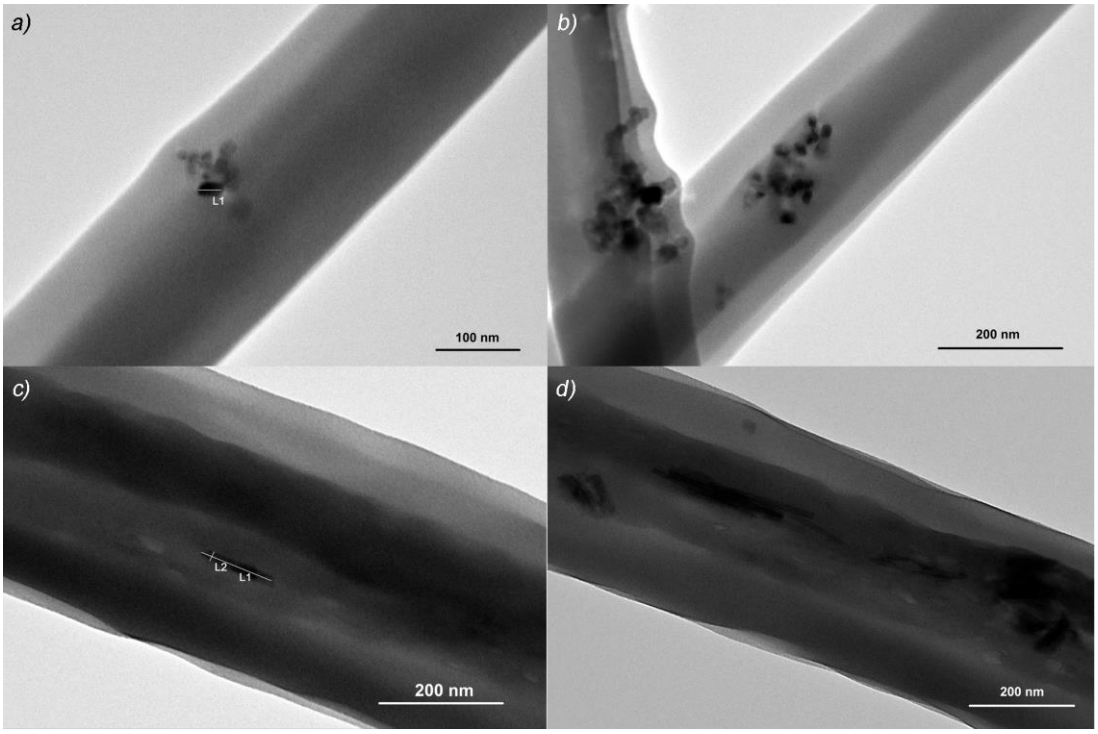

Figure 39. TEM images of: (a, b) TTNP and (c, d) TTNT inside PVB fibers

According to the obtained TEM images (Figure 39), the TTNP and TTNT were well dispersed without any chemical modification or ultrasonic treatment. The majority of them were in diameter between 21 nm and 40 nm (the length L1 of the nanoparticle is 27.6 nm, Figure 39(a)). Some of the nanoparticles fused into aggregates up to 275 nm in diameter. The titania nanotubes lengths was from 79 nm to 268 nm with their width within the range 13.6 nm-36 nm (in Figure 39 (c) the length L1 is 121.9 nm while the width L2 is 19.3 nm). The results indicate that electrospinning is a simple and general approach to create the satisfactory dispersion of nanoreinforcements in the polymer matrix.

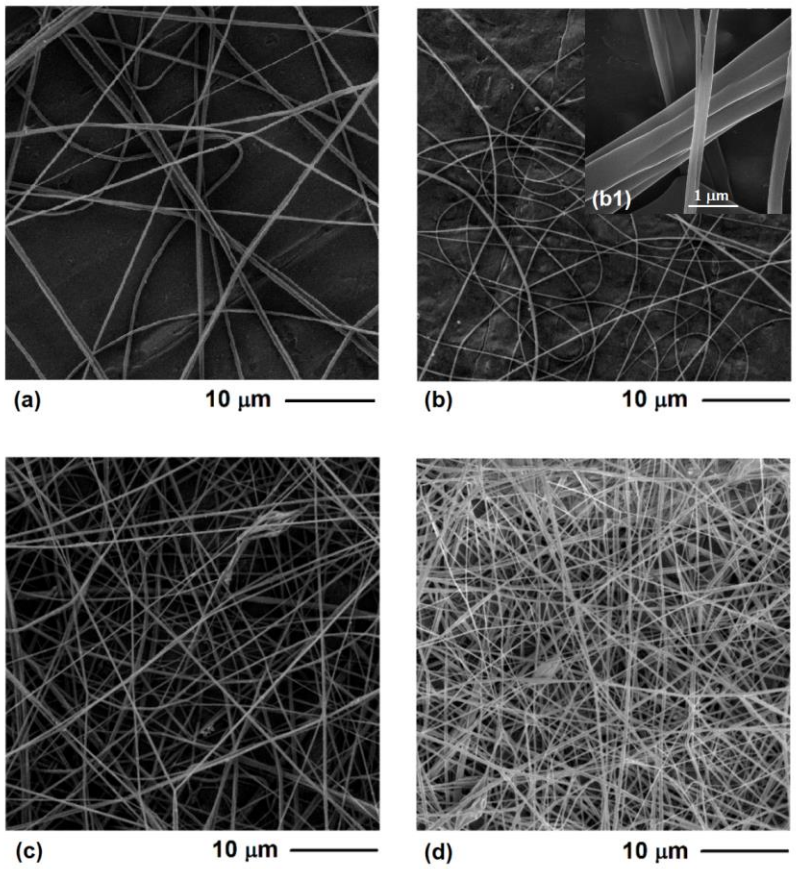

Figure 40. FESEM images: (a) PVB fibers (single-needle, 10 wt.%); (b) PVB fibers ((multi-needle, 8 wt.%), (b1) PVB fibers (multi-needle, 10 wt.%) ; (c) PVB fibers with TTNP (multi-needle, 8 wt.%); (c) PVB fibers with TTNT (multi-needle, 8 wt.%)

The SEM images of fiber types are depicted in Figure 40. The PVB fibers produced with single jet had the largest mean diameter, probably as a result of the higher concentration of PVB in acetic acid/ethanol (10 wt.%). The mean diameter of the PVB/TTNT fibers was smaller than in the case of the PVB/TTNP fibers, since the nanotubes inside the fibers influenced their elongation (Table 7). The histogram shows that most of the PVB fibers from the multi-needle system were in diameter between 0.2-0.25 μm, while the most of the PVB fibers with TTNT were in the range from 0.15 μm to 2 μm (Figure 41).

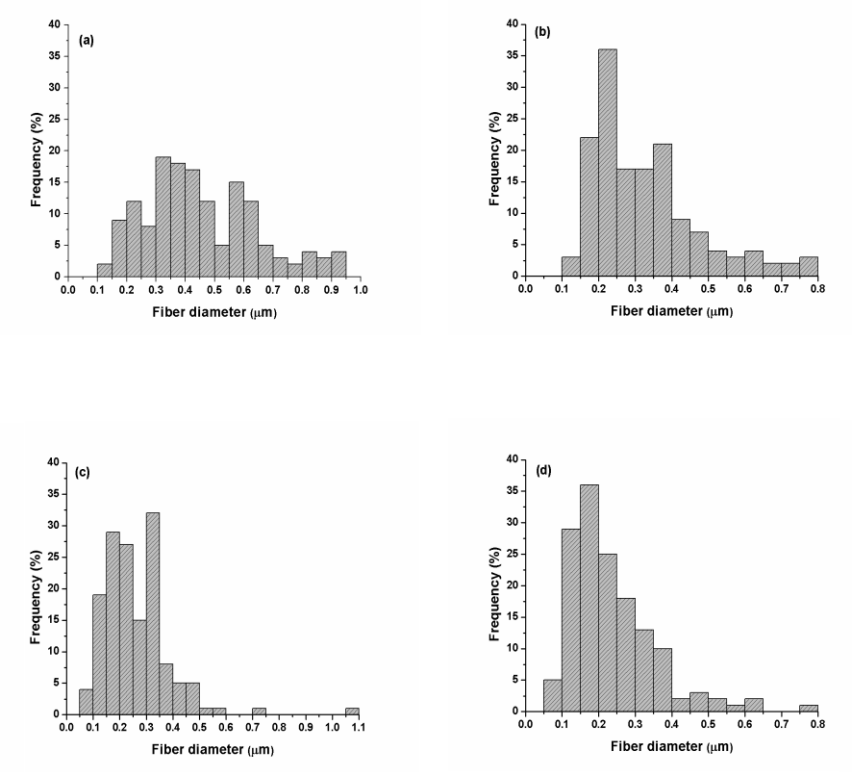

Figure 41. Histogram of fiber diameter distribution: (a) PVB fibers (single-needle, 10 wt.%); (b) PVB fibers (multi-needle, 8 wt.%); (c) PVB fibers with TTNP, (multi-needle, 8 wt.%); (c) PVB fibers with TTNT, (multi-needle, 8 wt.%)

Table 7. Fiber diameter distribution

Parameter	**PVB fibers (single-needle, 10 wt.%)**	**PVB fibers (multi-needle, 8 wt.%)**	**PVB/TTNP fibers (multi-needle, 8 wt.%)**	**PVB/TTNT fibers (multi-needle, 8 wt.%)**
Mean (μm)	0.454	0.328	0.261	0.237
Minimum (μm)	0.128	0.132	0.085	0.053
Maximum (μm)	0.933	0.785	1.085	0.767
Standard deviation (μm)	0.191	0.146	0.127	0.119
Count	150	150	148	147

The average diameters of the electrospun fibers were measured by *Image-Pro Plus 6.0* software (Media Cybernetics).

4.4 Results and Discussion

4.4.1 Antibacterial activity

The antibacterial activity of titania nanocomposite mats was quantitatively evaluated by using the Gram-negative *E. Coli* (ATCC 52922) as a model organism. It is well known that the bactericidal activity of the samples is closely related to the morphology, crystalline structure, and photocatalytic properties of synthesized titania [234]. A previous work [235] has reported modest antimicrobial activity of PVB with TTNPs. Given that different antimicrobial assays were applied, our results are not directly comparable.

However, the apparent higher antimicrobial activity of the materials tested in this study could be attributed to the increased photocatalytic–antibacterial performance of titania, which was stimulated by UV radiation used for sterilization [236]. The UV light was found to be more effective in expediting the antimicrobial activity of titania due to the suitable bandgap energy of UV light and the higher hydroxyl radical concentration on the surface of the materials [237].

Pant et al. [238] compared the photocatalytic oxidation efficiency of TTNP incorporated into the electrospun Nylon-6 fibers and pure TTNP. Their results showed that the photocatalytic efficiency of pure TTNP is almost the same as the photocatalytic efficiency of TTNP loaded in the electrospun Nylon-6 mats. As a result of titania UV irradiation, the reactive oxygen species (OH•, O2•, and HO2•) are generated on its surface [239]. Among them, OH• hydroxyl radical is considered to be the most important oxidizing agent providing inactivation of bacterial cell [240]. According to the obtained results, the maximum amount of active oxygen forms and hydroxide radicals was accumulated during this UV irradiation, which is sufficient for long-term inactivation of *E. coli* bacterial culture. These properties were evaluated after 30 min of UV light exposure.

The diffusion zone diameter for the PVB/TTNP composite mat was 15.6 mm, while this diameter for PVB/TTNT composite mat was 16.4 mm (Figure 42). The results showed that the composite mats with PVB nanofibers incorporating TTNP

exhibited similar zones of inhibition and antibacterial activity compared with the mats containing the TTNT nanofiber composites.

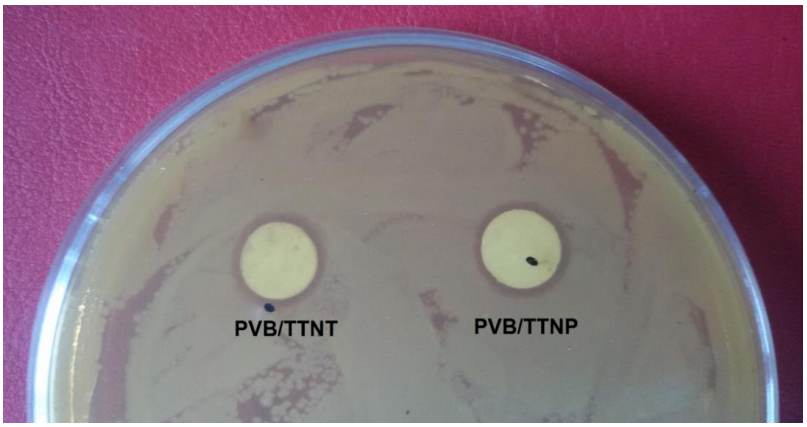

Figure 42. Antimicrobial activity of composite mats after UV irradiation against *E. coli*

4.4.2 Dynamic mechanical analysis

The strength value or the stress/strain ratio is in the form of relative modulus E* which was calculated from the measured data and the sample geometry for a dual cantilever mode. The stainless steel sample holder with dimensions of 60 × 13 × 1 mm (Figure 43) was employed for the characterization of the glass transition temperature of PVB fiber mats [241].

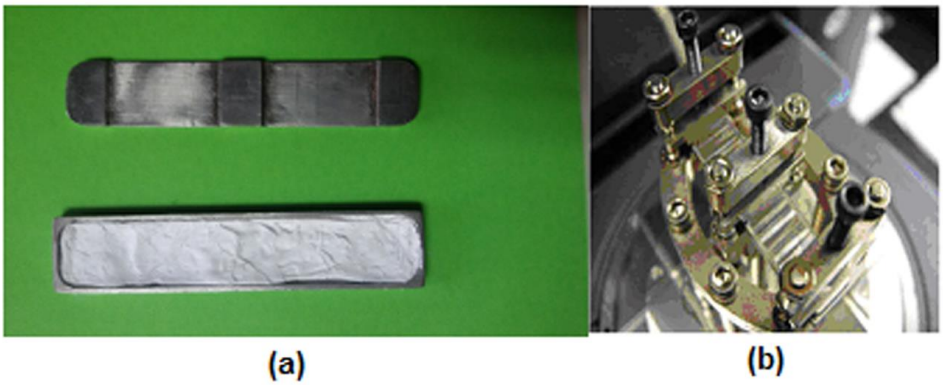

Figure 43. The (a) stainless steel sample holder in the (b) dual cantilever mode

In the glassy state, the modulus remained roughly constant; by increasing the temperature, a sharp drop in the modulus occurred at around 70 °C (Figure 44(a)), which corresponded to the primary relaxation process, glass–rubbery transition. The glass transition temperature was calculated as the onset of the E* drop or as the tan δ peak (Figure 44 (b)), [242].

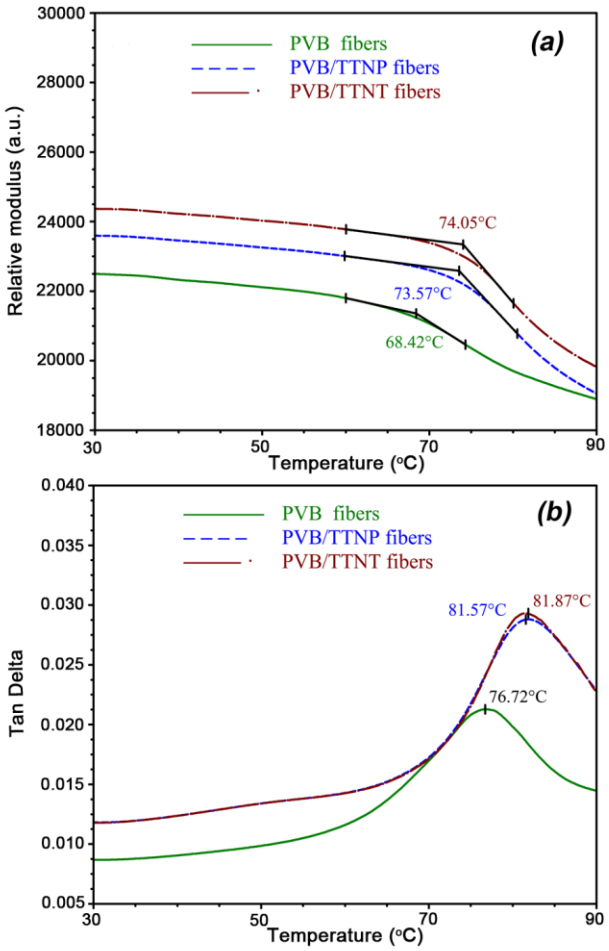

Figure 44. A typical sample holder DMA response for nanofibrous mats showing a comparison between the (a) relative modulus versus temperature signals and (b) Tan Delta versus temperature signals of PVB, PVB/ TTNP, and PVB/TTNT nanofiber mats

These results suggest that the presence of the titania nanofillers decreases the mobility of the polymer chains, which resulted in increase of the glass transition temperature. The temperatures (T_g) of the PVB/TTNP and PVB/TTNT fiber mats

were about 5 °C higher than with the PVB fiber mats, which indicated enhanced mechanical properties (relative modulus) of the PVB fibers with TTNP and TTNT as well (Figure 44(a)).

4.4.3 Nanoindentation testing

Figure 45 is a schematic presentation of the nanoindentation with indentation imprint. The nanoindentation testing of the PVB fiber mats included indentation hardness (H), reduced elastic modulus (E_r), and H/E_r ratio (Figure 45).

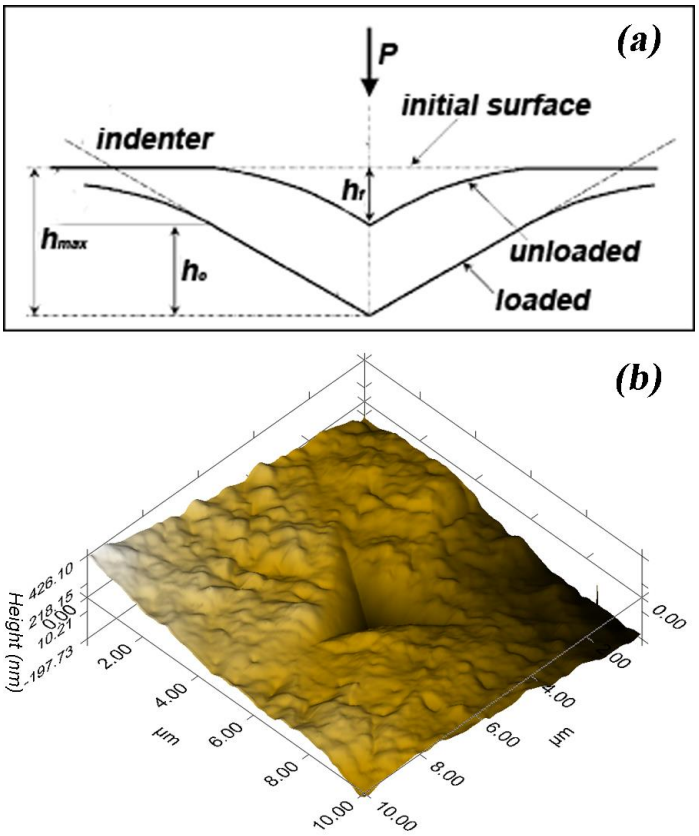

Figure 45. (a) Schematic presentation of indentation cross section and (b) 3D image of the Berkovich nanoindentation imprint.

The reduced elastic modulus and hardness values increased due to the addition of nanoreinforcement, and the best results were obtained with the PVB/TTNT fibers.

The results confirmed that the PVB/TTNP fibers, as well as the PVB/TTNT fibers, gave 80% and 163% improvement in indentation hardness together with 61% and 84% improvement in the reduced elastic modulus, respectively, compared with the neat PVB fibers (produced from the multi-needle system; Table 8).

Table 8. Reduced modulus (E_r) and hardness (H) results for all the samples

Multi-needle mats	H (GPa)	E_r (GPa)	H/E_r
PVB fibers	0.326 (0.204*)	4.823 (1.627*)	0.064 (0.020*)
PVB/TTNP fibers	0.587 (0.243*)	7.749 (1.634*)	0.074 (0.024*)
PVB/TTNT fibers	0.856 (0.371*)	8.914 (1.836*)	0.093 (0.027*)

*- Standard deviation

On the other hand, improved mechanical properties may result from the orientation of nanofibers [243] and the presence of TTNTs into aligned fibers. The highest value for the H/E_r ratio was reached for the PVB/TTNT fibers (0.093) which demonstrated that this configuration was characterized by the best wear resistance [244]. Elastic recovery parameter (*ERP*) is determined as *ERP* (%)=(h_{max}-h_f)/h_{max}×100, where h_{max} is a depth at maximal load in sample and h_f is a nonrecovered depth after unloading the indenter tip from the sample [245] and Fig. 46 (d).

This figure displays load-depth nanoindentation curves for all tested samples. Therefore, with higher *ERP* value, the higher is the elastic recovery of the fiber mats, which implies better elastic behavior of the fibrous material. In contrast, when *ERP* values are low, this implies that the fibrous material mainly presents plastic behavior. *ERP* for PVB fibers was 37%, while for PVB/TTNP fibers and PVB/TTNT fibers it was 49% and 54%, respectively. Due to these results, there was increase in the

hardness compared to unreinforced PVB fibers. The highest hardness is achieved with PVB/TTNT fiber mats. These results were in coherence with the results for reduced modulus and hardness determined by nanoindentation.

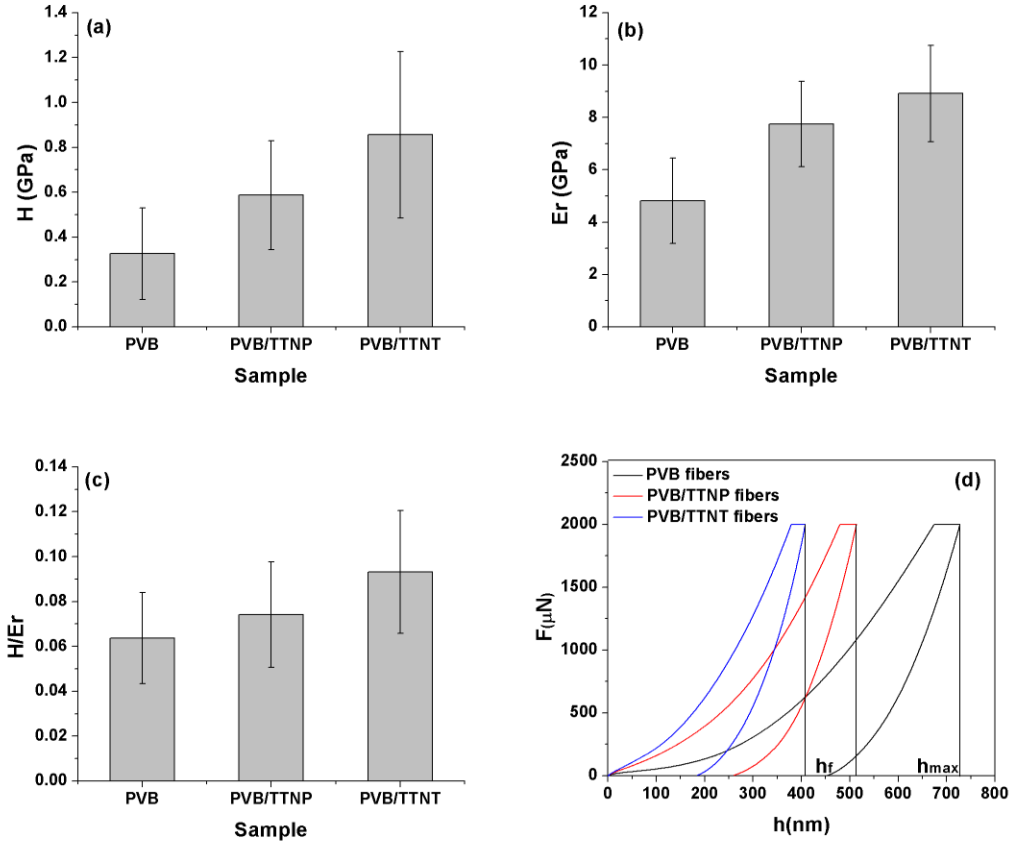

Figure 46. Nanoindentation results for all the samples: (a) hardness, (b) reduced modulus, (c) H/E_r ratio, and (d) load versus depth curves obtained by nanoindentation.

It is very difficult to compare results obtained from DMA and nanoindentation due to technical dissimilarities, different scale of the volumes of deformations and different direction of applied stresses [246]. Comparison of the modulus values obtained by means of DMA with those obtained by means of nanoindentation revealed that the later technique yielded significantly higher values than the former - [247]. The results obtained by nanoindentation were in coherence with the results of

relative modulus verified by dynamic mechanical analysis, confirming the better mechanical properties of the PVB mats with nanoreinforcement in comparison to the neat PVB fibrous material.

4.5 Conclusions

In this study, titania nanoparticles and titania nanotubes were used as reinforcement in electrospun PVB mats, which were produced by single and multi-needle electrospinning system. The thermo-mechanical properties and antibacterial activity against gram-negative *E. coli* was investigated, and characterized using FESEM, TEM, DMA and nanoindentation. The results of this study confirmed the mechanical improvement of the PVB mats with TTNP and TTNT through higher values of the indentation hardness and reduced modulus determined by nanoindenation when compared to the neat PVB mats. It produces the best results for PVB/TTNT composite fibers, with a significant increase in mechanical performance displayed in the increases of indentation hardness 163%, reduced elastic modulus 84% and elastic recovery 54%, respectively. The results obtained by DMA analysis were in coherence with the previous ones, making the PVB mats with TTNT the best one with the thermal and mechanical properties. Beside these properties, PVB/TTNP and PVB/TTNT electrospun composite mats displayed favorable antibacterial activity.

CHAPTER 5

ENHANCEMENT MECHANICAL PROPERTIES OF TRANSPARENT POLY (METHYL METHACRYLATE) THERMOPLASTIC COMPOSITES REINFORCED WITH POLY (VINYL BUTYRAL)/TITANIA NANOFIBERS

5.1 Introduction

Poly (methyl methacrylate) (PMMA) is an important thermoplastic material with excellent transparency, and it has been widely used in optical and porous materials, biomedical materials, dental and surgical applications, and electronics. However, brittleness limits its applications. Many studies have been extensively carried out in order to enhance the physical and mechanical properties of PMMA. Of which polymer-polymer composite is a promising approach, which incorporates polymer fibers into the PMMA polymer matrix to provide the toughening mechanisms for the composite. The fibers can redistribute the stress load on the composite and the small inter-fiber distance can stop crack propagation in the composite [248, 249]. In recent years, electrospun nanofibers have attracted interest as reinforcements for composite materials due to their small diameter (20 nm - 1μm) and high aspect ratio. Electrospun nanofibers have been evaluated as reinforcements in polymer matrices such as polyvinyl alcohol (PVA), styrenebutadiene rubber, epoxy resin, melamine formaldehyde resin, thermoplastic polyurethane, etc.. So far very few studies have reported the mechanical properties for electrospun composite nanofibers that are ideal candidates as reinforcement fillers [250].

Nanocomposite fibers constitute a new class of materials in which the polymeric nanofibers are reinforced by dispersed inorganic fillers with at least one dimension in nanometer-scale. In addition, electrospinning has the following

advantages: (a) the diameters of fibrous materials are reduced from micrometers to nanometers (b) it can produce nanofibrous mats with large surface area to mass ratio for better bonding and excellent mechanical strength of the matrix material; (c) it allows the nanoparticles to disperse in the spin solution; and (d) it does not compromise the chemical stability of the nanoparticles during spinning and composite fabrication [251].

The scope of this work is to demonstrate the feasibility of making high performance poly (vinyl butyral)/titania nanofiber reinforced composites with optimized optical and mechanical properties. To the best knowledge of the authors, this is the first time the preparation of electrospun nanofibers filled polyvinyl bytura/TiO_2 nanofibers composites has been reported. The PVB/TiO_2 nanofibers were embedded into PMMA/MMA/AIBN solution to fabricate reinforced composite films by polymerization technique. The mechanical and optical properties of PMMA composite films steadily improved with 20 wt. % polyvinyl bytura/TiO_2 nanofiber content. This study will pave a new way towards preparing high performance PMMA/PVB/TiO_2 composites for superior structural properties. In this study, to demonstrate the feasibility for the preparation of transparent poly (methyl methacrylate) (PMMA) electrospun nanofiber composites. Poly (vinyl butyral) (PVB) has the same refractive index as PMMA, and as a result, the PMMA/PVB nanofiber composites were completely optical clear. The reinforcing and toughening effects of PVB/TiO_2 nanofibers on PMMA matrix were investigated. Transparent PMMA electrospun nanofibers composites exhibit improved mechanical properties compared to the initial polymers. At a titania content of 3 wt.% and 5 wt.% TiO_2 nanoparticles, the indentation hardness (H) and reduced modulus (E_r) of the transparent nanocomposites increased slightly by 24% and 28%, and 60% and 35%, respectively. However, the fracture toughness dramatically improved by 55% at nanoparticles additions of 3 wt. %, while the transmittance of the nanocomposite maintained above 75-80% in the visible light wavelength range of 400– 800 nm.

5.2 Experimental part

5.2.1. Materials

PVB (Mowital B75H, Kuraray) is a resin usually used for applications that require strong binding, optical clarity, adhesion to many surfaces, toughness and flexibility. The experiments were carried out with the PVB solution in a concentration of 8 wt. % where acetic acid/ethanol was used as the solvent for production neat and composite nanofibers (Chapter 4). Commercially available PMMA Acryrex® CM205 (Chi Mei Corp., Taiwan) pellets, liquid monomer (methyl methacrylate, (MMA) and 2,2 Azobisisobutyronitrile (AIBN) initiator (Sigma Aldrich)), were used for preparing samples. Commercial TiO_2 powder (Aeroxide P25) with a mean diameter of 21 nm was obtained from Evonik-Degussa, Germany.

5.2.2. Composite fabrication

The neat PVB mat and PVB mat reinforced TiO_2 nanoparticles (20 wt.%) was soaked in the PMMA/MMA/AIBN solution for 3 h in the aluminum mold, followed by drying in a vacuum oven at room temperature for 20 min. and cured at 55 °C about 10 h.

5.3 Characterizations

The influence of the poly(vinyl butyral)/titania nanofibers on the mechanical and optical properties PMMA were studied using nanoidentation measurements, while the influence on the optical properties were studied using UV-Vis spectroscropy.

5.3.1 Nanoindentation of PMMA composite film

The mechanical properties of neat PMMA and PMMA composite film were tested using a a Hysitron TI 950 TriboIndenter equipped with *in situ* SPM imaging

(Hysitron, MN). A Berkovich indenter was used, and the indentation hardness, reduced elastic modulus and fracture toughness were calculated and recorded from nine different testing points. The analysis of nanoindentation data was performed using the Oliver and Pharr method, assuming a value of 0.45 for the Poisson's ratio. The indentation maximum load was set at 2 mN for each tested sample. The loading and unloading times as well as the hold time at the peak force were all set to 25 s.

5.3.2. Optical properties

Optical transmission spectra of the various kinds of prepared composite films and pure polymer films as a control were measured in VIS and IR ranges using DU 720 General purpose UV-VIS spectrometer in the wavelength range from 200 to 1100 nm.

5.4 Results and discussion

5.4.1 Mechanical Considerations

Indentation testing at nanoscale was used to investigate the nanomechanical properties, including indentation hardness (H), reduced elastic modulus (E_r), and fracture toughness (K_c) of the neat PMMA and PVB/PMMA/TiO_2 nanocomposites. Prior to experiments, the tip area function was calibrated by using Oliver and Pharr method with a standard alumina and fused quartz sample. The nanoindentation tests were operated in force-control mode where the load applied was controlled according to a programmed loading function.

$$P = A\left(h - h_f\right)^m \quad (1)$$

where h_f is the residual penetration depth and A is the projected contact area.

The derivative of the power law relation (with respect to h) is evaluated at the maximum load to calculate contact stiffness (S). The contact depth, h_c, is calculated with:

$$h_c = h_{\max} - 0.75 \times \frac{P_{\max}}{S} \quad (2)$$

where h_{max} was taken as the maximum penetration depth achieved after the holding period. The indentation hardness, H, is determined from the maximum load, P_{max}, divided by the projected contact area A at the contact depth h_c:

$$H = \frac{P_{\max}}{A(h_c)} \quad (3)$$

The reduced modulus is obtained from:

$$E_r = \frac{\sqrt{\pi} S}{2\sqrt{A(h_c)}} \quad (4)$$

The relationship between indentation modulus, E, and the reduced modulus, E_r, of the sample is given by:

$$\frac{1}{E_r} = \frac{\left(1 - \nu^2\right)}{E} + \frac{\left(1 - \nu_i^2\right)}{E_i} \quad (5)$$

where E and ν are, respectively, the elastic modulus and the Poisson's ratio ascribed to the tested sample, whereas E_i and ν_i are the same parameters for the indenter. In this work ν was set as 0.45, E_i and ν_i are equal to 1140 GPa and 0.07 for Berkovich diamond tips, respectively. The indentation maximum load is set to be 2000 μN for each tested samples; at least nine indents were performed at different points on the surface.

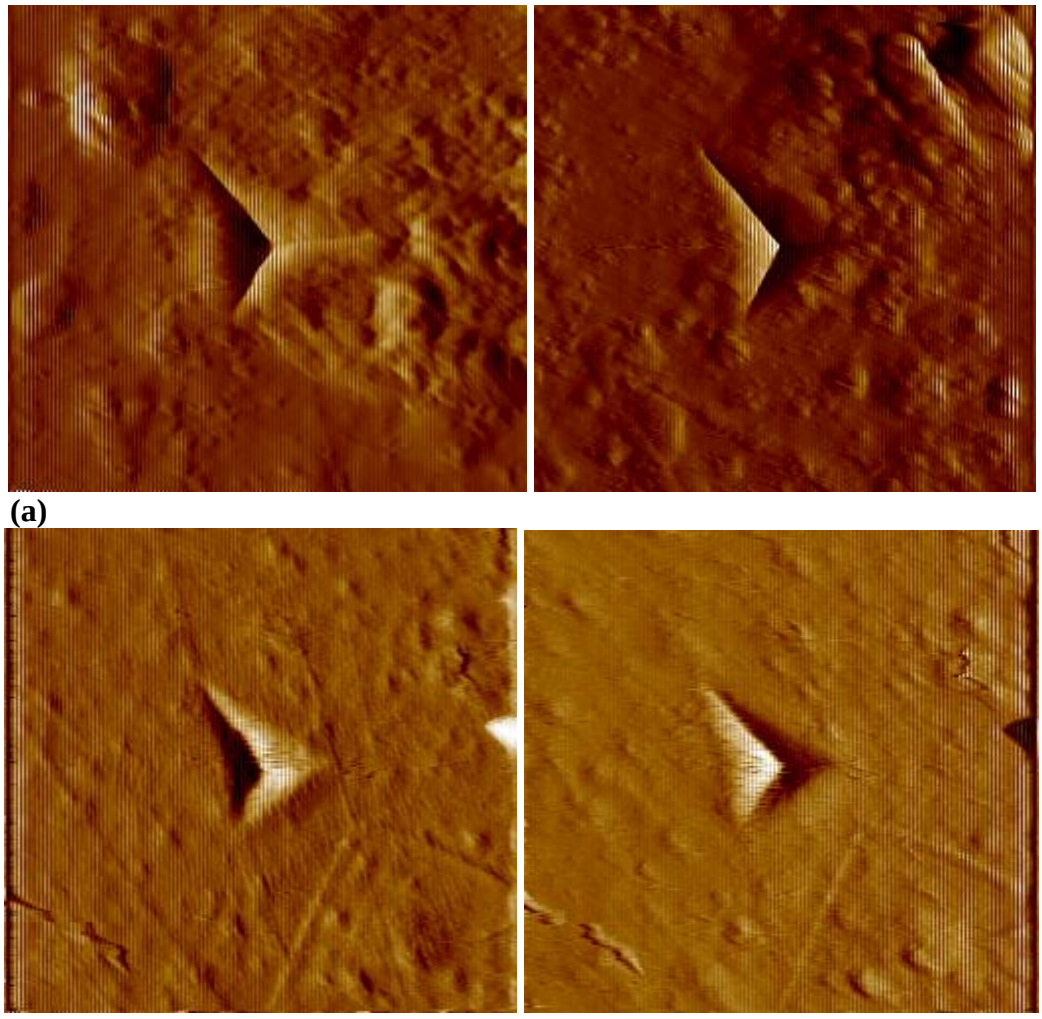

Figure 47. Gradient *in-situ* SPM images (scan size of 10×10 µm) of (a) neat PMMA and (b) PMMA/PVB/TiO_2 nanocomposites

The fracture toughness can be calculated from the indentation hardness, reduced elastic modulus, and the length of the crack size after nanoindentation:

$$K_c = k\left(\frac{E_r}{H}\right)^n \frac{P_{\max}}{c^{3/2}} \qquad (6)$$

where k is a calibration constant (0.016 for sharp indentation geometries, such as Berkovich), the value of the exponent n was estimated to be ½, c is the length of the

surface radial crack (as measured from the center of the indentation to the crack tip using *in-situ* SPM images) and P_{max} is the maximum applied load [252].

Table 9. Nanomechanical properties of neat PMMA and PMMA/PVB/TiO_2 nanocomposites

Samples	***H*/GPa**	***E*$_r$/GPa**	***K*$_c$/MPa m$^{1/2}$**
(a) Neat PMMA	4.27 (0.060)	0.229 (0.208)	2.73 (0.128)
(b) PMMA/PVB/$TiO_2$3wt. %	5.76 (0.188)	0.366 (0.343)	4.24 (0.154)
(c) PMMA/PVB/TiO_2 5wt.%	5.05 (0.676)	0.284 (0.717)	3.16 (0.495)

Values in parentheses indicate (±) standard deviations

The resulting PMMA/PVB/TiO_2 composite containing 3 wt.% nanoparticles showed an increase in hardness by 35% and elastic modulus by 60% relative to neat PMMA, as determined using the nanoindentation technique.

The results in the Table 9 indicate that PMMA/PVB/TiO2 composite containing 3 wt% and 5 wt.% nanoparticles have significantly higher fracture toughness compared with the neat polymer (2.73 (0.128), 4.24 (0.154) and 3.16 (0.495)) MPa m$^{1/2}$, respectively.

5.4.2. Optical Considerations

The transmission of polymer composite films depends on scattering and absorption of light by the particles, as well as, absorption of light in the pure matrix polymer itself.

The amount of scattered and absorbed energy on the single particle related to the incident radiation is expressed in terms of scattering and absorption cross sections. The total energy loss based of both processes is called extinction and it is presented by extinction cross section as a sum of scattering and absorption cross sections [253].

One way of presenting both propagating and absorbing properties of a material for some kind of electromagnetic radiation is to introduce complex index of refraction. The existence of the imaginary part of the index of refraction shows that the material is absorbed for that kind of electromagnetic radiation and its value directly influences the absorption coefficient of the material [253].

In the case of non-absorbing medium the scattering and extinction cross section are the same, and the complex part of the index of refraction is zero or almost zero.

Materials used both as a matrix or reinforcement for the described polymer composites in this research were non absorbing so in order to predict transmission coefficients the scattering properties of particles, ie. the scattering cross section should be calculated.

5.4.3 Theory and model

The scattering cross section is defined as a ratio of scattered radiation power, Ps on the particle and radiation flux density F_{in} incident on it [254]:

$$\sigma_s = \frac{P_s}{F_{in}} \tag{7}$$

One way to calculate scattering cross section is to use Mie scattering theory. It presents the solution for the electromagnetic scattering by a sphere of radius *R* embedded in a homogeneous and isotropic medium illuminated by a plane wave. If the index of refraction of a particle material is n_p, and of medium n_m, for some electromagnetic radiation of wavelength λ_0 in vacuum, the scattering cross section depends on: size parameter which compare dimension of a particle and medium wavelength, given as $\chi=2\cdot\pi\cdot R\cdot n_m/\lambda_0$, for spherical particle, and ratio of indices of refraction of particle and medium given as $m=n_p/n_m$ [254].

This calculation based on my theory is very complicated using the sum of the parameters obtained using special functions. And generally they are infinite power

series of χ. There is a nowadays lot of developed softwares for calculation of scattering cross section.

The values for the particular composite can be obtained using Mie scattering calculator [255], a free software.

If the size parameter $\chi \leq 1$, than the Mie calculated solutions can be approximated with Rayleigh scattering model values. Rayleigh scattering cross section is given by equation (8):

$$\sigma_s = \frac{128 \cdot \pi^5}{3} \cdot \left(\frac{m^2-1}{m^2+2}\right) \cdot \frac{r^6}{\lambda^4} \tag{8}$$

where $r=d/2$ represents particle radius [249].

For the composites prepared in this research, where particle and agglomerate in composites are from 20 to 140 nm and using the indices of refraction of the matrix and particles to calculate scattering cross section based on Rayleigh and Mie theory, the values are similar and differ up to 10% for larger particles. So for this kind of composite the Rayleigh theory should be used for less precise calculations.

In the following text, the scattering cross section calculated using Mie theory is denoted as σ_{sM}.

If particles in a composite are spherical with diameter d, their number concentration in a polymer is n_d, and their scattering cross section at a wavelength λ_0 is σ_{sM}, the scattering coefficient of the polymer composite sample at that wavelength γ_S can be obtained as:

$$\gamma_s = n_d \cdot \sigma_{sM}. \tag{9}$$

The total volume of all particles in the composite is denoted as V_p and it is connected with composite volume V_{comp} as:

$$V_p = f_V \cdot V_{comp} \tag{10}$$

where f_V is a total volume fraction of particles. If the volume of one spherical particle of diameter d is

$$V_d = \pi \cdot \frac{d^3}{6} \tag{11}$$

then, total particle volume is:

$$V_p = N_d V_d = N_d \cdot \pi \cdot \frac{d^3}{6} = f_V \cdot V_{comp} \tag{12}$$

and number concentration:

$$n_d = \frac{N_d}{V_{comp}} = \pi \cdot \frac{d^3}{6} = \frac{f_V \cdot 6}{\pi \cdot d^3}. \tag{13}$$

If two parallel planes, at distance *L*, inside a polymer composite are imagined and if I_0 is the intensity of incoming light at first plane and *I* is the intensity of transmitted light reaching the second plane, the transmission coefficient T can be calculated as [253]:

$$. T = \frac{I}{I_0} = e^{-\gamma_S \cdot L} \tag{14}$$

Thus obtained value T in equation (14) is the transmission or the transmission coefficient of the composite sample normalized to the transmission of the pure polymer sample of the same width and for the same wavelength. In order to calculate the transmission spectra of a sample normalized to the air, calculated transmission *T* should be multiplied with the transmission coefficients of the pure polymer film of the same width.

5.4.4 Calculation of the transmission coefficient of polymer composites

The calculations were done using Mie calculator software [255] for spherical particles and the concentration was given in $1/\mu m^3$ unit. Input data for the calculations were: mass density of PMMA ρ_{PMMA} = 1.18 g/cm^3, mass density of PVB ρ_{PVB} = 1.075 g/cm^3 and mass density of TiO_2 ρ_{Ti} = 3.915 g/cm^3. Based on those data

the total volume fraction f_V of TiO_2 in composite samples is calculated based on Equation (15) [253]:

$$f_V = \frac{\rho_{pol} \cdot f_W}{(1-f_W) \cdot \rho_{Ti} + \rho_{pol} \cdot f_W} \quad (15)$$

where f_W represents the total mass fraction of particles in the polymer composite, ρ_{pol} is a mass concentration of a matrix polymer. The values of f_w for the polymer composite in the research were 3 w.%t or 5 wt. %.

The indices of refraction values for used materials were taken from the literature [256].

Since the imaginary parts of indices of refraction for TiO_2 and used polymers were zero, obtained scattering coefficients are the same as the extinction coefficients of the samples.

Transmission for four different samples are calculated and compared with the measured ones.

The calculation was done for four samples. Sample No1. has pure PVB as matrix and 3 wt.% of T_iO_2 particles. Sample No. 2 has the same particles and matrix but the mass fraction of particles is 5 wt.%. Sample No. 3 was made from PVB nanofibers with 3 wt.%. of TiO_2 particles in the pure PMMA matrix.The nanofibers mass fraction in a composite is 20 wt.%. The sample No.4 was made from the similar nanofibers but the mass fraction of T_iO_2 in the nanofibers was 5 wt%. Than mass fraction of nanofibers in the pure PMMA matrix was 20 wt.%.

A) Calculation of the transmission coefficient of polymer composites with pure PVB as matrix and TiO_2 particles (samples No.1 and No.2).

The scattering cross sections σ_{sM} were calculated with Mie scattering calculator for spherical particles of various diameter *d*, where *d* was taken in the range 20 nm–140 nm at 10 nm steps, and for wavelengths from 450 nm to 1100 nm in 50 nm steps. This range of diameters is chosen based on SEM images.

The nominal value of the real particle diameter before embedding is 21 nm and the calculations were done for this diameter too.

In this type of calculation, it is supposed that all the particles in the composite have the same value, and the mass of particles is the same for all samples.

Then for sample No.1 with 3 wt.% of particles, the f_v is calculated, and based on this value the number concentrations n_d using Equation (13) is obtained.

Taking into account that the thickness of a composite films was L=1mm, the transmission coefficients are calculated for different diameters versus wavelength using Equation (14). Thus calculated values represent the transmission coefficient versus pure polymer transmission. In order to get transmission coefficients normalized to air transmission, the obtained values were multiplied with the measured transmission of pure polymer (in this case pure PVB films of 1 mm thickness).

In case of comparing composite samples based on the same polymer matrix it is more often to measure or calculate transmission normalized to transmission of pure polymer. Since our composite samples are based on different polymer matrices, their transmissions, normalized to the air, are compared mutually and compared to the corresponding measured values.

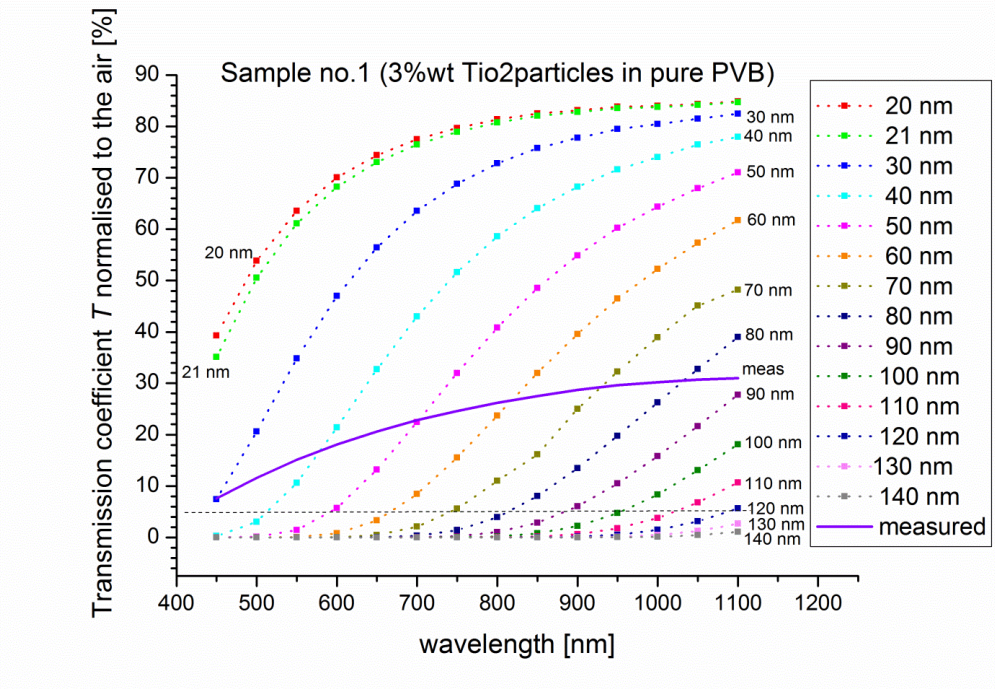

Figure 48. Transmission coefficients vs. wavelength for sample No.1

Graphs at Figure 48 represent the dependence of transmission coefficients of sample No.1 versus wavelength, for different diameters of embedded particles. As a comparison the measured transmission versus wavelength of the sample No.1 is presented at the same graph as a solid line.

For every wavelength there is characteristic maximum particle diameter value enabling the transmission coefficient at least 5% or greater. For example, for 450 nm wavelength particles should be smaller than 30 nm, for 600 nm smaller than 70 nm, etc. Also from the graph in Figure 48 it is obvious that when all particles are greater than 100 nm the transmission at all wavelengths in the range is below 5%.

So, since the measured transmission matches the calculated values for different diameter values it is obvious that the diameters of the particles in a real composite are in some range and have some diameter distribution. The rough comparison of measured and calculated results based transmission match on different diameters shows that range of particle diameters that most influence the transmission is from 20 to 90 nm.

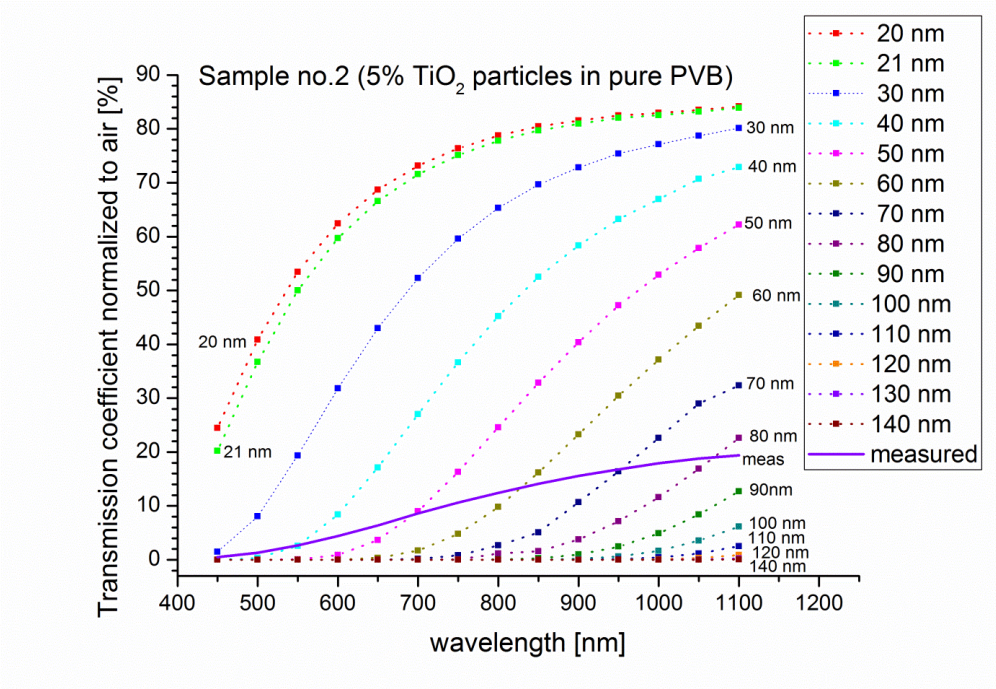

Figure 49. Transmission coefficients vs. wavelength for sample No.2

In Figure 49 the similar results are presented for sample No.2. Transmissions are generally smaller because of the greater mass fraction of particles. The comparison of measured and calculated values roughly shows that particles are in range from 30 nm to 90 nm.

B) Calculation of the transmission coefficient of polymer composites with TiO_2 - PVB nanofibers and pure PMMA matrix particles (samples No.3 and No.4).

Since in this polymer composites the mass fraction of TiO_2 is 3 wt.% or 5 wt.% in fibers, and the fibers are 20 wt.% mass fraction of the polymer composites with PMMA matrix. The real TiO_2 particles have 0.6 wt.% (sample No.3) or 1 wt.% (sample No.4) in the composite and the matrix consist respectively, of the 19.4 wt.% or 19 wt.% of pure PVB and 80 wt.% of pure PMMA. These data are used for f_v calculations for those two samples.

In Figure 50, the graphs represent obtained calculated transmission values for different diameters of the particles for the sample No.3. Also the measured transmission coefficient versus wavelengths for real sample is presented as a solid line. In this case it is obvious that smaller diameter particles have greater influence on transmission and their roughly estimated range is from 20 to 40 nm.

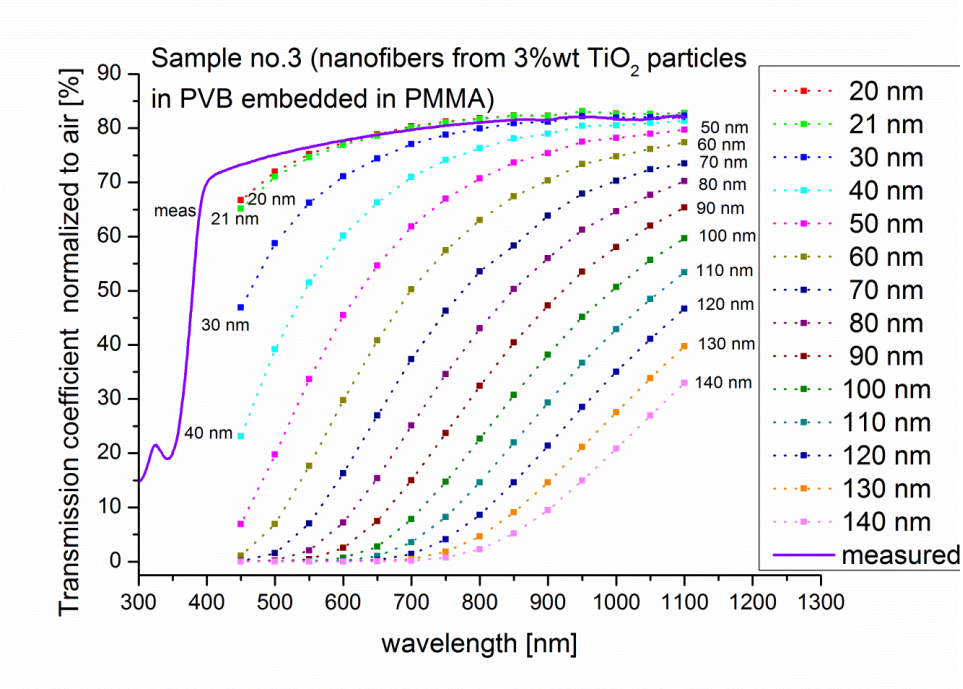

Figure 50. Transmission coefficients vs. wavelength for sample No.3

In Figure 51 the similar graphs for sample No.4 are presented. The calculated and measured transmission coefficients are smaller than of sample No.3 as expected. Estimated particles diameter range based on comparison of measured and calculated transmission coefficients is from 30 to 60 nm.

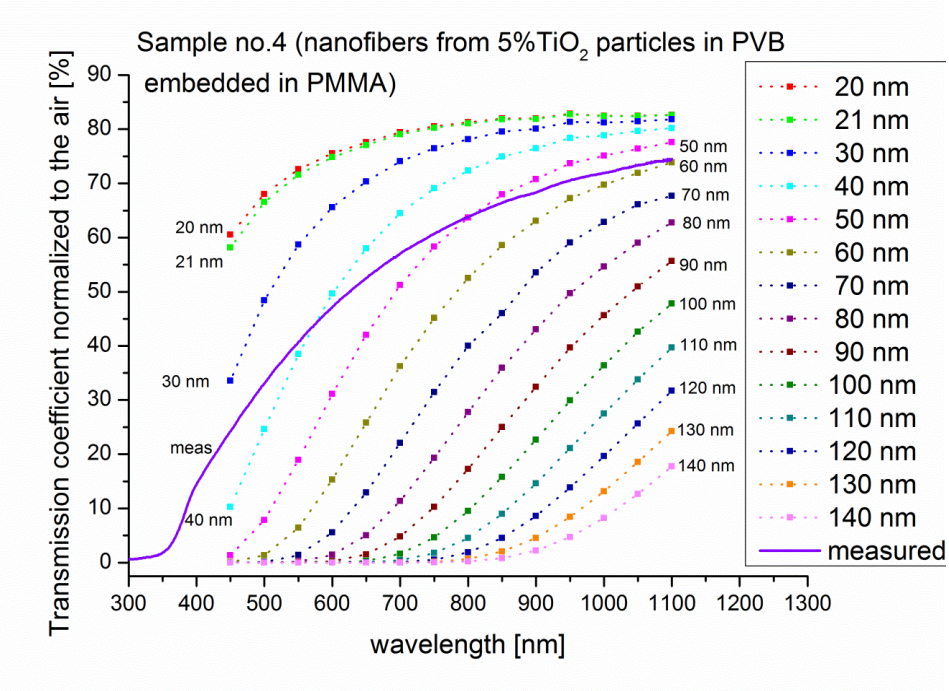

Figure 51. Transmission coefficients vs. wavelength for sample No.4.

Comparing graphs for different kind of particles, it can be concluded that composites from nanofibers have smaller agglomerates of the same type of particles.

The purpose of this research was to evaluate the mechanical and optical properties of PMMA based composites reinforced with poly (vinyl butyral)/titania nanofibers. Moreover, the effect of different contents of poly (vinyl butyral)/titania nanofibers on the mechanical and optical properties of the composites as well as a comparative study of the mechanical and optical properties of the composites have also been conducted in this work.

5.5 Conclusion

Poly(methyl methacrylate) was used as a matrix and two contens of nanofillers were added into the matrix to form the hybrid composites The concentration of TiO_2 particles were 3 wt.%, 5 wt.% in the PVB nanofibers while the total concentration of PVB/titania nanofibers in PMMA/MMA/AIBN solution were 20 wt%. In this work, we investigated polymerization techniques for the manufacture of functional electrospun nanofiber composites with optimized mechanical and optical properties. These processing methods are effective for achieving good dispersion of nanofillers and coherent nanofiber−matrix interfaces, with further functionality demonstrated for optically transparent electrospun nanofiber composites. The addition of poly (vinyl butyral)/titania nanofibers into acrylic matrix clearly show improvement in fracture toughness properties.

REFERENCES

[1] K. J. Anusavice, R. W. Phillips. Phillips' science of dental materials. 12th ed. St. Louis: W.B. Saunders (2012).

[2] J. F. McCabe, A. W. G. Walls, Applied Dental Materials, 9th edition (2013).

[3] K. J Söderholm, Fracture of Dental Materials, Applied Fracture Mechanics, Dr. Alexander Belov (Ed.), (2012). DOI: 10.5772/48354. Available from: http://www.intechopen.com/books/applied-fracture-mechanics/fracture-of-dental-materials

[4] R. G. Craig, J. M. Powers, R. L. Sakaguchi, Craig's restorative dental materials. 13th ed. St. Louis: Mosby Elsevier; 2012.

[5] R. Rudolf, I. Anžel, D. Stamenković, *MJoM*, 135-142. UDC:611.314:615.464/.465.001.575=20

[6] https://pocketdentistry.com/7-general-classes-of-biomaterials/

[7] M. Gladwin, M. Bagby. Clinical Aspects of Dental Materials. 4th ed. Lippincott Williams & Wilkins; Auflage: 4. Auflage, (2012).

[8] I. Denry, J.A. Holloway, *Materials* **2010**, *3*, 351-368. doi:10.3390/ma3010351

[9] M. S. Spiller. Dental composites: A Comprehensive Review. Albany, NY 12212, (2012).

[10] B. Zimmerli, M. Strub, F. Jeger, O. Stadler, A. Lussi, *Schweiz Monatsschr. Zahnmed.* **2010**, *120* (11), 972-986.

[11] I. D. Sideriou, D. S. Achilias, *J. Biomed. Mater. Res. Part B: Appl. Biomater.* **2005**, *74B*, 617-626.

[12]https://adohta.net.au/webroot/filebrowser/upload/files/PS9%20Restorative%20Materials.pdf

[13] Y. Ucar, W. Brantley, *Int. J. Dent.* **2011**, 1-7.

[14] K. H. S. Chan,Y. Mai, H. Kim, K. C. T. Tong, Desmond Ng, J. C. M. Hsiao, *Materials (Basel)* **2010,** *3*(2), 1228-1243.

[15] Glass Ionomer Cements. Available at: http://airforcemedicine.afms.mil/idc/groups/public/documents/afms/ctb_108335.pdf.

[16] M. Dehghan, A. D. Braxton, J. F. Simon, An Overview of Permanent Cements, Inside dentistry site, November **2012**, *8* (11).

[17] S. Y. Cho, A. C. Cheng, *JCDA*, October **1999**, *65*(9), 491-495.

[18] https://pocketdentistry.com/6-restorative-paediatric-dentistry/

[19] A. Shenoy, N. Shenoy, *J. Conserv. Dent.* **2010**, *13*, 195-203.

[20] S. Nandini, *J. Conserv. Dent.* **2010**, *13*(4), 184-194.

[21] A. Gupta, EJBPS, **2018**, *5*(4), 360-363.

[22] http://www.drjjalvarez.com/dental-materials-2/gold/

[23] https://pocketdentistry.com/2-properties-used-to-characterise-materials/

[24] https://www.slideshare.net/physics101/mechanical-properties-of-matter

[25] C. Luebkeman, D. Peting, Stress–strain curves. Retrieved from http://pages.uoregon.edu/struct/courseware/461/461_lectures/461_lecture24/461_lecture24.html.

[26]http://www.learneasy.info/MDME/MEMmods/MEM30007A/properties/Properties.html

[27] A. Ramalho, J. Miranda, *Wear* **2006**, *260*, 361-367.

[28] H. Chai, JJ-W Lee, P. J. Constantino, P. W. Lucas, B. R. Lawn, *Proc. Natl. Acad. Sci. USA* **2009**, *106*, 7289-7293.

[29] B. R. Lawn, JWJ-W Lee, H. Chai, *Annu. Rev. Mater. Res.* **2010**, *40*, 55-75.

[30] A. Lee, L. H. He, K. Lyons, M. V. Swain, *J. Oral. Rehabil.* **2012,** *39*, 217-225.

[31] L. Piccoli, L. Konstantinos Besharat, M. Cassetta, G. Migliau, S. Di Carlo, G. Pompa, *Ann. Stomatol. (Roma)* **2014**, *5*(2), 52-60.

[32] Z. Zhou, J. Zheng, *J. Phys. D: Appl. Phys.* **2008**, *41*, 113001.

[33] J. Zheng, Z. R. Zhou, *Tribol. Int.* **2007**, *40*, 278-284.

[34] American Dental Association: Dental product spotlight: Dental shade guides. *J. Am. Dent. Assoc.* **2002**, *133*, 366-367.

[35] J. R. Calamia, M. S. Wolff, R. J. Simonsen, Dental Clinics of North America: Successful Esthetic and Cosmetic Dentistry for the Modern Dental Practice. Elsevier Saunders Inc., (2007).

[36] S. Chu, A. Devigus, A. Mieleszko, The Fundamentals of Color: Shade Matching and Communication in Esthetic Dentistry. Carol Steam, IL, Quintessence, 2004.

[37] C. J. Goodacre, R. D. Paravina, S. F. Bergen, J. D. Preston. A contemporary guide to color and shade selection for prosthodontists. American College of Prosthodontists, (2009).

[38] https://pocketdentistry.com/physical-and-chemical-properties-of-solids-2/

[39] K. J. Anusavice, C. Shen, H. Ralph Rawls. Phillips' Science of Dental Materials. 12th ed, Elsevier Saunders Inc, (2013).

[40] R. Paravina, J. Powers. Esthetic Color Training in Dentistry. 1st Edition, Mosby, July (2004). eBook ISBN: 9780323087667

[41] http://www.ndhu.edu.tw/ezfiles/29/1029/img/2481/Chapter21-OpticalProperties.pdf

[42] E. D. Palik. Handbook of Optical Constants of Solids. Chapter 2 - Refractive Index. Academic Press, (1997), Pages 5-114. ISBN 9780125444156

[43] D. Upadhyay, M. A. Panchal, R. S. Dubey, V. K. Srivastava, *Mater. Sci. Eng. A* **2006**, *432*, 1-11. doi:10.1016/j.msea.2006.05.003

[44] D. F. Williams, *ACS Biomater. Sci. Eng.* **2017**, *3*(1), 2-35.

[45] J. C. Wataha, *J. Prosthet. Dent.* **2001**, *86*(2), 203-209.

[46] C. R. Lanza, C. A. de Souza Costa, M. Furlan, A. Alécio, J. Hebling, *Cell Biol. Toxicol.* **2009**, *25*, 533-543.

[47] L. Bianchi, A. P. Ribeiro, M. R. de Oliveira Carrilho, D. H. Pashley, C. A. de Souza Costa, J. Hebling, *J. Dent. Mater.* **2013**, *29*, 980-990.

[48] J. C. Wataha, *Dent. Mater.* **2012**, *28*, 23-40.

[49] J. M. Anderson, *Annu. RevMater. Sci.* **2001**, *31*, 81-110.

[50] C. A. S. Costa, J. Hebling, C. T. Hanks, *Dent. Mater.* **2000**, *16*, 188-197.

[51] I. A. Mjör, *J. Oral Rehabil.* **2007**, *34*, 907-912.

[52] S. C. Bayne, *J. Oral Rehabil.* **2007**, *34*, 921-932.

[53] G. Schmalz. Determination of biocompatibility. In: G. Schmalz, D. Arenholt-Bindslev. Biocompatibility of dental materials. Springer; (2010), pp. 13-40.

[54] J. C. Wataha, *J. Prosthet. Dent.* **2001**, *86*, 203-209.

[55] S. C. Bayne, *Dent. Mater.* **2012**, *28*, 52-71.

[56] J. M. Anderson, *Annu. Rev. Mater. Sci*. **2001**, *31*, 81-110.

[57] T. Subbiah, G. S. Bhat, R. W. Tock, S. Pararneswaran, S. S. Ramkumar, *J. Appl. Polym. Sci.* **2005**, *96*, 557-569.

[58] C. S. Ki, D. H. Baek, K. D. Gang, K. H. Lee, I. C. Um, Y. H. Park, *Polymer* **2005**, *46*, 5094-5102.

[59] A. Rogina, *Appl. Surf. Sci.* **2014**, *296*, 221-230.

[60] A. Welle, M. Kroger, M. Doring, K. Niederer, E. Pindel, S. Chronakis *Biomaterials* **2007**, *28*, 2211-2219.

[61] D. H. Reneker, A. L. Yarin, H. Fong, S. Koombhonge, *J. Appl. Phys.* **2000**, *87*, 4531-4547.

[62] X.-H. Qin, Y.-Q. Wan, J.-H. He, J. Zhang, J.-Y. Yu, S.-Y. Wang, *Polymer* **2004**, *45*, 6409-6413.

[63] F. K. Ko, S. Sukigara, M. Gandhi, J. Ayutsede, Electrospun carbon nanotube reinforced silk fibers. US patent no. 0082197; 2007.

[64] A. Baji, Y-W Mai, S-C Wong, M. Abtahi, P. Chen, *Compos. Sci. Technol.* **2010**, *70*, 703-718.

[65] S. K. Tiwari, S. S. Venkatraman, *Mater. Sci. Eng.*: *C* **2012**, *32*, 1037-1042.

[66] Jian Yao, C. W. M. Bastiaansen, T. Peijs, *Fibers* **2014**, *2*, 158-187. doi:10.3390/fib2020158

[67] J. M. Deitzel, J. D. Kleinmeyer, J. K. Hirvonen, N. C. BeckTan, *Polymer* **2001**, *42*, 8163-8170.

[68] V. Ciobotaru, D. Avram, F. Pantilimonescu, *AUO-FMTE* **2014**, *15*(2), 39-42.

[69] X. Yuan, Y. Zhang, C. Dong, J. Sheng, *Polym. Int.* **2004**, *53*(11), 1704-1710. doi:10.1002/pi.1538

[70] C. S. Ki, J. W. Kim, J. H. Hyun, K. H. Lee, M. Hattori, D. K. Rah, Y. H. Park, *J. Appl. Polym. Sci.* **2007**, *106*(6), 3922-3928.doi:10.1002/app.26914

[71] Z. Li, C. Wang, Chapter 2: Effects of Working Parameters on Electrospinning, One-Dimensional Nanostructures, Springer Briefs in Materials, (2013). DOI: 10.1007/978-3-642-36427-3_2

[72] A. K. Haghi, M. Akbari, *Phys. Status. Solidi.* **2007**, *204*, 1830-1834.

[73] G. Eda, S. Shivkumar, *J. Appl. Polym. Sci.* **2007**, *106*(1), 475-487. doi:10.1002/app.25907

[74] Q. Yang, Z. Li, Y. Hong, Y. Zhao, S. Qiu, C. Wang, Y. Wei, *J. Polym. Sci., Part B: Polym. Phys.* **2004**, *42*(20), 3721-3726. doi:10.1002/polb.20222

[75] https://www.slideshare.net/beckerbudwan/fabrication-of-semiconductor-materials-by-using-electrospinning

[76] M. G. McKee, J. M. Layman, M. P. Cashion, T. E. Long, *Science* **2006**, *311*(5759), 353–355. doi:10.1126/science.1119790

[77] S. Ramakrishna, K. Fujihara, W.-E. Teo, T.-C. Lim, Z. Ma, An Introduction to Electrospinning and Nanofibers, National University of Singapore, World Scientific Publishing, (2005).

[78] W. K. Son, J. H. Youk, T. S. Lee, W. H. Park, *J. Polym. Sci, B Polym. Phys.* **2004b**, *42*, 5-11.

[79] N. Bhardwaj, S. C. Kundu, *Biotechnol. Adv.* **2010**, *28*, 325-347.

[80] A. He, J. Zheng, C. C. Han, *Biomacromolecules* **2006a**, *7*, 2243-2247.

[81] D. Li, G. Ouyang, J. T. McCann, Y. Xia, *Nano Lett* **2005**, *5*(5), 913-916.

[82] Y. Z. Zhang, J. Venugopal, Z. M. Huang, C. T. Lim, S. Ramakrishna, *Polymer* **2006**, *47*, 2911-2917.

[83] S. Zhong, W. E. Teo, X. Zhu, R. W. Beuerman, S. Ramakrishna, L. Y. L. Yung, *J. Biomed. Mater. Res. A* **2006**, *79A*, 456-463.

[84] D. I. Zeugolis, S. T. Khew, E. S. Y. Yew, A. K. Ekaputra, Y. W. Tong, L. Y. L. Yung, D. W. Hutmacher, C. Shepard, M. Raghunath, *Biomaterials* **2008**, *29*, 2293-2305.

[85] K. S. Rho, L. Jeong, G. Lee, B. M. Seo, Y. J. Park, S. D. Hong, S. Roh, J. J. Cho, W. H. Park, B. M. Min, *Biomaterials* **2006**, *27*, 1452-1461.

[86] I. K. Kwon, T. Matsuda, *Biomacromolecules* **2005**, *6*, 2096-105.

[87] E. D. Boland, T. A. Telemeco, D. G. Simpson, G. E. Wnek, G. L. Bowlin, *J. Biomed. Mater. Res. B Appl. Biomater.* **2004a**, *71B*, 144-152.

[88] F. Yang, R. Murugan, S. Ramakrishna, X. Wang, Y. X. Ma, S. Wang. *Biomaterials* **2004**, *25*, 1891-1900.

[89] E. P. S. Tan, S. Y. Ng, C. T. Lim, *Biomaterials* **2005**, *26*, 1453-1456.

[90] S. R. Bhattarai, N. Bhattarai, H. K. Yi, P. H. Hwang, D. I. Cha, H. Y. Kim, *Biomaterials* **2004**, *25*, 2595-2602.

[91] X. M. Mo, C. Y. Xu, M. Kotaki, S. Ramakrishna, *Biomaterials* **2004**, *25*, 1883-1890.

[92] C. Y. Xu, R. Inai, M. Kotaki, S. Ramakrishna, *Biomaterials* **2004**; *25*, 877-886.

[93] Y. Wang, D. D. Rudym, A. Walsh, L. Abrahamsen, H.-J. Kim, H. S. Kim, C. KirkerHead, D. L. Kaplan, *Biomaterials* **2008**, *29*, 3415-3428.

[94] V. Thomas, D. R. Dean, Y. K. Vohra, *Curr. Nanosci.* **2006**, *2*, 155-177.

[95] E. K. Brenner, J. D. Schiffman, E.A. Thompson, L. J. Toth, C. L. Schauer, *Carbohydr.Polym.* **2012**, *87*, 926-929.

[96] Y. Liu, G. Ma, D. Fang, J. Xu, H. Zhang, J. Nie, *Carbohydr. Polym.* **2011**, *83*, 1011-1015.

[97] D. Li, G. Ouyang, J. T. McCann,Y. Xia, *Nano Lett*. **2005**, *5*(5), 913-916.

[98] I. C. Um, D. F. Fang, B. S. Hsiao, A. Okamoto, B. Chu, *Biomacromolecules* **2004**, *5*, 1428-1436.

[99] S. Haider, S. Y. Park, S. H. Lee, *Soft. Matter.* **2008**, *4*, 485-492.

[100] K. Desai, K. Kit, J. J. Li, S. Zivanovic, *Biomacromolecules* **2008**, *9*, 1000-1006.

[101] K. Saeed, S. Haider, T. J. Oh, S. Y. Park, *J. Membr. Sci.* **2008**, *322*, 400-405.

[102] K. J. Pawlowski, C. P. Barnes, E. D. Boland, G. E. Wnek, G. L. Bowlin, *Mater. Res. Soc. Symp. Proc.* **2004**, *827*, 17-28.

[103] S.-C. Wu, W.-H. Chang, G.-C. Dong, K.-Y. Chen, Y.-S. Chen, C.-H. Yao, *J. Bioact. Compat. Polym.* **2011**, *26*, 565-577.

[104] M. Angarano, S. Schulz, M. Fabritius, R. Vogt, T. Steinberg, P. Tomakidi, C.Friedrich, R. Mülhaupt, *Adv. Funct. Mater.* **2013**, *23*, 3277-3285.

[105] G. M. Peretti, M. A. Randolph, V. Zaporojan, L. J. Bonassar, J. W. Xu, J. C. Fellers, M. J. Yaremchuk, *Ann. Plast. Surg*. **2001**, *46*, 533-537.

[106] S. Underwood, A. Afoke, R. A. Brown, A. J. MacLeod, P. A. Shamlou, P. Dunnill, *Biotechnol. Bioeng.* **2001**, *73*, 295-305.

[107] T. T. Yuan, A. M. DiGeorge Foushee, M. C. Johnson, A. R. Jockheck-Clark, J. M. Stahl, *Nanoscale Res Lett* **2018**, 13:88.

[108] M. Wang, A. J. Hsieh, G. C. Rutledge, *Polymer* **2005a**, *46*, 3407-3418.

[109] D. Liang, B. S. Hsiao, B. Chu, *Adv. Drug. Deliv. Rev.* **2007**, *59*(14), 1392-1412.

[110] J. Lyons, F. Ko, *Polym. News* **2005**, *30*, 1-9.

[111] J. Ayutsede, M. Gandhi, S. Sukigara, M. Micklus, H. E. Chen, F. Ko, *Polymer* **2005**, *46*, 1625-1634.

[112] K. E. Park, S. Y. Jung, S. J. Lee, B. M. Min, W. H. Park, *Int. J. Biol. Macromol*. **2006**, *38*, 165-173.

[113] J. S. Kim, D. H. Reneker, *Polym. Compos.* **1999**, *20*, 124-131.

[114] H. Schreuder-Gibson, P. Gibson, K. Senecal, M. Sennett, J. Walker, W. Yeomans, D. Ziegler, P. Tsai, *J. Adv. Mater*. **2002**, *34*, 44-55.

[115] E. Zussman, A. L. Yarin, D. Weihs, *Exp. Fluids* **2002**, *33*, 315-320.

[116] L. Huang, R. A. McMillan, R. P. Apkarian, B. Pourdeyhimi, V. P. Conticello, E. L. Chaikof, *Macromolecules* **2000**, 33, 2989-2997.

[117] C. Zhao, J. Tao, H. Masuda, R. Kishore, T. Asakura, *Biopolymers* **2003**, *69*, 253-259.

[118] S. Y. Chew, Y. Wen, Y. Dzenis, K. W. Leong, *Curr. Pharm. Des*. **2006**, *12*, 4751-4770.

[119] Z. M. Huang, Y. Y. Zhang, S. Ramakrishna, C. T. Lim, *Polymer* **2004**, *45*, 5361-5368.

[120] E. P. S. Tan, S. Y. Ng, C. T. Lim, *Biomaterials* **2005**, *26*, 1453-1456.

[121] S. Y. Chew, T. C. Hufnagel, C. T. Lim, K. W. Leong, *Nanotechnology* **2006**, *17*, 3880-3891.

[122] K. Ramanathan, M. A. Bangar, M. Yun, W. Chen, N. V. Myung, A. Mulchandani, *J. AmChem. Soc.* **2005**, *127*, 496-497.

[123] L. Yang, C. F. C. Fitie, K. O. V. Werf, M. L. Bennink, P. J. Dijkstra, J. Feijen, *Biomaterials* **2008**, *29*, 955-962

[124] E. P. S. Tan, C. T. Lim, *Compos. Sci. Technol.* **2006**, *66*, 1102-1111.

[125] E. Valarezo, Innovative processes for the production of new nanocomposite materials by electrospinning technique, PhD thesis, Università degli Studi di Salerno, 2009.

[126] C. P. Barnes, S. A. Sell, E. D. Boland, D. G. Simpson, G. L. Bowlin, *Adv. Drug. Deliv. Rev.* **2007**, *59*, 1413-1433.

[127] P. X. Ma, Tissue engineering. In encyclopedia of polymer science and technology, NJ, John Wiley & Sons (2004).

[128] X. M. Mo, C. Y. Xu, M. Kotaki, S. Ramakrishna, *Biomaterials* **2004**, *25*(10), 1883-1890.

[129] D. Rubenstein, D. Han, S. Goldgraben, H. El-Gendi, P.-I. Gouma, M. D. Frame, *Microcirculation* **2007**, *14*(7), 723-737.

[130] A. Balguid, A. Mol, M. H. van Marion, R. A. Bank, C. V. C. Bouten, F. P. T. Baaijens, *Tissue Eng., Part A* **2009**, *15*(2), 437-444.

[131] S. A. Sell, M. J. McClure, C. P. Barnes, D. C. Knapp, B. H. Walpoth, D. G. Simpson, G. L. Bowlin, *Biomed. Mater.* **2006**, *1*(2), 72-80.

[132] H. Yoshimoto, Y. M. Shin, H. Terai, J. P. Vacanti, Biomaterials **2003**, *24*, 2077-2082.

[133] A. S. Badami, M. R. Kreke, M. S. Thompson, J. S. Riffle, A. S. Goldstein, *Biomaterials* **2006**, *27*, 596-606.

[134] K. Sombatmankhong, N. Sanchavanakit, P. Pavasant, P. Supaphol, *Polymer* **2007**, *48*, 1419-1427.

[135] K. Fujihara, M. Kotaki, S. Ramakrishna, *Biomaterials* **2005**, *26*(19), 4139-4147.

[136] B. Duan, L. Wu, X. Li, X. Yuan, X. Li, Y. Zhang, K. J. Yao, *Biomater. Sci., Polym. Ed.* **2007**, *18*(1), 95-115.

[137] Z. G. Chen, P. W. Wang, B. Wei, X. M. Mo, F. Z. Cui, *Acta Biomater.* **2010b**, *6*(2), 372-382.

[138] S. C. Baker, N. Atkin, P. A. Gunning, N. Granville, K. Wilson, D. Wilson, D. Southgate, *J. Biomaterials* **2006**, *27*(16), 3136-3146.

[139] D. J. Wong, H. Y. Chang, E. Biology, Skin tissue engineering. StemBook, 1-9, 2009.

[140] S. G. Priya, H. Jungvid, A. Kumar, *Tissue Eng. Part B Rev.* **2008**, *14*(1), 105-118.

[141] H. M. Powell, S. T. Boyce, *Tissue Eng. Part A* **2009**, *15*(8), 2177-2187.

[142] Y. Yang, X. Zhu, W. Cui, X. Li, Y. Jin, *Macromol. Mater. Eng.* **2009**, *294*(9), 611-619.

[143] Y. Zhou, D. Yang, X. Chen, Q. Xu, F. Lu, J. Nie, *Biomacromolecules* **2008**, *9*(1), 349-354.

[144] T. Sun, S. Mai, D. Norton, J. W. Haycock, A. J. Ryan, S. MacNeil, *Tissue Eng.* **2005**, *11*(7-8), 1023-1033.

[145] J. C. Vickers, A. E. King, A. Woodhouse, M. T. Kirkcaldie, J. A. Staal, G. H. McCormack, C. A. Blizzard, R. E. Musgrove, S. Mitew, Y. Liu, J. A. Chuckowree, O. Bibari, T. C. Dickson, *Brain Res. Bull.* **2009**, *80*, 217-223.

[146] V. J. Mukhatyar, M. Salmeron-Sanchez, S. Rudra, S. Mukhopadaya, T. H. Barker, A. J. Garcia, R. V. Bellamkonda, *Biomaterials* **2011**, *32*(16), 3958-3968.

[147] G. T. Christopherson, H. Song, H.-Q. Mao, *Biomaterials* **2008**, *30*(4), 556-564.

[148] H. B. Wang, M. E. Mullins, J. M. Cregg, C. W. McCarthy, R. J. Gilbert, *Acta Biomater*. **2010**, *6*(8), 2970-2978.

[149] K. J. Senecal, D. P. Ziegler, J. He, R. Mosurkal, H. Schreuder-Gibson, L. A. Samuelson, *Mater. Res. Soc. Symp. Proc.* **2002**, *708*, 285-289.

[150] G. Verreck, I. Chun, J. Peeters, J. Rosenblatt, M. E. Brewster, *Pharm. Res.* **2003**, *20*, 810-817.

[151] Y. K. Luu, K. Kim, B. S. Hsiao, B. Chu, M. Hadjiargyrou, *J. Control Release* **2003**, *89*, 341-353.

[152] W. Sambaer, M. Zatloukal, D. Kimmer, *Polym. Test.* **2010**, *29*(1), 82-94.

[153] K. Yoon, K. Kim, X. Wang, D. Fang, B. S. Hsiao, B. Chu, *Polymer* **2006**, *47*(7), 2434-2441.

[154] Z. Tang, C. Qiu, J. R. McCutcheon, K. Yoon, H. Ma, D. Fang, E. Lee, C. Kopp, B. S. Hsiao, B. Chu, *J. Polym. Sci., Part B: Polym. Phys*. **2009**, *47*(22), 2288-2300.

[155] X. H. Qin, S. Y. Wang, *J. Appl. Polym. Sci.* **2008**, *109*(2), 951-956.

[156] S. S. Homaeigohar, K. Buhr, K. Ebert, *J. Membr. Sci.* **2010**, *365*(1-2), 68-77.

[157] Q. Zhang, J. Welch, H. Park, C. Wu, W. Sigmund, J. C. M. Marijnissen, *J. Aerosol Sci.* **2010**, *41*(2), 230-236.

[158] D. Figeys, D. Pinto, *Anal. Chem.* **2000**, *72*, 330A-335A.

[159] K. Ramanathan, M. A. Bangar, M. Yun, W. Chen, N. V. Myung, *J. Am. Chem. Soc.* **2005**, *127*, 496-497.

[160] N. L. Lala, R. Ramaseshan, L. Bojun, S. Sundarrajan, R. S. Barhate, Y. L. Liu, S. Ramakrishna, *Biotechnol. Bioeng.* **2007**, *97*, 1357-1365.

[161] H. L. Schreuder-Gibson, P. Gibson, K. Senecal, M. Sennett, J. Walker, W. Yeomans, D. Ziegler, P. P. Tsai, *J. Adv. Mater.* **2002**, *34*, 44-55.

[162] K. J. Senecal, D. P. Ziegler, J. He, R. Mosurkal, H. Schreuder-Gibson, L. A. Samuelson, *Mater. Res. Soc. Symp. Proc.* **2002**, *708*, 285-289.

[163] P. Ye, Z. K. Xu, A. F. Che, J. Wu, P. Seta, *Biomaterials* **2005**, *26*, 6394-6403.

[164] H. F. Jia, G. Y. Zhu, B. Vugrinovich, W. Kataphinan, D. H. Reneker, P. Wang, *Biotechnol. Prog.* **2002**, *18*, 1027-1032.

[165] R. Gopal, S. Kaur, Z. W. Ma, C. Chan, S. Ramakrishna, T. Matsuura, *J. Membr. Sci.* **2006**, *281*, 581-586.

[166] S. Kaur, R. Gopal, M. Kotaki, Z. W. Ma, S. Ramakrishna, *Int. J. Nanosci.* **2006**, *5*, 1-11.

[167] R. A. Freitas, Personal choice in the coming era of nanomedicine. Nanoethics: The Ethical and Social Implications of Nanotechnology, John Wiley, NY (**2007**) pp.161-172.

[168] P. Rodgers. Nanoelectronics: Single file. *Nat. Nanotechnol.* **2006.**

[169] H. H. Xu, J. L. Moreau, L. Sun, L. C. Chow, *Biomaterials* **2008,** *29*(32), 4261-4267.

[170] C. Rahiotis, G. Vougiouklakis, *J. Dent.* **2007**, *35*, 695-698.

[171] G. Mendonca, D. B. Mendonca, F. J. Aragao, L. F. Cooper, *Biomaterials* **2008**, *29*, 3822-3835.

[172] M. Tian, Y. Gao, Y. Liu, Y. Liao, N. E. Hedin, H. Fong, *Dent. Mater.* **2008**, *24*(2), 235-243.

[173] M. Tian, Y. Gao, Y. Liu, Y. Liao, R. Xu, N. E. Hedin, H. Fong, *Polymer* (Guildf) **2007**, *48*(9), 2720-2728.

[174] K. V. P. Rao, J. S. Kumar, *KDJ* **2013**, *36*, 56-59.

[175] B. Park, Current and Future Applications of Nanotechnology. The Royal Society of Chemistry, Cambridge, UK, (2007).

[176] E. Pinon-Segundo, A. Ganem-Quintanar, V. Alonso-Perez, D. Quintanar-Guerrero, *Int. J. Pharm.* **2005**, *294*(1-2), 217-232.

[177] C. Du, G. Falini, S. Fermani, C. Abbott, Moradian-Oldak, *J. Science* **2005**, *307*, 1450-1454.

[178] S. Jain, A. P. Jain, S. Jain, O. N. Gupta, A. Vaidya, *J. Dent. Sci.* **2013**, http://dx.doi.org/10.1016/j.jds.2013.08.

[179] Y. Xia, F. Zhang, H. Xie, N. Gu, *J. Dent*. **2008**, *36*, 450-455.

[180] C. D. Mayworm, J. S. S. Camargo, F. L. Bastian, *J. Dent.* **2008**, *36*, 703-710.

[181] H. F. Chen, B. H. Clarkson, K. Sun, J. F. Mansfield, *J. Colloid. Interf. Sci.* **2005**, *288*, 97-103.

[182] F. Zhang, Y. Xia, L. Xu, N. Gu, *J. Biomed. Mater. Res. B App.l Biomater.* **2008**, *86*, 90-97.

[183] F. A. Alzarrug, M. M. Dimitrijević, R. M. Jančić Heinemann, V. Radojević, D. B. Stojanović, P. S. Uskoković, R. Aleksić, *Mater. Des.* **2015**, *86*(5), 575-581.

[184] B. Marrs, R. Andrews, T. Rantell, D. Pienkowski. *J. Biomed. Mater. Res.* **2006**, *77A*, 269-276.

[185] H. W. Kim, H. E. Kim, *J. Biomed. Mater. Res. B Appl. Biomater.* **2006**, *77*, 323-328.

[186] M. Tian, Y. Gao, Y. Liu, Y. Liao, N. E. Hedin, *Dent. Mater.* **2008**, *24*, 235-243.

[187] https://en.wikipedia.org/wiki/Poly(methyl_methacrylate)

[188] J. H. Yu, A. J. Hsieh, G. C. Rutledge, U.S. Army Research Laboratory, September **2010**, pp 1-10, XP002649570, Internet Retrieved from the Internet: URL:http://www.dtic.mil/dtic/tr/fulltext/u 2/a531405.pdf

[189] G. Bayraktar , B. Guvener, C. Bural, Y. Uresin, *J. Biomed. Mater. Res. Part B: Appl. Biomater.* **2006**; *76B*, 340-345.

[190] J. Zhang, J. Liao, A. Mo, Y. Li, J. Li, X. Wang, *Appl. Surf. Sci.* **2008**, *255*, 328-330.

[191] X. Wang, L. Wang, Q. Su, J. Zheng, *Compos. Sci. Technol.* **2013**, *89*, 52-60.

[192] M. B. Correa, M. A. Peres, K. G. Peres, B. L. Horta, A. D. Barros, F. F. Demarco, *J. Dent.* **2012**, *40*, 703-710.

[193] M. E. Khalaf, Q. D. Alomari, R. Omar, *J. Dent.* **2014**, *42*, 785-792.

[194] A. M. Ballo, I. Cekic-Nagas, G. Ergun, L. Lassila, A. Palmquist, P. Borchardt, J. Lausmaa, P. Thomsen, P. K. Vallittu, T. O. Närhi, *Dent. Mater.* **2014**, *30*, 384-395.

[195] J. Pino-Mínguez, A. Jorge-Mora, R. Couceiro-Otero, C. García-Santiago, *Revista Española de Cirugía Ortopédica y Traumatología (English Edition)* **2015**, *59*, 122-128.

[196] P. S. Stein, J. Sullivan, J. E. Haubenreich, P. B. Osborne, *J. Long Term. Eff. Med. Implants* **2005**, *15*, 641-654.

[197] J. W. Stanford, L. Burns Claire, G. C. Paffenbarger, *J. Am. Den.t Assoc.* **1955**, *51*, 307-315.

[198] D. Rentería-Zamarrón, D. A. Cortés-Hernández, L. Bretado-Aragón, W. Ortega-Lara, *Mater. Des.* **2009**, *30*, 3318-3324.

[199] R. Q. Frazer, R. T. Byron, P. B. Osborne, *J. Long. Term. Eff. Med. Implants* **2005**, *15*, 629-639.

[200] C. Chen, D. Li, Q. Hu, R. Wang, *Mater. Design* **2014**, 56, 1049-1056.

[201] M. Barathi, A. Santhana Krishna Kumar, N. Rajesh, *Ultrason. Sonochem.* **2014**, *21*, 1090-1099.

[202] C. Peng, P. Liu, J. Hu, T. Hua, Y. Shen, B. Zhao, G. Tang, *Colloid Surf. A*, **2014**, *457*, 1-7.

[203] A. Mahapatra, B. G. Mishra, G. Hota, *Ceram. Int.* **2011**, *37*, 2329-2333.

[204] V. Maneeratana, W. M. Sigmund, *Chem. Eng. J.* **2008**, *137*, 137-143.

[205] R. Jančić, R. Aleksić, *Mater. Lett.* **2000**, *42*, 350-355.

[206] P. Milanović, M. Dimitrijević, R. Jančić Heinemann, J. Rogan, D. B. Stojanović, A. Kojović, R. Aleksić, *Ceram. Int.* **2013**, *39*, 2131-2134.

[207] S. Ahmed Ben Hasan, M. M. Dimitrijević, A. Kojović, D. B. Stojanović, K. Obradović - Đuričić, R. M. Jančić-Heinemann, R. Aleksić R, *J. Serb. Chem. Soc.* **2014**, *79*, 1295-1307.

[208] M. Hussain, A. Nakahira, K. Niihara, *Mater. Lett.* **1996**, *26*, 185-191.

[209] W. C. Oliver, G. M. Pharr, *J. Mat. Res.* **1992**, *7*, 1564-1583.

[210] D. B. Stojanović, M. Zrilić, R. Jančić-Heinemann, I. Živković, A. Kojović, P. S. Uskoković, R. Aleksić, *Polym. Advan. Technol.* **2013**, *24*, 772-776.

[211] D. H. Reneker, I. Chun, *Nanotechnology* **1996**, *7*, 216-223.

[212] Z. Ding, A. Salim, B. Ziaie, *Langmuir* **2009**, *25*(17), 9648-9652.

[213] S. Zargham, S. Bazgir, A. Tavakoli, A. S. Rashidi, R. Damerchely, *J. Eng. Fiber. Fabr.* **2012**, *7*(4), 42-49.

[214] Y. C. Ahn, S. K. Park, G. T. Kim, Y. J. Hwang, C. G. Lee, H. S. Shin, J. K. Lee, *Curr. Appl. Phys.* **2006**, *6*(6), 1030-1035.

[215] G. G. Chase, J. S. Varabhas, D. H. Reneker, *J. Eng. Fiber. Fabr.* **2011**, *6*(3), 32–38.

[216] P. Ramesh Kumar, N. Khan, S. Vivekanandhan, N. Satyanarayana, A. K. Mohanty, M. Misra, *J. Nanosci. Nanotechnol.* **2012**, *12*, 1-25.

[217] Y. Yang, Z. Jia, Q. Li, L. Hou, Z. Guan, *J. Phys.: Conf. Ser.* **2008**, *142*, 012027.

[218] L. Tian, C. Zhao, J. Li, Z. Pan, *Text. Res. J.* **2015**, *85*(6), 621–631.

[219] D. B. Stojanović, M. Zrilić, R. Jančić-Heinemann, I. Živković, A. Kojović, P. S. Uskoković, R. Aleksić, *Polym. Adv. Technol.* **2013**, *24*(8), 772–776.

[220] H. Xu, H. Li, J. Chang, *J. Mater. Chem. B.* **2013**, *1*, 4182-4188.

[221] K. Lee, S. Lee, *J. Appl. Polym. Sci.* **2012**, *124*, 4038-4046.

[222] F. Yalcinkaya, M. Komarek, D. Lubasova, F. Sanetrnik, J. Maryska, *J. Nanomater.* **2016**, 7565972, 1-7.

[223] A. M. Torki, I. Živković, V. R. Radmilović, D. B. Stojanović, V. J. Radojević, P. S. Uskoković, R. R. Aleksić, *Int. J. Mod. Phys. B.* **2010**, *24*(6-7), 805-812.

[224] D. G. Medeiros, P. M. Jardim, M. K. V. de Tatagiba, J. R. M. d'Almeida, *Polym. Test.* **2015**, *42*, 108-114.

[225] L. Mancic, P. I. Pontón, S. Letichevsky, A. M. Costa, B. A. Marinkovic, F. C. Rizzo, *Compos. Part B- Eng.* **2016**, *93*, 153-162.

[226] P. Ahmadpoor, A. S. Nateri, V. Motaghitalab, *J. Appl. Polym. Sci.* **2013**, *130*(1), 78-85.

[227] Y. Lv, Z. L. Xu, H. Asai, N. Shimada, K. Nakane, *RSC Adv.* **2016**, *6*, 21043-21047.

[228] M. Radoicic, G. Ciric-Marjanovic, Z. V. Saponjic, M. Mitric, Z. Konstantinovic, M. Stoiljkovic, J. M. Nedeljkovic, *J. Mater. Sci.* **2013**, *48*, 5776-5787.

[229] M. Kulkarni, A. Mazare, E. Gongadze, Š. Perutkova, V. Kralj-Iglič, I. Milošev, P. Schmuki, A. Iglič, M. Mozetič, *Nanotechnology* **2015**, *26*, 062002, 1-18.

[230] S. M. Z. Klaled, R. M. Miron, W. D. Hamilton, P. A. Charpentier, A. S. Rizkalla, *Dent. Mater.* **2010**, *26*, 169-178.

[231] Z. V Saponjic, N. M Dimitrijevic, D. M Tiede, A. J Goshe, X. Zuo, L. X Chen, A. S Barnard, P. Zapol, L. Curtiss, T. Rajh, *Adv. Mater.* **2005**, *17*(8), 965-971.

[232] D. B. Stojanovic, A. Orlovic, M. Zrilic, I. Balac, C. Y. Tang, P. S. Uskokovic, R. Aleksic, *Polym. Composite.* **2013**, *34*, 1710-1719.

[233] W. C. Oliver, G. M. Pharr, *J. Mater. Res.* **2004**, *19*, 3-20.

[234] Y. Cai, M. Stromme, K. Welch, *PLOS One* **2013**, *8*(10), e75929.

[235] F. Yalcinkaya, D. Lubasova, *Polym. Adv. Technol.* **2016**, DOI: 10.1002/pat.3883V

[236] K. Cendrowski, M. Peruzynska, A. Markowska-Szczupak, X. Chen, A. Wajda, J. Lapczuk, M. Kurzawski, R. J. Kalenczuk, M. Drozdzik, E. Mijowska. *Biomed. Microdevices.* **2014**, *16*, 449-458.

[237] S. H. Othman, N. R. A. Salam, N. Zainal, R. K. Basha, R. A. Talib, *Int. J. Photogr.* **2014**, (Article ID 945930), 1-6.

[238] H. R. Pant, D. R. Pandeya, K. T. Nam, W. I. Baek, S. T. Hong, H. Y. Kim, J. *Hazard. Mater.* **2011**, *189*(1-2), 465-471.

[239] J. Chen, A. Zhao, H. Chen, Y. Liao, P. Yang, H. Sun, N. Huang, *Colloid. Surface. B.* **2014**, *122*, 709-718.

[240] W. A. Daoud, J. H. Xin, Y. H. Zhang, *Surf. Sci.* **2005**, *599*(1-3), 69-75.

[241] S. Ahmed Ben Hassan, D. B. Stojanović, A. Kojović, I. Janković-Častvan, Dj. Janaćković, P. S. Uskoković, R. Aleksić, *Ceram. Int.* **2014**, *40*, 1139-1146.

[242] K. Menard, Dynamic Mechanical Analysis: A Practical Introduction, 2nd Ed. CRC Press, Boca Raton (2007).

[243] A. L. S. Borges, E. A. Münchow, A. C. O. Souza, T. Yoshida, P. K. Vallittu, M. C. Bottino, *J. Mech. Behav. Biomed.* **2015**, *48*, 134-144.

[244] H. Yahyaei, M. Mohseni, *Tribol. Int.* **2013**, *57*, 147-155.

[245] H. Chakraborty, A. Sinha, N. Mukherjee, P. P. Chattopadhyay, *J. Nanotechnol.* **2012**, 940516, 1-5.

[246] A. M. Díez-Pascual, M. A. Gómez-Fatou, F. Ania, A. Flores, *Prog. Mater. Sci.* **2015**, *67*, 1-94.

[247] D. Stojanovic, A. Orlovic, S. Markovic, V. Radmilovic, P. S. Uskokovic, R. Aleksic, *J. Mater. Sci.* **2009**, *44*, 6223-6232.

[248] Y. Xia, M. Mrksich, E. Kim, George M. Whitesides, *J. Am. Chem. Soc.* **1995**, *117*, 9576-9577; J. A. Foster, D. W. Johnson, M. O. M. Pipenbrock, J. W. Steed, *New J. Chem*. **2014**, *38*, 927-932.

[249] M. E. Fowler, H. Keskkula, D. R. Paul, *Polymer* **1987**, *28*, 1703-1711; X. L. Xie, R. K. Y. Li, Q. X. Liu, Y. W. Mai, *Polymer* **2004**, *45*, 2793-2802; K. Cho, J. H. Yang, C. E. Park, *Polymer* **1998**, *39*, 3073-3081; K. Cho, J. H. Yang, C. E. Park, *Polymer* **1997**, *38*, 5161-5167.

[250] S. Jiang, Electrospun Nanofiber Reinforced Composites: Fabrication and Properties, PhD Thessis, Geboren in Xin'Gan, Jiangxi Province, China, Bayreuth 2014.

[251] S. Ahmed Ben Hassan, Structure and the Physical and Mechanical Properties of Dental Hybrid Composite Materials, PhD Thessis, Faculty of Technology and Metallurgy, Belgrade, 2014.

[252] D. B. Stojanović, A. Orlović, M. Zrilić, I. Balać, C. Y. Tang, P. S. Uskoković, R. Aleksić, *Polym. Compos.* **2013**, *34*(10), 1710-1719.

[253] Lj. M. Brajovic, D. B. Stojanovic, P. M. Mihailovic, S. B. Markovic, M. J. Romcevic, M. N. Mitric, V. Lazovic, D. M. Dramlic, S. J. Petricevic, N. Z. Romcevic, *J. Alloys Compd.* **2017**, *695*, 841-849.

[254] W. G. Rees, Physical Principles of Remote Sensing, Third edition, Cambridge University Press, NewYork (2012)

[255] Mie scaterring by Scott Prahl, http://omlc.org/calc/mie_calc.html

[256] Refractive index database, www.refractiveIndex.info, 2015.

BIOGRAFIJA

Faisal Ali Alzarrug rođen je 10.03.1983. u Nalutu, Libija. Diplomirao je medicinsku tehnologiju 2005. na El-Jabel Univerzitetu El Garbi, Libija, Nalut. Master studije je završio 2011. godine na Univerzitetu u Beogradu, Tehnološko-metalurški fakultet, profil Inženjerstvo materijala. Doktorske studije upisao je 2011. godine na Univerzitetu u Beogradu, Tehnološko-metalurški fakultet, profil Inženjerstvo materijala

BIOGRAPHY

Faisal Ali Alzarrug was born 10.03.1983. in Nalut-Libya. He received his bachelor degree in medical technology 2005. at El-jabel El-Garbi University, Libya, Nalut. He obtained his master degree in Materials Science and Engineering 2011. at the Department of Materials Science & Engineering, the Faculty of Technology and Metallurgy, the University of Belgrade, Serbia. Since 2011, he has been enrolled in PhD studies at the Faculty of Technology and Metallurgy, the University of Belgrade.

Прилог 1.

Изјава о ауторству

Потписани-а Faisal Ali Al Zarrug

број индекса 4071/2011

Изјављујем

да је докторска дисертација под насловом

"Sinteza i karakterizacija dentalnih materijala ojačanih nanovlaknima"

Synthesis and characterisation of dental materials reinforced with nanofibers

- резултат сопственог истраживачког рада,
- да предложена дисертација у целини ни у деловима није била предложена за добијање било које дипломе према студијским програмима других високошколских установа,
- да су резултати коректно наведени и
- да нисам кршио/ла ауторска права и користио интелектуалну својину других лица.

Потпис докторанда

У Београду, _____

Прилог 2.

Изјава о истоветности штампане и електронске верзије докторског рада

Име и презиме аутора Faisal Ali Al Zarrug

Број индекса 4071/2011

Студијски програм Инжењерство Материјала

Наслов рада "Sinteza i karakterizacija dentalnih materijala ojačanih nanovlaknima"

Synthesis and characterisation of dental materials reinforced with nanofibers

Ментори Ускоковић Петар

Душица Стојановић

Потписани/а _____

_____

Изјављујем да је штампана верзија мог докторског рада истоветна електронској верзији коју сам предао/ла за објављивање на порталу **Дигиталног репозиторијума Универзитета у Београду.**

Дозвољавам да се објаве моји лични подаци везани за добијање академског звања доктора наука, као што су име и презиме, година и место рођења и датум одбране рада.

Ови лични подаци могу се објавити на мрежним страницама дигиталне библиотеке, у електронском каталогу и у публикацијама Универзитета у Београду.

Потпис докторанда

У Београду, _____

_____

Прилог 3.

Изјава о коришћењу

Овлашћујем Универзитетску библиотеку „Светозар Марковић" да у Дигитални репозиторијум Универзитета у Београду унесе моју докторску дисертацију под насловом:

"Sinteza i karakterizacija dentalnih materijala ojačanih nanovlaknima"

Synthesis and characterisation of dental materials reinforced with nanofibers

која је моје ауторско дело.

Дисертацију са свим прилозима предао/ла сам у електронском формату погодном за трајно архивирање.

Моју докторску дисертацију похрањену у Дигитални репозиторијум Универзитета у Београду могу да користе сви који поштују одредбе садржане у одабраном типу лиценце Креативне заједнице (Creative Commons) за коју сам се одлучио/ла.

1. Ауторство

2. Ауторство - некомерцијално

3. Ауторство – некомерцијално – без прераде

4. Ауторство – некомерцијално – делити под истим условима

5. Ауторство – без прераде

6. Ауторство – делити под истим условима

(Молимо да заокружите само једну од шест понуђених лиценци, кратак опис лиценци дат је на полеђини листа).

Потпис докторанда

У Београду, _____